Development of anticancer nanomedicine targeting Neuraminidase-1

（ノイラミニダーゼ-1 をターゲットとした抗がんナノ医薬の開発）

September 2025

Doctoral Thesis

Ken Murakami

Laboratory of Advanced Chemical Biology

Graduate School of Life Science, Hokkaido University

Table of Contents

Abbreviations

1D	1 dimension
2D	2 dimension
AO	Aminooxy
Ac	Acetyl
AcOH	Acetic acid
AuNP	Gold nanoparticles
Boc	Tert-butyl
$CHCl_3$	Chloroform
DAST	N, N-diethylaminosulfur trifluoride
DDS	Drug delivery system
DIC	N, N-diisopropylcarbodiimide
DHB	Dihydroxybenzoic acid
EDC	1-ethyl-3-(3-dimethylaminopropyl) carbodiimide
eq.	Equal
ESI	Electro spray ionization
Gal	Galactose
GlcNAc	N-acetylglucosamine
Ki	Binding constant
Kinact	Inactivation rate
Man	Mannose
MALDI	Matrix assisted laser desorption ionization
Me	Methyl
MeCN	Acetonitrile
MeOH	Methanol
MS	Mass spectra
NANA	N-acetyl neuraminic acid
NaOMe	Sodium methoxide
NAG	N-acetylglucosaminidase
NEU1	Neuraminidase-1
NMR	Nuclear magnetic resonance
p-NP	p-Nitrophenol
NP	Nanoparticles
NS	Nanosomes
PC	Phosphocholine

QDs	Quantum dots
r.t.	Room temperature
SAM	Self-assembled monolayer-coated
t1/2	Half-time for inhibition
THF	Tetrahydrofuran
TOF	Time of flight
TOPO	Tri-n-octylphosphine oxide
UDP	Uridine-5'-phosphate
UV	Ultraviolet

Chapter 1　General Introduction

1-1. Lysosomes

Lysosomes are organelles surrounded by cell membranes that function as sites of digestion within cells. Substances taken up from outside the cell are transported to lysosomes by endocytosis (a mechanism for taking substances into cells) and broken down by autophagy (a process of self-digestion) that breaks down proteins within the cell[1,2] (Figure. 1-1-1). Endocytosis includes the following types: (1) Clathrin-dependent endocytosis: A process in which clathrin-coated pits are formed for the transport of compounds through ligand-receptor binding. (2) Caveolae-mediated endocytosis: A process in which caveolae, a special form of lipid rafts generated by the oligomerization of caveolin, are formed and vesicle transport occurs. (3) Macropinocytosis: A phenomenon in which cells non-specifically take up relatively large amounts of extracellular fluid and compounds, form vesicles, and transport them. The vesicles formed in all these transports are eventually delivered to lysosomes, where the compounds are degraded[3]. Lysosomes contain various hydrolytic enzymes, such as proteases, glycosidases, and phosphatases, which are used to break down delivered compounds. Furthermore, the interior of lysosomes is constantly maintained in an acidic state and covered with sugar chains to prevent escape from enzymatic hydrolysis.[1,2,3] However, lysosomes in cancer cells have an additional feature that they can take up many compounds due to active endocytosis. In addition, hydrolases levels including a variety of glycosidases are elevated in cancer cells[5]. The nutrient source obtained by degrading large amounts of compounds will result in various cancer cell characteristics such as aberrant cell surface glycosylation (Figure. 1-1-2). The Aberrant glycan structure is involved in cancer progression such as proliferation, invasion, angiogenesis and metastasis[6]. Therefore, it is natural that glycosidases localized in lysosomes are promising targets. Many proteins secreted on the cell surface and extracellularly are glycoproteins, so glycoprotein-degrading enzymes that break them down are abundant in lysosomes[1]. In addition, hyaluronic acid and chondroitin sulfate, which exist as extracellular matrix, are also hydrolyzed by glycosidase (Figure. 1-1-3).

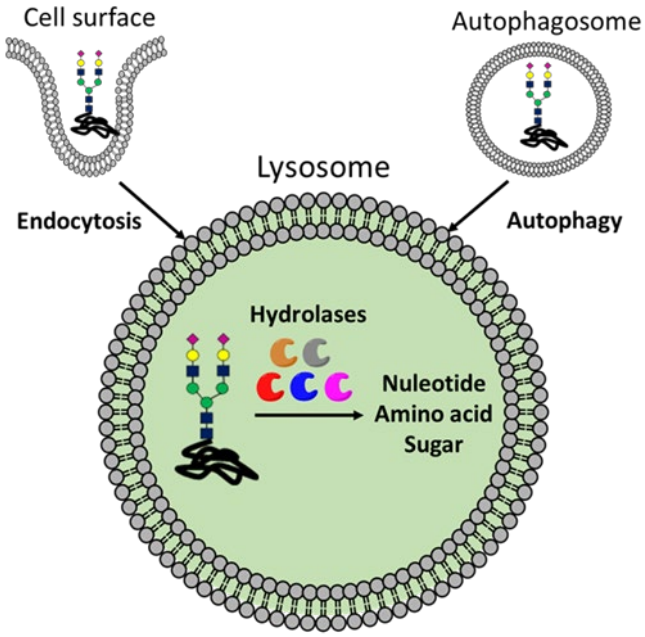

Figure 1-1-1. Cells take up compounds by endocytosis and autophagy

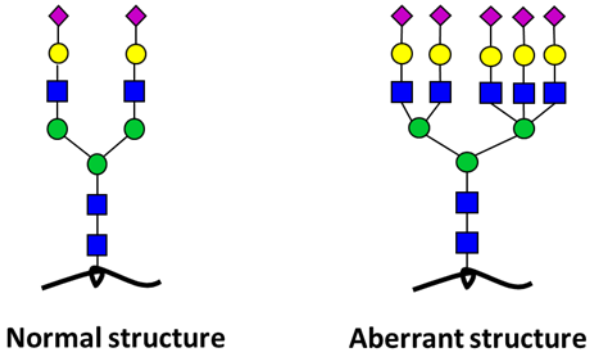

Figure 1-1-2. An example of normal and aberrant N-glycan structures

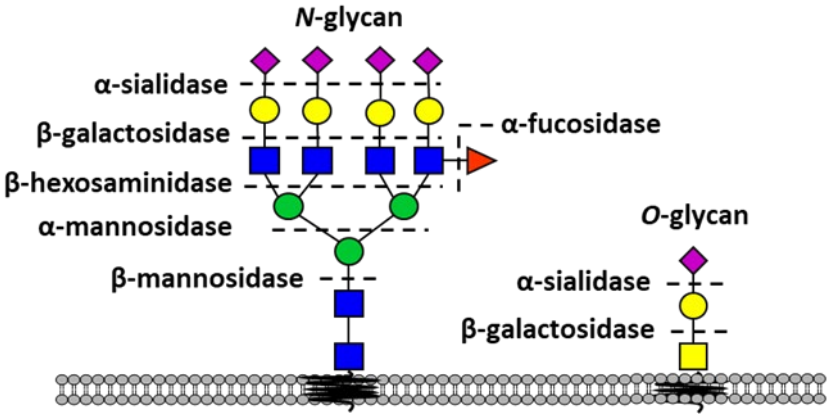

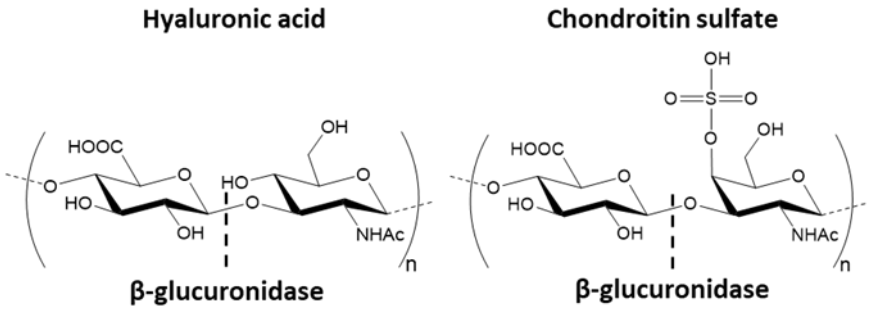

Figure 1-1-3. Examples of glycans and their glycosidases

1-2. Suicide substrate

Previously, our laboratory reported various suicide substrate[7-9]. These compounds are characterized by the presence of a methyl difluoride group that inhibits enzyme activity by forming covalent bonds with enzymes. The inhibition mechanism is as follow: (Ⅰ) Suicide substrate is recognized by the enzyme and hydrolysis of the glycan parts occurs, producing reactive methide. (Ⅱ) The methide react with a nucleophile in the glycosidase (i.e., the carboxylate of Asp or Glu) and form a covalent linkage between the glycosidase and the released aryl moiety. This mechanism allows for irreversible enzyme inhibition[7,8] (Figure. 1-2-1).

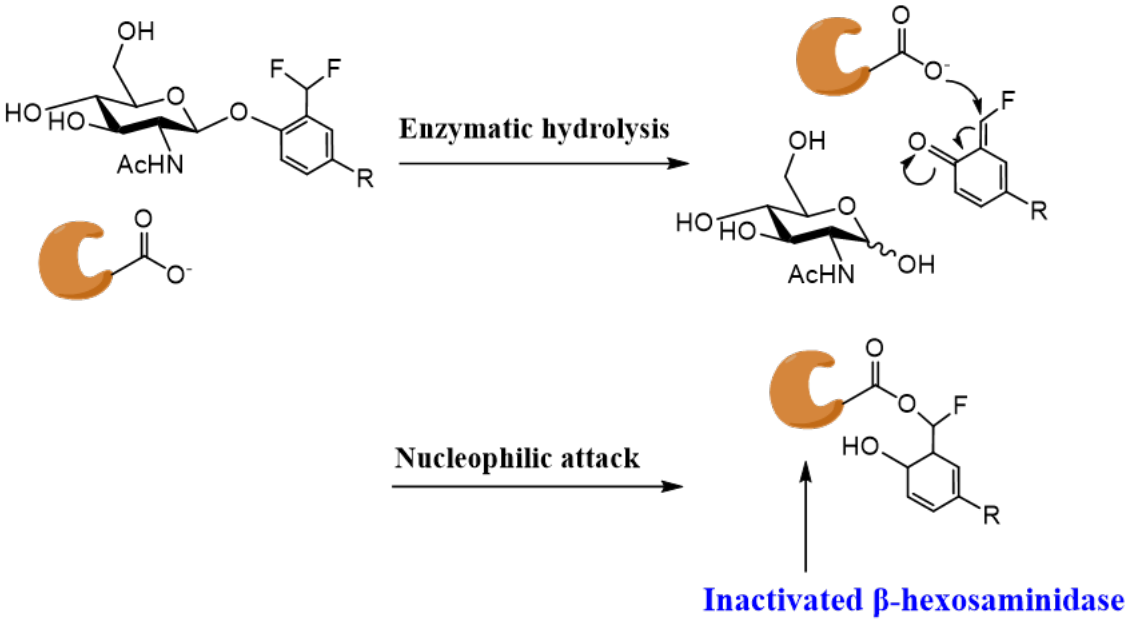

Figure 1-2-1. Inhibition mechanism of suicide substrate (example of β-hexosaminidase)

1-3. Nanosomes

Currently, drug delivery systems (DDS) based on nanoparticles (NPs) are being researched worldwide[10-12]. Research using nanoparticles has led to groundbreaking advances in the development of new imaging agents, therapeutic drugs, genome editing tools, nanomachines, and other biotechnological tools. Furthermore, the size, shape, surface chemistry, rigidity, and chemical composition of nanoparticles are key factors in controlling various biological interactions such as intracellular uptake efficiency and biodistribution[13-19]. In our previous studies, we have demonstrated that "nanosomes" consisting of a core metal coated with an anti-adhesive mixed self-assembled monolayer can avoid non-specific surface protein corona and enable target molecule delivery via activated endocytosis[20,21]. Nanosomes are obtained by coating a linker called phosphorylcholine (PC) linker, which mimics phosphatidylcholine widely distributed in biological membranes, to the surface of nanoparticles. The coating of the PC linker has several advantages, such as improving water solubility and preventing the formation of protein corona. In addition, by simultaneously coating an Aminooxy (AO) linker with an amino group at the end, compounds with aldehyde or ketone groups can be conveniently presented under production conditions through oxime formation reactions[13,20,21] (Figure. 1-3-1). Nanosomes are taken up into cells by endocytosis, and their final delivery to lysosomes has been confirmed by live cell imaging using fluorescent nanoparticles[21]. Nanosomes targeting β-hexosaminidase and β-galactosidase were synthesized and confirmed to exhibit high anticancer activity[20].

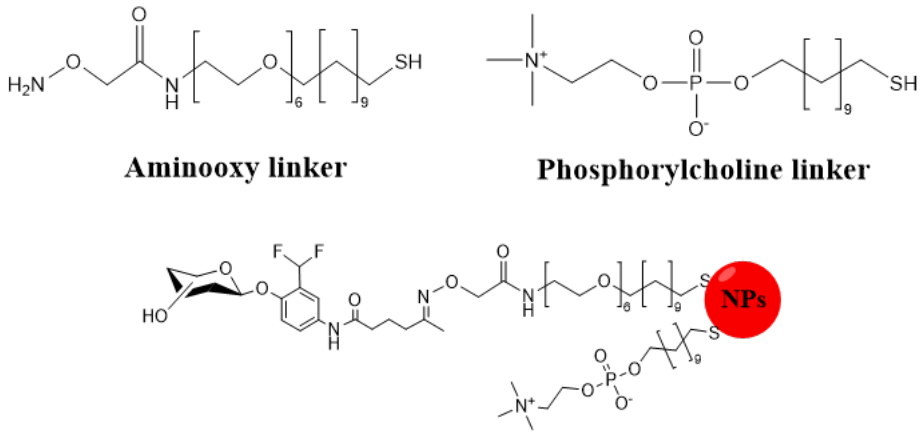

Figure 1-3-1. Presenting compounds on NPs by utilizing AO and PC linker

In Chapter 2, we first synthesized five types of lysosome inhibitors. The resulting inhibitors were presented on the surface of nanosomes via oxime bonds mediated by aminooxy groups.

Subsequently, to evaluate the antitumor effects of these nanoparticles, we conducted cell survival assays using human liver cancer cells (HepG2), human lung cancer cells (A549), and human colon cancer cells (HT-29). The results showed that each lysosome inhibitor-loaded nanosomes exhibited anticancer activity against cancer cells, but the nanosomes loaded with sialidase inhibitor demonstrated universal and significant proliferation inhibitory effects against all cell lines. Furthermore, fluorescence microscopy using fluorescent dyes revealed that the nanosomes were efficiently taken up by cancer cells, and their colocalization with lysosomes suggested enhanced LMP.

In Chapter 3, we simultaneously loaded sialidase inhibitor-carrying nanosomes with sorafenib (multikinase inhibitor) and SN-38 (active metabolite of the topoisomerase inhibitor irinotecan). The sorafenib-loaded nanosomes exhibited potent antitumor activity against HepG2 cells with an IC_{50} of 8.57 nM. Additionally, similar cytotoxicity assays were conducted using PANC-1 (human pancreatic cancer cells) and OUS-11 (human normal lung cells) with SN-38 derivative-loaded nanosomes. The IC_{50} value in PANC-1 was 8.07 nM, indicating extremely high anticancer activity, while toxicity toward normal cells was suppressed. These results suggest that NEU1-targeted nanosomes irreversibly inhibit NEU1 on the cell surface and within lysosomes in cancer cells, inducing lysosomal membrane permeabilization (LMP) and effectively causing cell death. Additionally, co-delivery with sorafenib or SN-38 derivatives enables a dual attack of targeted therapy and cytotoxic drugs, potentially enhancing therapeutic efficacy.

In Chapter 4, we conducted animal experiments using nude mice with subcutaneously transplanted PANC-1 cells to demonstrate the antitumor effects of nanosomes. When the tumor volume reached 100 mm^3 subcutaneously, five groups were administered via the tail vein: saline, nanosomes without drugs, nanosomes loaded with sialidase inhibitors, nanosomes loaded with irinotecan, and nanosomes co-loaded with sialidase inhibitors and irinotecan. As a result, tumor growth was inhibited in the two groups containing neuraminidase inhibitor-loaded nanosomes and irinotecan-loaded nanosomes. Furthermore, no significant weight loss was observed in the nanosome-administered groups, and no obvious systemic toxicity was demonstrated.

1-4. Reference

[1] B. Winchester, Lysosomal metabolism of glycoproteins. *Glycobiology* **2005**, 15, 1R-15R

[2] B. A. Schröder, C. Wrocklage, A. Hasilik, P. Saftig, The proteome of lysosomes. *Proteomics* **2010**, 10, 4053-4076

[3] Y. Mosesson, G. B. Mills, Y. Yarden, Derailed endocytosis: an emerging feature of cancer. *Nat. Rev. Cancer* **2008**, 8, 835–850

[4] J. L. Goldstein, Richard G. W. Anderson, M. S. Brown, Coated pits, coated vesicles, and receptor- mediated endocytosis. *Nature* **1979**, 21, 670-685

[5] R. J. Bernacki, M. J. Niedbala, W. Korytnyk, Glycosidases in cancer and invasion. *Cancer Metastasis Rev.* **1985**, 4, 81-102

[6] M. M. Fuster, J. D. Esko, The sweet and sour of cancer: glycans as novel therapeutic targets. *Nat. Rev. Cancer* **2005**, 5, 526-542

[7] H. Hinou, M. Kurogochi, H. Shimizu, and S.-I. Nishimura, Characterization of Vibrio cholerae Neuraminidase by a Novel Mechanism-Based Fluorescent Labeling Reagent. *Biochemistry* **2005**, 44, 11669-11675

[8] M. Kurogochi, S.-I. Nishimura, Y. C. Lee, Mechanism-based Fluorescent Labeling of β-Galactosidases. *J. Biol. Chem.* **2004**, 279, 44704–44712

[9] H. Kai, H. Hinou, S.-I. Nishimura, Aglycone-focused randomization of 2-difluoromethylphenyl-type sialoside suicide substrates for neuraminidases. *Bioorgan. Med. Chem.* **2012**, 20, 2739–2746

[10] C. E. Probst, P. Zrazhevskiy, V. Bagalkot, X. Gao, Quantum dots as a platform for nanoparticle drug delivery vehicle design. *Adv. Drug Delivery. Rev.* **2013**, 65, 703–718

[11] S. Wilhelm, A. J. Tavares, Q. Dai, S. Ohta, J. Audet, H. F. Dvorak, Warren C. W. Chan, Analysis of nanoparticle delivery to tumours. *Nat. Rev. Mater.* **2016**, 1, 1-12

[12] W. Poon, B. R. Kingston, B. Ouyang, W. Ngo, Warren C. W. Chan, A framework for designing delivery systems Wilson. *Nat. Nanotechnol.* **2020**, 15, 819–829

[13] T. Ohyanagi, N. Nagahori, K. Shimawaki, H. Hinou, T. Yamashita, A. Sasaki, T. Jin, T. Iwanaga, M. Kinjo, S.-I. Nishimura, Importance of Sialic Acid Residues Illuminated by Live Animal Imaging Using Phosphorylcholine Self-Assembled Monolayer-Coated Quantum Dots. *J. Am. Chem. Soc.* **2011**, 133, 12507–12517

[14] C. Kinnear, T. L. Moore, L. R. -Lorenzo, B. R. -Rutishauser, A. P. -Fink, Form Follows Function: Nanoparticle Shape and Its Implications for Nanomedicine. *Chem. Rev.* **2017**, 117, 11476－11521

[15] B. D. Chithrani, A. A. Ghazani, Warren C. W. Chan, Determining the Size and Shape Dependence of Gold Nanoparticle Uptake into Mammalian Cells. *Nano Lett.* **2006**, 6, 662-668

[16] M. Borkowska, M. Siek, D. V. Kolygina, Y. I. Sobolev, S. Lach, S. Kumar, Y. -K. Cho, K. K. -Grzybowska, B. A. Grzybowski, Targeted crystallization of mixed-charge nanoparticles in lysosomes induces selective death of cancer cells. *Nat. Nanotechnol.* **2020**, 15, 331–341

[17] A. E. Nel1, L. Mädler, D. Velegol , T. Xia1 , E. M. V. Hoek , P. Somasundaran, F. Klaessig , V. Castranova, M. Thompson, Understanding biophysicochemical interactions at the nano–bio interface. *Nat. Mater.* **2009**, 8, 543-557

[18] F. Alexis, E. Pridgen, L. K. Molnar, O. C. Farokhzad, Factors Affecting the Clearance and Biodistribution of Polymeric Nanoparticles. *Mol. Pharm.* **2008**, 5, 505–515

[19] S. D. Perrault, C. Walkey, T. Jennings, H. C. Fischer, Warren C. W. Chan, Mediating Tumor Targeting Efficiency of Nanoparticles Through Design. *Nano Lett.* **2009**, 9, 1909-1915

[20] R. Koide, S.-I. Nishimura, Antiadhesive Nanosomes Facilitate Targeting of the Lysosomal GlcNAc Salvage Pathway through Derailed Cancer Endocytosis. *Angew. Chem. Int. Ed.* 2019, 58, 14513-14518

[21] R. S. Tan, K. Naruchi, M. Amano, H. Hinou, S.-I. Nishimura, Rapid Endolysosomal

Escape and Controlled Intracellular Trafficking of Cell Surface Mimetic Quantum-Dots-Anchored Peptides and Glycopeptides. *ACS Chem. Biol.* **2015**, 10, 2073-2086

Chapter 2　Nanosomes targeting cancer lysosomal glycosidase

2-1. Introduction

Cancer remains one of the leading causes of death worldwide, and its complex biology poses significant challenges to the development of effective treatments. Among the molecules involved in tumorigenesis, human neuraminidase-1 (NEU1) has emerged as an important regulator of cell signaling on the surface of cancer cells. NEU1, a sialidase, has been shown to regulate receptor tyrosine kinases (RTKs) and Toll-like receptors (TLRs) by hydrolyzing terminal sialic acid residues bound to N-glycans in the extracellular domain[1,2,3]. This desialylation is essential for receptor activation, and it promotes processes such as dimerization, phosphorylation, and downstream signal transduction, thereby promoting cancer cell proliferation[4]. For example, N1, which forms a complex with matrix metalloproteinase-9 (MMP-9) and G protein-coupled receptors (GPCRs), has been demonstrated to be an important mediator in the activation of the epidermal growth factor receptor (EGFR). Pharmacological inhibition of NEU1 by oseltamivir phosphate (Tamiflu) has been shown to effectively attenuate EGFR phosphorylation, supporting the potential for NEU1-targeted therapy in cancer[2].

At the same time, lysosomal function is being recognized as a metabolic vulnerability in rapidly dividing and invasive cancer cells. The abnormal endocytosis and macropinocytosis pathways utilized by cancer cells enable the uptake of extracellular glycoproteins and their intracellular transport, supplying the essential monosaccharides and amino acids necessary for the biosynthesis of complex carbohydrates[5-7]. Lysosomal glycosidases (such as β-hexosaminidase and β-galactosidase) are overexpressed in various cancers and are promising molecular targets for anticancer drug therapy. Previous studies have demonstrated that the delivery of inhibitors (suicide substrates) based on a mechanism targeting lysosomal β-hexosaminidase using nanoparticles can cause irreversible enzyme inactivation, lysosomal membrane permeabilization, and subsequent apoptosis of cancer cells.[8,9,10]. This approach exploits the critical role of lysosomal β-hexosaminidase in the hexosamine biosynthetic pathway, which provides the essential sugar donor UDP-GlcNAc for cancer-associated glycoconjugates.

Interestingly, the dynamics of NEU1 localization further highlight its multifaceted role in cancer progression. The newly synthesized NEU1 is initially targeted to the endosomal/lysosomal compartment, but it can relocalize to the plasma membrane by forming a complex with cathepsin A. At the membrane, NEU1 is involved in receptor signaling cross-talk, amplifying its effects on tumorigenesis[1-3,11]. This dual distribution of NEU1 provides a unique opportunity for therapeutic intervention, as it is possible to target both the cell surface and the lysosomal compartment simultaneously.

Given the important role played by NEU1 and lysosomal glycosidases in cancer biology, our research aims to develop next-generation nanomedicines that exploit the vulnerability of these molecules. Specifically, we hypothesize that irreversible inactivation of NEU1 on the surface of cancer cells will promote the endocytosis and intracellular transport of nanoparticle-based sialidase inhibitors to the lysosome. These nanoparticle-based drugs are conjugated with an adhesion-inhibitory suicide substrate, acting as a "suicide bag"[10] to specifically induce cancer cell death while sparing normal cells. This study is the first to demonstrate the potential of NEU1-targeted nanoparticles as a versatile platform for drug delivery systems (DDS) that addresses a key challenge in targeting intracellular molecules via endocytosis through the cancer cell surface.

In Chapter 2, we have provided a new framework for the development of molecularly targeted cancer therapy by integrating the functional roles of NEU1 and lysosomal glycosidases into nanoparticle-based therapeutic strategies. The findings of this study not only deepen our understanding of cancer cell biology but also pave the way for innovative DDS approaches to combat cancer.

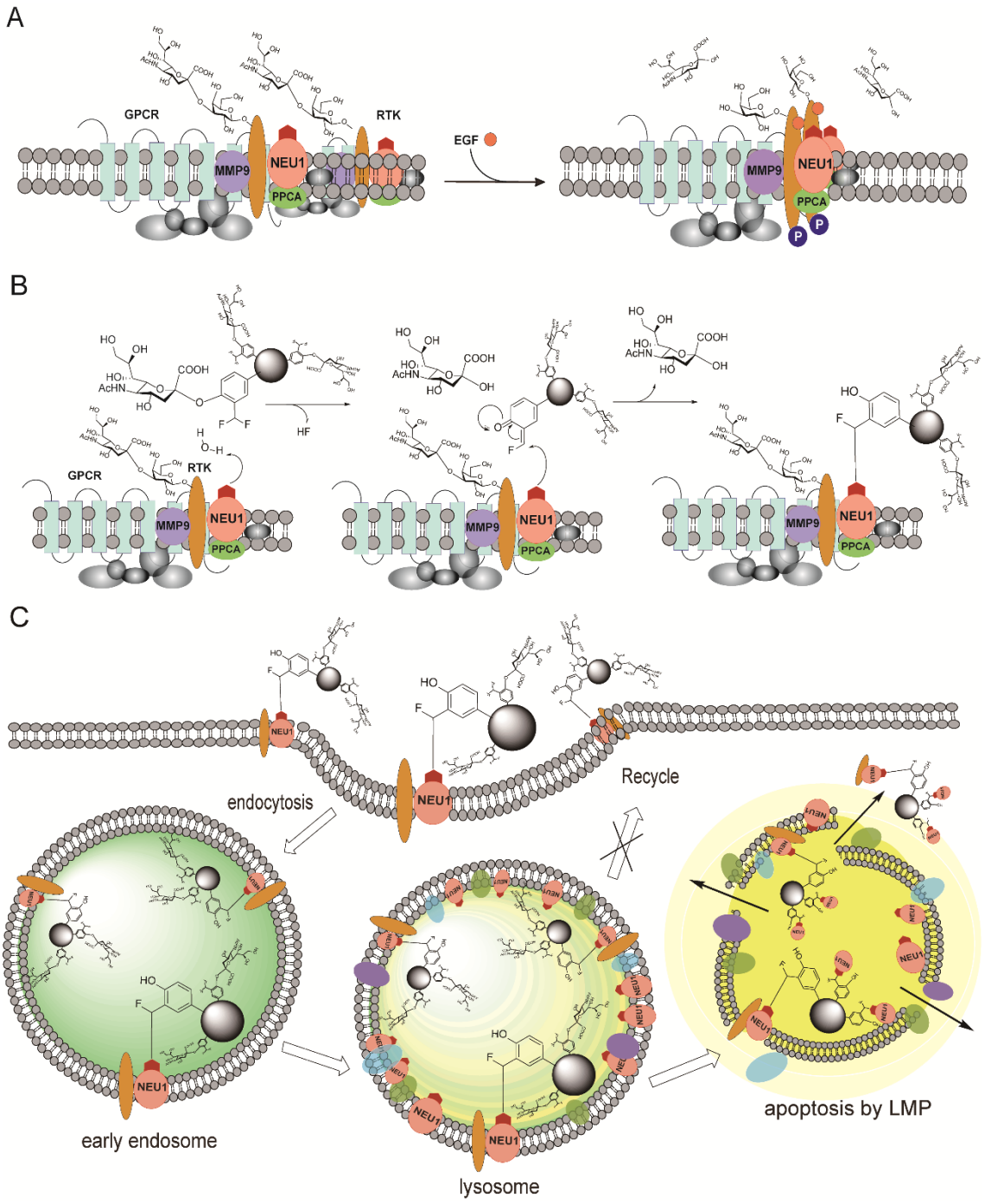

Figure 2-1. Human NEU1 sialidase plays crucial roles at the cancer cell-surface molecular platform during various stages of tumorigenesis. (A) NEU1 existing in a trimeric complex with MMP-9 and GPCR at cancer cell surface plays critical roles in ligand (EGF)-induced activation of RTKs upregulated in various stages of tumorigenesis. Prerequisite hydrolysis of the glycoside bond in the terminal Neu5Ac α 2→3Gal moiety of N-glycans is proposed to remove steric hindrance of ecto-domain of RTK (EGFR) to facilitate receptor dimerization and phosphorylation. (B) Mechanism-based irreversible inactiva-tion of cancer cell surface

NEU1 could be achieved by nanoparticle displaying multiple suicide substrates for sialidase. (C) Proposed endocytic mechanism of cancer cell membrane tethered NEU1 covalently anchored with nanoparticles, in which early endosomes might involve RTKs and other cargoes related to the NEU1-MMP-9-GPCR signaling platform. Then, internalized materials from plasma membrane are delivered to lysosomes (pH~5) and to be degraded or recycled in a context dependent manner[15]. A variety of lysosomal hydro-lases such as cathepsins and glycosidases colored by green, light blue, or purple are traveled from the trans-Golgi network to the lysosomal compartment. However, multiple sui-cide substrates on the nanomedicine may still have a suffi-cient ability to inactivate lysosomal sialidases irreversively to afford insoluble particles covalently harboring multiple sial-idases that disrupt the integrity of the lysosomal membranes, resulting in the LMP, a critical step for cathepsin-mediated cell death[16]. GPCR (G-protein-coupled receptor), MMP-9 (ma-trix metalloproteinase-9), RTK (receptor tyrosine kinase), PPCA (protective protein cathepsin A), and LMP (lysosomal membrane permeabilization). These schematic images are taken in part from the paper reported by Szewczuk et al.[2,3]

2-2. Results and Discussion

2-2-1. Nanomedicine targeting cancer cell surface NEU1

Because NEU1 plays an important role in both the signaling platform[1-3] on the surface of cancer cells and the endolysosomal compartment[14] within the cell, we evaluated the antitumor activity of nanostructures (NS)[15] immobilized with a mechanism-based NEU1 inhibitor (**NS-8103**) compared to other NS targeting major lysosomal glycosidases targeted NS, we evaluated the antitumor activity of the nano-structured material (NS) immobilized with the mechanism-based NEU1 inhibitor (**NS-8103**) compared to other major lysosomal glycosidases, such as α-mannosidase (**NS-8104**), β-glucuronidase (**NS-8105**), β-hexosaminidase (**NS-8101**)[9], and β-galactosidase (**NS-8102**)[9]. Since the removal of the non-reducing terminal Neu5Ac residue by NEU1 initiates the degradation of sugar chains by other lysosomal glycosidases, hydrolysis mediated by NEU1 is thought to be an important step in the metabolism of glycoproteins within the lysosome. Furthermore, it appears that β-glucuronidase and β-hexosaminidase are involved in the lysosomal degradation of hyaluronic acid and may function as an alternative pathway to hyaluronidase.

We have established a synthetic procedure for novel cargoes **103**, **104**, and **105**, which have a double functional group in the aglycone portion. The suicide substrates **101-105** are designed to generate an active intermediate for irreversible enzyme inactivation and can be coupled to NS by a nucleophilic addition reaction under mild conditions in combination with a ketone-terminated linker. These NSs are synthesized using a semiconductor single-crystal quantum dot (QD)-based platform and incorporate self-assembled monolayers (SAMs) consisting of AO-linkers and phosphorylcholine-based PC-linkers[9,15] to impart antifouling properties. The highly organized SAM structure prevents protein corona formation and enhances the specificity and stability of the NSs[9,16,17].

Fluorescence staining using anti-NEU1 antibodies and CellLight markers confirmed that, in contrast to the absence of NEU1 in normal human fibroblasts, membrane-bound NEU1 is overexpressed in HepG2 cells. **NS-8103** targets other lysosomal glycosidases compared to NS, which targets other lysosomal glycosidases, showed significantly higher anti-tumor activity against various cancer cell lines, including lung cancer A549 (IC50=9.57 nM), HepG2 (IC50=13.5 nM), and colorectal cancer HT-29 (IC50=11.1 nM). These cancer cells were completely eliminated by 25 nM **NS-8103**, highlighting the outstanding efficacy of **NS-8103** and confirming that NEU1 is a universal molecular target for anti-cancer therapy. In contrast, **NS-8101** and **NS-8102** had negligible effects on the proliferation of A549 and HT-29 cells,

while cisplatin required significantly higher concentrations (≥50 μM) and longer incubation periods to induce cell death.

Live cell imaging using a fluorescence microscope revealed that **NS-8103** is efficiently taken up by cancer cells within 4 hours of incubation. In particular, the red fluorescent signal increased significantly after 4 hours, suggesting that **NS-8103** may escape from lysosomes, but after 1 hour it was mainly co-localized with early endosomes. These findings highlight the potential for precise and effective intracellular drug delivery using NEU1-targeted nanomedicine and pave the way for the development of advanced therapeutic strategies.

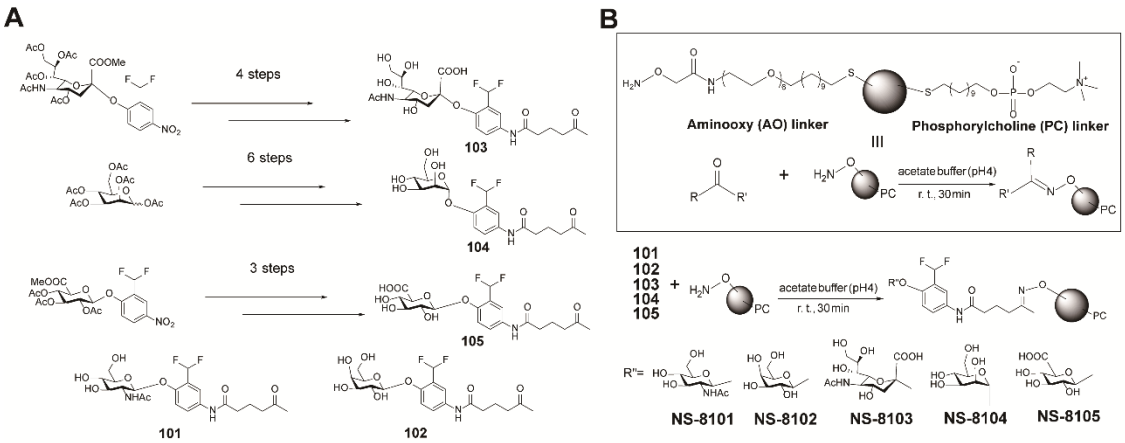
A
4 steps
6 steps
3 steps
103
104
105
101
102
B
Aminooxy (AO) linker
Phosphorylcholine (PC) linker
acetate buffer (pH4)
r. t., 30 min
NS-8101
NS-8102
NS-8103
NS-8104
NS-8105

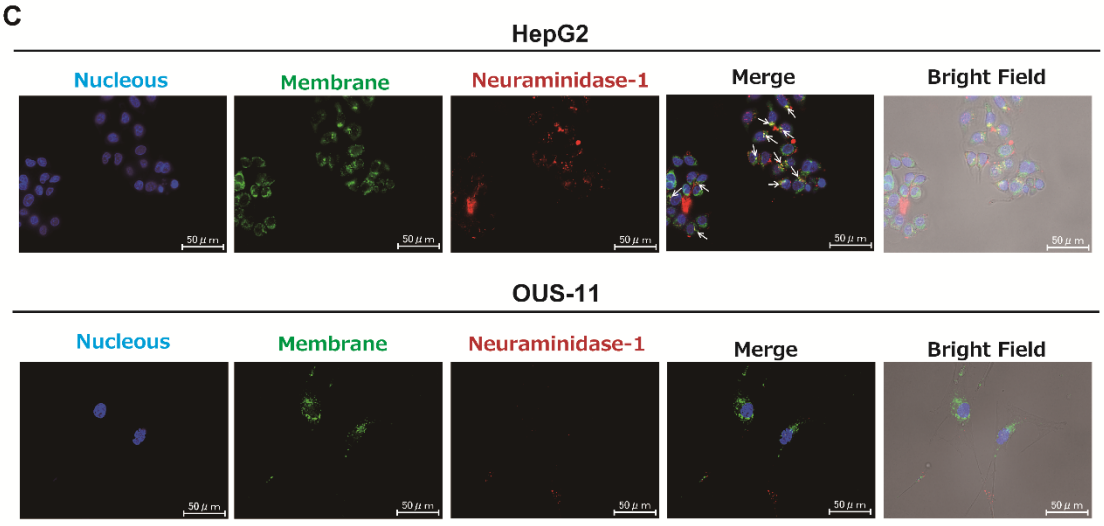
C
HepG2
Nucleous
Membrane
Neuraminidase-1
Merge
Bright Field
OUS-11
50 μm

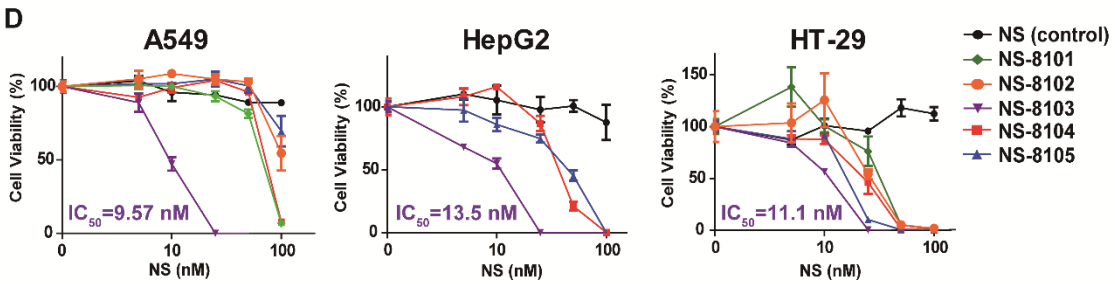
D
A549
HepG2
HT-29
Cell Viability (%)
NS (nM)
IC50=9.57 nM
IC50=13.5 nM
IC50=11.1 nM
NS (control)
NS-8101
NS-8102
NS-8103
NS-8104
NS-8105

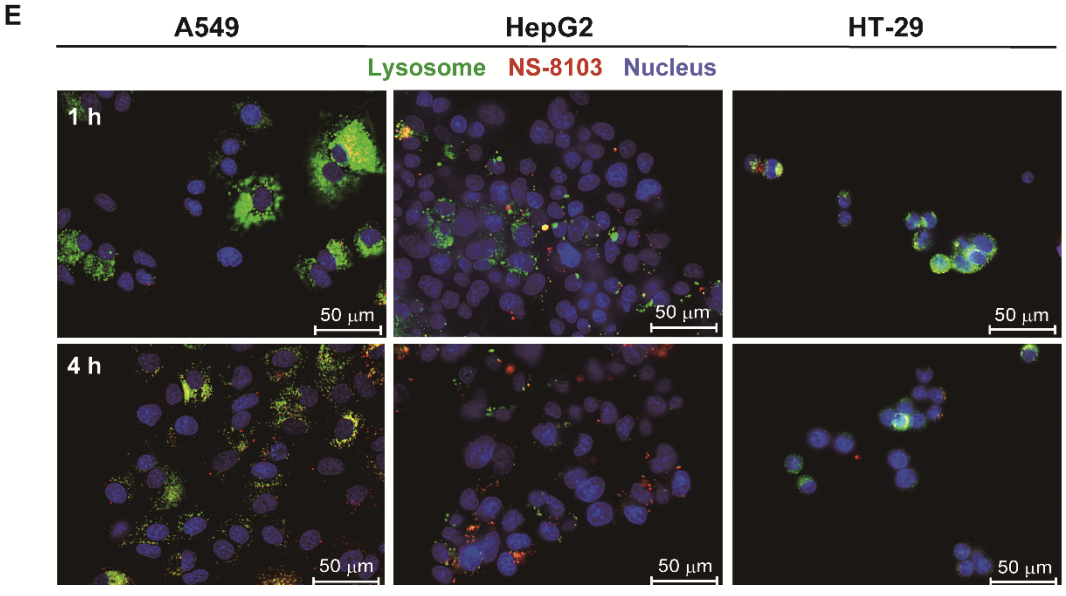
E
A549
HepG2
HT-29
Lysosome
NS-8103
Nucleus
1 h
4 h
50 μm

Figure 2-2. NEU1 sialidase is a promising and universal molecular target for anticancer nanomedicines. (A) Synthetic process of novel mechanism-based inhibitors of NEU1 sialidase **103**, α-mannosidase **104**, and β-glucuronidase 105, respectively. (B) A concept of surface loading of aldehyde/ketone auxiliary to NSs. **NS-8101**-**NS-8105** were prepared by treating AO/PC-NSs with the corresponding mechanism-based glycosidase inhibitors **101**-**105** according to the method described previously[9]. (C) Live cell NEU1 fluorescent staining of HepG2 and OUS-11 (normal control cell line) by anti-NEU1 antibody (F-8) Alexa Fluor® 546. Nuclei and cell membrane were stained with Hoechst 33342 (blue) and CellLight™ Plasma Membrane-GFP, BaeMam 2.0 (green), respectively. (D) Antitumor activity of NSs represented by loss of viability determined by the MTT assay of human cancer cells such as A549, HepG2, and HT-29 cells after 96 h coincubation with 1-100 nM NSs. (E) Intracellular distribution of **NS-8103** (red) after 1 and 4 h after co-culturing with A549, HepG2, and HT-29 cells. Scale bar: 50 μm. Nuclei and lysosomes were stained with Hoechst 33342 (blue) and LysoTracker Green DND-26 (green). Human NEU1 sialidase plays crucial roles at the cancer cell-surface molecular platform during various stages of tumorigenesis.

2-2-2. An irreversible inhibition is critical for endocytosis

To understand the mechanism of the enhanced anti-cancer activity of **NS-8103**, we investigated whether its endocytosis is specifically mediated by membrane-bound NEU1 sialidase. The uptake of 10 nM **NS-8103** by HepG2 cells uptake of 10 nM **NS-8103** was significantly reduced when the cells were incubated with 1 mM DANA (2,3-dideoxy-2-deoxy-N-acetylneuraminic acid) for 4 or 8 hours, compared to incubation without DANA (Figure. 2-3A). Furthermore, cell suspension assays revealed that the addition of DANA at concentrations of 1.0, 2.5, and 5.0 mM significantly inhibited the sialidase activity of HepG2 cells, especially the sialidase activity of NEU1 on the cell surface.

Previous studies have demonstrated that dansylated derivatives structurally like **103** functions as competitive and irreversible inhibitors of Vibrio cholerae neuraminidase (VCNA).[9] Kinetic analysis by fluorescence correlation spectroscopy (FCS) showed that **NS-8103** aggregates in the presence of VCNA. This indicates that multiple suicide substrates on **NS-8103** irreversibly inactivate lysosomal NEU1 sialidase. This inactivation leads to the formation of large insoluble nanoparticles covered with a “NEU corona”.

We hypothesized that the initial complex formation of NEU1 and **NS-8103** at the cell surface, mediated by the irreversible inhibition mechanism, is important for the efficient and multiple inactivation of lysosomal NEU1 sialidase, leading to lysosomal membrane permeabilization (LMP), as proposed in Figure 2-1B. Excessive addition of DANA, a compound with a

significant inhibitory effect on human NEU1 (IC50 = 49 ± 8 μM)[18], is thought to occupy the active center pocket of NEU1 and prevent the nucleophilic attack on the suicide substrate exposed on **NS-8103**. This competitive inhibition effectively blocks the endocytosis of **NS-8103** mediated by NEU1.

These findings provide compelling evidence that irreversible and mechanism-based inactivation of cell surface-bound NEU1 is essential for the accelerated endocytic uptake of **NS-8103**. This process leads to multiple inactivation of lysosomal sialidases, resulting in LMP and cancer cell death. However, further research is needed to determine whether the observed cell death is due to apoptosis, necrosis, or a combination of both. In addition, further investigation is needed into the exact mechanism of LMP and lysosomal damage.

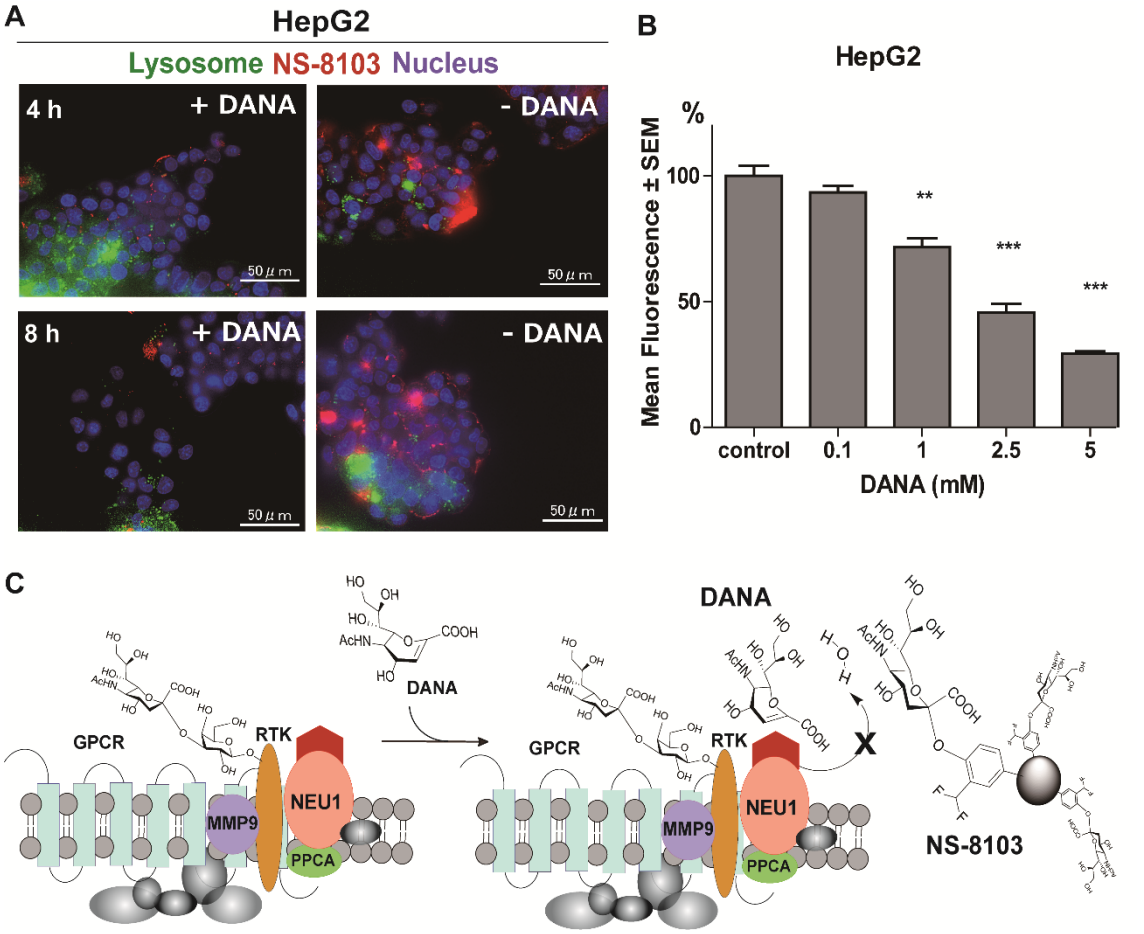

Figure 2-3. Irreversible mechanism-based inactivation of cell surface NEU1 is critical for accelerated endocytosis, intracellular traffic, and ultimately LMP. (A) Intracellular distribution of **NS-8103** (red) at 4 and 8 h after co-culturing with HepG2 cells in the presence (+DANA) and absence (-DANA) of 1 mM DANA. Scale bar: 50 μm. Nuclei and lysosomes were stained with Hoechst 33342 (blue) and LysoTracker Green DND-26 (green). (B) Cell suspension sialidase assay using 0.5 mM of 2′-(4-methylumbbelliferyl)- α -D-*N*-

acetylneuraminic acid (4-MUNANA) in the presence of DANA (0, 0.1, 1.0, 2.5, and 5.0) demonstrates that DANA inhibits significantly cancer cell NEU1 activity (**p=0.0008, ***p<0.0001, n=5). (C) Schematic depicting that excess DANA impedes interaction between **NS-8103** and membrane-tethered NEU1 by occupying a binding pocket for the sialic acid residue in the active center of NEU1. This schematic image is taken in part from the paper reported by Szewczuk et al.[2]

2-3. Conclusion

This study provides groundbreaking evidence that human neuraminidase-1 (NEU1), which is widely distributed on the surface of cancer cells, is a promising molecular target for innovative anticancer nanomedicines. In addition to regulating important aspects of tumor formation, NEU1 also facilitates the intracellular delivery of therapeutics via the NEU1-mediated endocytosis pathway. In this study, targeting NEU1 will introduce anti-adhesive nanomedicines such as **NS-8103**, effectively inactivating NEU1 on the surface of cancer cells, internalizing it into the cytoplasm, localizing it in the endolysosomal compartment, disrupting the lysosomal membrane, and ultimately inducing cancer cell death.

Furthermore, our results highlight the importance of the glycocalyx, especially the expression of sialic acid-terminated sugar chains, in determining the circulation and biodistribution of nano-drugs in vivo. Anti-adhesive nanocarriers equipped with multiple irreversible NEU1 inhibitors, such as **103**, provide an ideal platform for targeted drug delivery to cancer tissues and organs. These nanomedicines provide a robust and versatile framework for the intracellular delivery of various small-molecule anticancer drugs modified with appropriate auxiliary groups.

The broader impact of this research goes beyond the current study. The concept of targeting NEU1-mediated endocytosis can be applied to a variety of nanoparticle forms, including gold nanoparticles, dendrimers, exosome-like liposomes, and a new class of non-toxic quantum dots (QDs) that do not contain cadmium. Preliminary data using fluorescent QD cores highlight the potential to expand this strategy to other nanocarrier systems.

In conclusion, this study establishes nanomedicine targeting NEU1 as a breakthrough in cancer therapy. By integrating molecular-level insights into the role of NEU1 in cancer biology with innovative nanotechnology, this approach paves the way for the development of next-generation drug delivery systems. Future research will focus on elucidating the precise molecular mechanisms and further refining this platform for clinical application, thereby advancing the fight against cancer.

2-4. Experimental Section

General methods and materials

All solvents and reagents were purchased from Aldrich Chemical Co. (Milwaukee, WI), Tokyo Chemical Industry Co. Inc. (Tokyo, Japan), Wako Pure Chemical Industries Co. Inc. (Tokyo, Japan), Funakoshi Co., Inc. (Japan, Tokyo), Thermo Fisher Scientific K. K. Co. Inc. (Tokyo, Japan), Kanto Chemical Co. Inc. (Tokyo, Japan) and used without further purification. TOPO-coated QDs (655 nm) were purchased from Thermo Fisher Scientific K. K. Co. Inc. (Tokyo, Japan). Microcon YM50 was purchased from Millipore Co. Inc (Tokyo, Japan). 11-Mercaptoundecylphosphorylcholine (PC linker) was synthesized according to the procedure reported previously.[19], 11,11'-dithio bis [undec-11yl 12-(aminooxyacetyl) amino hexa (ethyleneglycol)] (AO linker) was synthesized by the method reported previously.[20] Proton and carbon NMR were recorded at 25 °C on BRUKER AVANCE 600 MHz (1H: 600 MHz, 13C: 150 MHz) Bruker AVANCE (Bruker Biospin Co., Germany). Chemical shifts are indicated by ppm. Electro-spray ionization mass (ESI-MS) spectra were obtained with a JMS-T100LP mass spectrometer (JEOL Co. Inc., Tokyo, Japan). Matrix Assisted Laser Desorption Ionization time-of-flight mass (MALDI-TOFMS) spectra were obtained with an Ultraflex III TOF mass spectrometer (Bruker Daltonik GmbsH Co. Inc, Germany) equipped with a reflector and controlled by the Flexcontrol 3.0 software package. Reactions were monitored by thin layer.

Statistical analysis was carried out in GraphPad Prism v8.0.2. Quantitative data are presented as mean ± s.d., if not stated otherwise. Differences were compared using the student's t-test. P values were 0.05 or less, the differences were considered statistically significant.

Synthesis

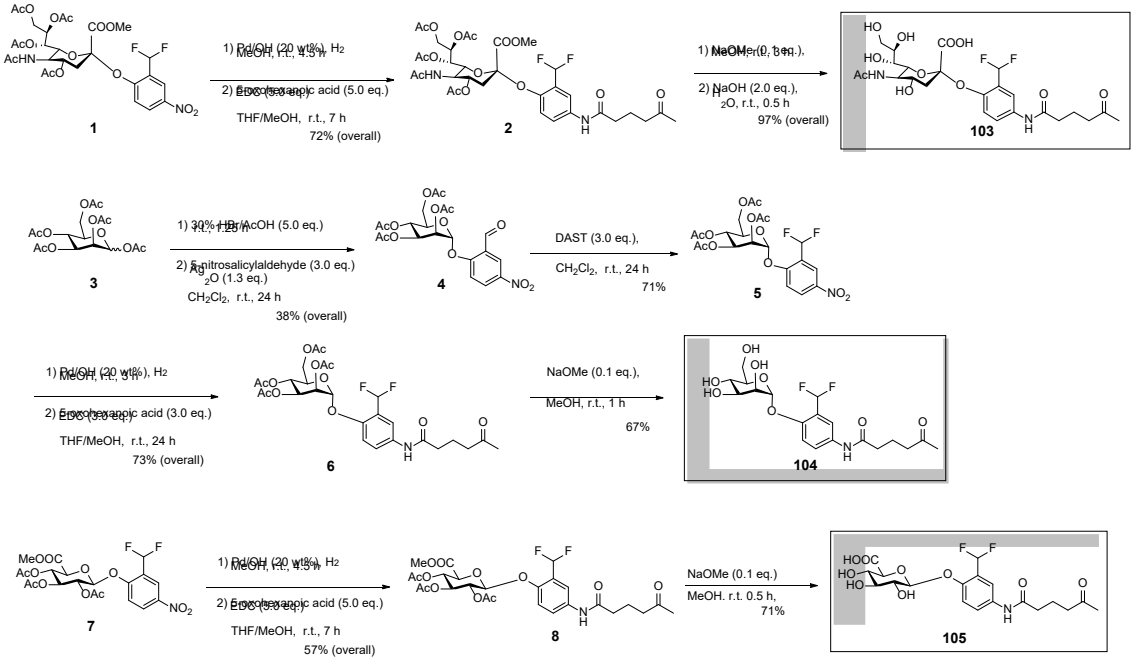

Scheme S2

Methyl [4,7,8,9-tetra-O-acetyl-5-acetamide-2-{2-difluoromethyl-4-N-(5-oxo-hexane-1-ly)phenyl}-3,5-dideoxy-D-glycero-α-D-galacto-2-nonulopyranosid]onate (**2**). To a solution of compound **1**[26] (300 mg, 0.453 mmol) in MeOH (20 mL) was added Pd/OH (20 wt.%, 60 mg) and stirred at room temperature under H2 gas for 4.5 h. The mixture was filtered by celite and then evaporated under reduced pressure and the residue was dissolved in THF (20 mL) and anhydrous MeOH (5 mL). To a solution was added 5-oxohexanoic acid (162 μL, 1.36 mmol) and 1-ethyl-3-(3-dimethylaminopropyl)-carbodiimide (EDC, 521 mg, 2.72 mmol) and the mixture was stirred at room temperature under argon gas for 1 day. The reaction mixture was extracted with chloroform and the organic layer was washed with 1N HCl aq., saturated $NaHCO_3$ aq., and brine. Then, the solvents were dried with $MgSO_4$ and evaporated under reduced pressure. Silica-gel chromatography (hexane/acetone, 4:3) of the crude product gave pure compound **2** in 72% yield (243 mg, 0.340 mmol). HR-ESI-MS: $C_{33}H_{42}F_2N_2O_{15}Na$ [M+Na]+ calcd. 767.24455, found 767.24456 (Figure S2-2a).

1H NMR (600 MHz, CDCl3) δ ppm 7.83 (s, 1 H), 7.53 (d, 1 H, J=8.7 Hz), 7.47 (s, 1 H), 7.27 (d, 1 H, J=9.1 Hz), 6.90 (t, 1 H), 5.38 (m, 2 H), 4.98 (m, 1 H), 4.45 (d, 1 H, J=10.6 Hz), 4.30 (m, 1 H), 4.16 (m, 1 H), 4.11 (m, 1 H), 3.67 (s, 3 H), 2.75 (dd, 1 H, J=13.0, 4.7 Hz), 2.62 (t, 2 H, J=6.8 Hz), 2.41 (t, 2 H, J=7.2 Hz), 2.25 (t, 1 H, J=12.7 Hz), 2.20 (s, 3 H), 2.17 (s, 6 H), 2.08 (s, 3 H), 2.07 (s, 3 H), 2.02 (m, 2 H), 1.94 (s, 3 H). 13C NMR (150 MHz, CDCl3) δ ppm 123.04, 120.10, 117.40, 110.29, 72.79, 68.63, 68.14, 66.67, 61.52, 53.19,

49.27, 41.92, 37.75, 36.03, 30.15, 23.04, 20.34, and 19.12 (Figure S2-2b).

5-Acetamide-2-{2-difluoromethyl-4-N-(5-oxo-hexane-1-ly)phenyl}-3,5-dideoxy-D-glycero-α-D-galacto-2-nonulopyranosonic acid (**103**). To a solution of compound 2 (100 mg, 0.134 mmol) in MeOH (10 mL) was treated with sodium methoxide (5.0 mg, 0.093 mmol) at room temperate for 3.5 h and the solution was evaporated under reduced pressure. The residue was dissolved in 1N NaOH aq. (10 mL) and the mixture was stirred at room temperature for 3.5 h. After confirming the completion of the reaction by using ESI-MS, the reaction mixture was neutralized to pH 7 with DOWEX-50. The solution was filtered and lyophilized to afford pure compound **103** as a white powder (73 mg, 0.130 mmol, 97%). HR-ESI-MS: $C_{24}H_{32}F_2N_2O_{11}Na$ [M+Na]+ calcd. 585.18664, found 585.18695 (Figure S2-3a).
1H NMR (600 MHz, D2O) δ ppm 7.57 (s, 1 H), 7.34 (d, 1 H, J=8.8 Hz), 7.26 (d, 1 H, J=9.1 Hz), 7.00 (t, 1 H), 3.82 (m, 1 H), 3.75 (m, 3 H), 3.66 (m, 1 H), 3.52 (m, 2 H), 2.81 (dd, 1 H, J=12.5, 4.5 Hz), 2.55 (t, 2 H, J=7.2 Hz), 2.31 (t, 2 H, J=7.3 Hz), 2.10 (s, 3 H), 1.94 (s, 3 H), 1.86 (m, 1 H), 1.81 (m, 2 H). 13C NMR (150 MHz, D2O) δ ppm 125.00, 121.59, 118.86, 111.82, 73.41, 71.36, 67.96, 62.27, 51.14, 41.59, 40.00, 35.00, 29.09, 21.82, and 18.86 (Figure S2-3b).

1-(2-Formyl-4-nitrophenyl)-2,3,4,6-tetra-O-acetyl-α-D-mannopyranoside (**4**). D-Mannose peracetate **3** (1.12 g, 2.87 mmol) was dissolved in hydrogen bromide (5.6 mL) and the solution was stirred in room temperature for 1.25 h. The reaction mixture was extracted with ethyl acetate and the organic layer was shaken with saturated $NaHCO_3$ aq. and brine, and dried with $MgSO_4$. The filtrate was evaporated under reduced pressure to afford crude per-O-acetyl mannosylbromide. To a solution of this intermediate in anhydrous dichloromethane (15 mL) was added 5-nitrosalicylaldehyde (1.43 g, 8.61 mmol), silver (I) oxide (0.86 g, 3.73 mmol), and Molecular Sieves (4A 1/16) and the mixture was stirred for 1 day. The reaction mixture was extracted with chloroform and the organic layer was washed with water, saturated $NaHCO_3$ aq., and brine. The solution was dried with $MgSO_4$ and evaporated under reduced pressure. Silica-gel chromatography (hexane/EtOAc, 3:1) of the crude product gave pure compound **4** (540 mg, 1.09 mmol, 38% overall yield). HR-ESI-MS: $C_{21}H_{23}NO_{13}Na$ [M+Na]+ calc. 520.10616, found 520.10620 (Figure S2-4a).
1H NMR (600 MHz, CDCl3) δ ppm 10.52 (s, 1 H), 8.79 (d, 1 H, J=3.0 Hz), 8.46 (dd, J=9.3, 2.8 Hz), 7.47 (d, 1 H, J=9.1 Hz), 5.81 (d, 1 H, J=1.5 Hz), 5.56 (dd, 1 H, J=3.4, 1.9 Hz), 5.53 (m, 1 H), 5.47 (m, 1 H), 4.32 (dd, 1 H, J=12.5, 5.3 Hz), 4.13 (dd, 1 H, J=12.1, 2.3 Hz), 4.07 (m, 1 H), 2.26 (s, 3 H), 2.10 (s, 3 H), 2.09 (s, 3 H), 2.07 (s, 3 H). 13C NMR (150 MHz, CDCl3) δ ppm 129.77, 124.55, 115.68, 95.91, 70.46, 68.18, 64.55, 61.59, and 20.68 (Figure

S2-4b).

1-(2-Difruoromethyl-4-nitrophenyl)-2,3,4,6-tetra-O-acetyl-α-D-mannopyranoside (**5**). To a solution of compound **4** (540 mg, 1.09 mmol) in anhydrous dichloromethane (10 mL) was added N,N-diethylaminosulfur trifluoride (DAST, 432 µL, 3.27 mmol) and the mixture was stirred at room temperature under argon gas for 1 day. The reaction was quenched by the addition of MeOH, and the reaction mixture was extracted with chloroform. The organic layer was washed with water, saturated $NaHCO_3$ aq., and brine. Then, the solution was dried with $MgSO_4$, filtered with celite, and evaporated under reduced pressure. Silica-gel chromatography (hexane/EtOAc, 4:1) of the crude product afforded pure compound 5 (400 mg, 0.770 mmol, 38%). HR-ESI-MS: $C_{21}H_{23}F_2NO_{12}Na$ [M+Na]+ calcd 542.10805, found 540.10806 (Figure S2-5a).
1H NMR (600 MHz, $CDCl_3$) δ ppm 8.54 (s, 1 H), 8.38 (d, 1 H, J=9.1 Hz), 7.38 (d, 1 H, J=9.1 Hz), 6.99 (t, 1 H), 5.75 (d, 1 H, J=1.9 Hz), 5.52 (dd, 1 H, J=3.2, 2.1 Hz), 5.48 (m, 1 H), 5.44 (m, 1H), 4.30 (dd, 1 H, J=12.5, 5.7 Hz), 4.09 (dd, 1 H, J=12.5, 2.3 Hz), 3.99 (ddd, 1 H, J=9.7, 5.4, and 2.3 Hz), 2.25 (s, 3 H), 2.10 (s, 3 H), 2.08 (s, 3 H), 2.06 (s, 3 H). 13C NMR (150 MHz, $CDCl_3$) δ ppm 127.61, 123.06, 114.55, 109.51, 95.46, 70.23, 68.18, 65.00, 60.68, and 20.46 (Figure S2-5b).

1-{2-Difruoromethyl-4-N-(5-oxo-hexane-1-ly)phenyl}-2,3,4,6-tetra-O-acetyl-α-D-mannopyranoside (**6**). To a solution compound **5** (400 mg, 0.770 mmol) in MeOH (20 mL) was added Pd/OH (20 wt.%, 80 mg) and the mixture was stirred at room temperature under H_2 gas for 3 h. The mixture was filtered with celite and then the solution was evaporated under reduced pressure to give 4-aminophenyl mannopyranoside intermediate. This intermediate was directly dissolved in THF (20 mL) and anhydrous MeOH (5 mL). To this solution was added 5-oxohexanoic acid (276 µl, 2.31 mmol) and 1-ethyl-3-(3-dimethylaminopropyl)-carbodiimide (EDC, 886 mg, 4.62 mmol). The reaction mixture was stirred at room temperature under argon gas for 1 day. The reaction mixture was extracted with chloroform. The organic layer was washed with 1N HCl aq., saturated $NaHCO_3$ aq., and brine, respectively. The solution was dried with $MgSO_4$, filtered with celite, and evaporated under reduced pressure. Silica-gel chromatography (hexane/EtOAc, 2:1) of the crude product gave pure compound 6 (330 mg, 0.563 mmol, 73%). HR-ESI-MS: $C_{27}H_{33}F_2NO_{12}Na$ [M+Na]+ calcd. 624.18630, found 624.18620 (Figure S2-6a).
1H NMR (600 MHz, CDCl3) δ ppm 7.76 (d, 1 H, J=8.9 Hz), 7.62 (s, 1 H), 7.56 (s, 1 H), 7.19 (d, 1 H, J=9.1 Hz), 6.93 (t, 1 H), 5.55 (d, 1 H, J=1.5 Hz), 5.48 (m, 2 H), 5.41 (m, 1 H), 4.31 (dd, 1 H, J=12.5, 5.7 Hz), 4.09 (m, 2 H), 2.62 (t, 2 H, J=6.8 Hz), 2.41 (t, 2 H, J=7.2 Hz),

2.22 (s, 3 H), 2.19 (s, 3 H), 2.09 (s, 6 H), 2.06 (s, 3 H), 2.01 (m, 2 H, J=7.0 Hz). 13C NMR (150 MHz, CDCl3) δ ppm 123.31, 117.93, 115.45, 112.82, 95.91, 69.49, 68.67, 65.41, 61.92, 42.33, 36.12, 30.18, 20.75, and 19.42 (Figure S2-6b).

1-{2-Difluoromethyl-4-N-(5-oxo-hexane-1-ly)phenyl}-α-D-mannopyranoside (**104**). To a solution of compound **6** (330 mg, 0.560 mmol) in MeOH (50 mL) was treated with sodium methoxide (10.0 mg, 0.185 mmol) at room temperature for 40 min. After the reaction, sodium methoxide was neutralized by DOWEX-50. Then, the solution was filtered and lyophilized to afford pure compound 104 as a white powder (162 mg, 0.374 mmol, 67%). HR-ESI-MS: $C_{19}H_{25}F_2NO_8Na$ [M+Na]+ calcd. 456.14404, found 456.14401 (Figure S2-7a).
1H NMR (600 MHz, D2O) δ ppm 7.53 (s, 1 H), 7.38 (d, 1 H, J=8.8 Hz), 7.23 (d, 1 H, J=9.1 Hz), 6.94 (t, 1 H), 5.59 (d, 1 H, J=1.5 Hz), 4.10 (dd, 1 H, J=3.4, 1.9 Hz), 3.93 (dd, 1 H, J=9.7, 3.5 Hz), 3.69 (m, 1 H), 3.63 (m, 2 H), 3.54 (m, 1 H), 2.56 (t, 2 H, J=7.2 Hz), 2.32 (t, 2 H, J=7.3 Hz), 2.10 (s, 3 H), 1.82 (m, 2 H). 13C NMR (150 MHz, D2O) δ ppm 125.68, 120.23, 115.46, 111.59, 97.27, 73.41, 70.00, 69.09, 66.36, 60.23, 41.82, 35.23, 29.09, and 19.09 (Figure S2-7b).

Methyl 1-{2-difluoromethyl-4-N-(5-oxo-hexane-1-ly)phenyl}-2,3,4-tri-O-acetyl-β-D-glucopyronuronate (**8**). To a solution of compound **7**[22] (530 mg, 1.05 mmol) in MeOH (20 mL) was added Pd/OH (20 wt.%, 106 mg) and the mixture was stirred at room temperature under H2 gas for 2.5 h. The reaction mixture was filtered with celite and evaporated under reduced pressure to give 4-aminophenyl glucopyronuronate intermediate. This intermediate was dissolved in THF (20 mL) and anhydrous MeOH (5 mL). To this solution was added 5-oxohexanoic acid (376 µl, 3.15 mmol) and 1-ethyl-3-(3-dimethylaminopropyl)-carbodiimide (EDC, 1.21 g, 6.30 mmol) and the mixture was stirred at room temperature under argon gas for 1 day. The reaction mixture was extracted with chloroform and the organic layer was washed with 1N HCl aq., saturated $NaHCO_3$ aq., and brine, respectively. The solution was dried with $MgSO_4$, filtered, and evaporated under reduced pressure to afford crude compound 8 (350 mg, 0.596 mmol, overall, 57%). Crude compound 8 was employed directly for the preparation of compound 105 without further purification.

1-{2-Difluoromethyl-4-N-(5-oxo-hexane-1-ly)phenyl}-β-D-glucopyronuronate (**105**). To a solution of compound **8** (350 mg, 0.596 mmol) in MeOH (50 mL) was treated with sodium methoxide (10.0 mg, 0.185 mmol) at room temperate for 3 h and the solution was evaporated under reduced pressure. To a solution of the residue dissolved in MilliQ (25 mL) was added sodium hydroxide (1 g, 0.0250 mmol) and the solution was stirred at room temperature for

0.5 h. After confirming the completion of the deprotection by using ESI-MS, the reaction mixture was neutralized to pH 7 with acetic acid. The solution was lyophilized to afford pure compound 105 as a white powder (189 mg, 0.423 mmol, 71%). HR-ESI-MS: $C_{19}H_{22}F_2NO_9Na$ [M]− calcd. 446.12681, found 446.12765 (Figure S2-8a).
1H NMR (600 MHz, D2O) δ ppm 7.57 (m, 1 H), 7.38 (m, 1 H), 7.19 (m, 1 H), 7.05 (t, 1 H), 5.02 (m, 1 H), 3.78 (m, 1 H), 3.50 (m, 3 H), 2.56 (m, 2 H), 2.32 (m, 2 H), 2.10 (s, 3 H), and 1.82 (m, 2 H). 13C NMR (150 MHz, D2O) δ ppm 125.91, 120.23, 116.36, 100.23, 76.14, 75.23, 72.73, 71.59, 41.59, 34.77, 28.86, and 18.86 (Figure S2-8b).

General protocol for preparation of nanosomes

CdSeS/ZnS quantum dots (QDs) with a fluorescence peak wavelength of 655 nm (Thermo Fisher Scientific K.K., Tokyo) were coated with tri-n-octylphosphine (TOPO) and dissolved in decane. TOPO-QDs (50 µL, 1 µM/decane) were added MeOH (50 µL) and i-PrOH (100 µL), then centrifuged at 5 min, 15000 rcf. to precipitate TOPO-QDs. The pellet-shaped TOPO-QDs were dissolved in n-hexane (100 µL). QDs were coated by using phosphocholine (PC) linker and aminooxy (AO) linker according to the method described in our previous reports.[9,15,23] The lyophilized PC linker was dissolved in MeOH to a final concentration of 100 mM and the lyophilized AO linker was also dissolved in water to a final concentration of 10 mM. The solution of PC linker (4 or 8 µL, 100 mM/MeOH) were added AO linker (10 µL, 10 mM/Milli Q), NaBH4 (1 µL, 12 wt%/14 N NaOH) and water (50 µL) and then added to QDs solution in a 2 x 10^5 (linker/QDs) ratio. The hexane/water two-layer solution was mixed in room temperature for 30 min. The n-hexane layer containing TOPO was removed and excess TOPO was washed by hexane. Excess linker was removed by washing 3 times with Milli Q through an Amicon Ultra-0.5 centrifugal Filter Unit with Ultracel-50 membrane (MWCO of 50kDa, Millipore UFC5050).

The conjugation of surface AO linker and aldehyde/ketone auxiliary were performed by oxime formation reaction in acid condition.[9,15,23] The AO/PC mixed SAM coated QDs (50 µL, 1 µM/Milli Q) were added compounds **3** and **103** (AO/PC=1/4) and sodium acetate buffer (200 µL, 100 mM, pH4.0). Then, intensely vortexed for 30 min at room temperature. Excess compounds were removed by washing four times with Milli Q through an Amicon Ultra-0.5 centrifugal Filter Unit with Ultracel-50 membrane (MWCO of 50 kDa, Millipore UFC5050).

Characterization of nanosomes

Hydrodynamic diameter based on Dynamic Light Scattering (DLS) and Zeta potential were determined with Zetasizer Nano ZS or NANOSIGHT LM10V TF (Malvern Panalytical, UK).

Ligand exchange and oxime formation reaction on the nanosomes was confirmed directly by MALDI-TOFMS analysis (Ultraflex Ⅲ TOF mass spectrometer, Bruker Daltonik GmbsH Co. Inc, Germany) in the presence of DHB (1 μL, 10 mg/mL).

Cell culture

Human hepatocellular carcinoma HepG2 (RIKEN cell bank, Sait ama, Japan), human lung cancer cells A549 (Health Science Research Resource Bank, Osaka, Japan), and human colon cancer cells HT-29 (American Type Culture Collection, Manassas, VA) were maintained in D-MEM High-glucose (Wako, Osaka, Japan), supplemented with 10% fetal bovine serum (FBS, Thermo Fisher Scientific, USA), and cultured in a humidified incubator at 37 ℃ with % CO_2. OUS-11 cells (Health Science Research Bank), normal human cell line from lung cancer patient, were grown in Eagle's Minimum Essential Medium (EMEM, Wako, Osaka, Japan) supplemented with 10% fetal bovine serum (FBS, Thermo Fisher Scientific, USA) at 37 ℃ with 5% CO_2.

Live cell imaging

Cells were suspended in medium supplemented with 10% FBS and plated in the wells of 8-well plate (Thermo Fisher Scientific, USA) at a seeding density of 5 x 104 cells/well. Cells were allowed to adhere overnight at 37 ℃ in a humidified incubator with 5 % CO_2 and the cell membrane was stained with CellLightTM Plasma Membrane-GFP, BacMam 2.0 (Thermo Fisher Scientific, USA) (2 μL) according to the recommended protocol. Cells were washed with Opti-MEM (gibco) three times and the nuclei were stained with Hoechst 33342 (2 μL, 1 ng/μL/Opti-MEM) and NEU1 was stained with NEU1 Antibody (F-8) Alexa Fluor®546 (Santa Cruz Biotechnology, Inc.) (1 μL) incubated at 37 ℃ in a humidified incubator with 5% CO_2 for 15 min. Stained cells were imaged an all-in-one fluorescence microscope BIOREV BZ-9000 series generation II (Keyence, Osaka, Japan) which was equipped with a 60×lens. Imaging pictures were analyzed by BZ-II Analyzer software (Keyence, Osaka, Japan).

Cells were suspended in medium supplemented with 10% FBS and seeded into 8-well cover glass (Thermo Fisher Scientific) at a seeding density of 5 x 104 cells/well. Cells were allowed to attach overnight in an incubator at 5 % CO_2 and 37 ℃. A stock solution of nanosomes was diluted with autoclaved MillQ and added to the existing medium; QD-derived nanosomes were added to a final concentration of 10 nM and co-cultured with the cells. At the indicated time points, cells were washed three times with Opti-MEM (Gibco) to remove nanosomes, stained with the lysosomal marker LysoTracker Green DND-26 (200 μL, 5 nM/Opti-MEM),

and incubated in an incubator at 37 ℃, 5 % CO_2 for 30 minutes. The nuclei were then stained with Hoechst 33342 (2 μL, 1 ng/μL/Opti-MEM) and incubated in an incubator at 37 ℃, 5 % CO_2 for 15 min.[9,23] Stained cells were photographed using a BIOREV BZ-9000 series 2nd generation all-in-one fluorescence microscope (Keyence, Osaka, Japan) equipped with a 60× objective. The captured images were analyzed using BZ-II Analyzer software (Keyence, Osaka, Japan).

Cell suspension sialidase assay[24]

HepG2 cells were suspended in sterile 1× phosphate buffered saline (PBS) in black 96-well plates at a density of 30,000 cells/well. As a control, 0.5 mM 4-MU-NANA (2-α-(4-Methylumbelliferyl)-N-acetylneuraminic acid, Tokyo Chemical Industry Co., Ltd.) was added alone or with the indicated concentration of the sialidase inhibitor 2,3-dehydro-2-deoxy-N-acetylneuraminic acid (DANA). Fluorescence intensity readings were taken immediately using SpectraMax M5 spectrophotometer (Molecular Devices Co., Sunnyvale Co., USA) at an emission of 450 nm following excitation at 365 nm. In Figure 2-3, Error bars represent ± SEM from three separate experiments performed in triplicates (n=5). Significance is represented in comparison to the cells without DANA added as a control by one-way ANOVA using the uncorrected Fisher's LSD multiple comparisons test with 95% confidence with indicated asterisks for statistical significance, **p = 0.0008, ***p < 0.0001, n = 5.

Cell viability assay

HepG2, A549, and HT-29 cells were seeded in 96-well plate (Thermo Fisher, USA), at 5 x 103 cells/well/100 μL and incubated at 37 ℃ with 5 % CO_2 for 24 h. After incubation, medium was replaced by D-MEM containing reagents (nanosomes in 0, 5, 10, 25, 50, and 100 nM concentrations, respectively), or (cisplatin in 0, 5, 10, 25, 50, and 100 μM), and incubated for 96 h at 37 ℃ with 5 % CO_2. Cell viability assay was performed according to the procedure of a Cell Counting Kit-8 solution (Dojindo, Kumamoto, Japan). After 96 h incubation, cells were washed with medium (100 μL) and then replaced with new medium (100 μL). 10 μL Cell Counting Kit-8 solution was added to the medium and incubated at 37 ℃ with 5 % CO_2 for 1 h. The optical density was measured with SUNRISE Thermo microplate reader (Tecan Japan Co. Ltd., Kawasaki, Japan). All values are expressed as means ± the standard error of the mean (SEM), and the assays were repeated three times. The error bar graphs in each picture were generated with Prism 4.0 (GraphPad Software, Inc., San Diego, CA). Cell viability assay after 24 h to 96 h coincubation. HepG2 and OUS-11 cells were seeded in 96-

well plate (Thermo Fisher, USA), at 5 × 10^4 cells/well, and incubated at 37 ℃ with 5 % for 24 h. The cells were treated with NSs for 24, 48, 72, 96 h. Cell growth was determined by adding 10 μL of a Cell Counting Kit8 solution (Dojindo, Kumamoto, Japan), and the mixture was incubated for 1.5 h and the optical density was measured using SpectraMax M5 spectrophotometer (Molecular Devices Co., Sunnyvale Co., USA). All values are expressed as means ± the standard error of the mean (SEM), and the assays were repeated three times. The bar graphs in each picture were generated with Prism 5.0 (GraphPad Software, Inc., San Diego, CA).

2-5. Reference

[1] Haxho, F. *et al.*, Neuraminidase-1: A novel therapeutic target in multistage tumorigenesis. *Oncotarget* **2016**, *7*, 40860-40881.

[2] (a) Gilmour, A. M. *et al.*, A novel epidermal growth factor receptor-signaling platform and its targeted translation in pancreatic cancer. *Cell. Signal.* **2013**, *25*, 2587-2603. (b) Abdulkhalek, S., Hrynyk, M., Szrwczuk, M. R., A novel G-protein-coupled receptor-signaling platform and its targeted translation in human disease. *Res. Rep. Biochem.* **2013**, *3*, 17-30.

[3] Abdulkhalek, S., Szewczuk, M. R. Neu1 sialidase and matrix metalloproteinase-9 cross-talk regulates nucleic acid-induced endosomal TOLL-like receptor-7 and -9 activation, cellular signaling and pro-inflammatory responses. *Cell. Signal.* **2013**, *25*, 2093-2105.

[4] Liu, Y-C. *et al.*, Sialylation and fucosylation of epidermal growth factor receptor suppress its dimerization and activation in lung cancer cells. *Proc. Natl. Acad. Sci. USA* **2011**, *108*, 11332-11337.

[5] Mosesson, Y., Mills, G. B., Yarden, Y. Derailed endocytosis: An emerging feature of cancer. *Nat. Rev. Cancer* **2008**, *8*, 835-850.

[6] Commisso, C. *et al.*, Macropinocytosis of protein is an amino acid supply route in Ras-transformed cells. *Nature* **2013**, *497*, 633-637.

[7] Kamphorst, J. J. *et al.*, Human pancreatic cancer tumors are nutrient poor and tumor cells actively scavenge extracellular protein. *Cancer Res.* **2015**, *75*, 544-553.

[8] Bernacki, R. J., Niedbala, M. J., Korytnyk, W. Glycosidases in cancer and invasion. *Cancer Metastasis Rev.* **1985**, *4*, 81-102.

[9] Koide, R., Nishimura, S.-I. Antiadhesive nanosomes facilitate targeting of the lysosomal GlcNAc salvage pathway through derailed cancer endocytosis. *Angew. Chem. Int. Ed.* **2019**, *58*, 14513-14518.

[10] Turk, B., Turk, V. Lysosomes as “suicide bags” in cell death: Myth or reality? *J. Biol. Chem.* **2009**, *284*, 21783-21787.

[11] Liang, F. *et al.*, Monocyte differentiation up-regulates the expression of the lysosomal sialidase, Neu1, and triggers its targeting to the plasma membrane via major histocompatibility complex class II-positive compartments. *J. Biol. Chem.* **2006**, *281*, 27526-27538.

[12] Sigismund, S. *et al.*, Endocytosis in the context-dependent regulation of individual and collective cell properties. *Nat. Rev. Cell Biol.* **2021**, *22*, 625-643.

[13] Boya, P., Kroemer, G. Lysosomal membrane permeabilization in cell death. *Oncogene* **2008**, *27*, 6434-6451.

[14] Kallunki, T., Olsen, O. D., Jäättelä, M. Cancer-associated lysosomal changes: friends or foes? *Oncogene* **2013**, *32*, 1995-2004.

[15] Ohyanagi, T. *et al.*, Importance of sialic acid residues illuminated by live animal imaging using phosphorylcholine self-assembled monolayer-coated quantum dots. *J. Am. Chem. Soc.* **2011**, *133*, 12507-12517.

[16] Koide, R. *et al.*, Antiadhesive nanosome elicits role of glycocalyx of tumor cell-derived exosomes in the organotropic cancer metastasis. *Biomaterials* **2022**, *280*, 121314.

[17] Love, J. C. *et al.*, Self-assembled monolayers of thiolates on metals as a form of nanotechnology. *Chem. Rev.* **2005**, *105*, 1103-1169.

[18] Bourguet, E., Figurska, S., Frączek, M. M. Human neuraminidases: Structures and stereoselective inhibitors. *J. Med. Chem.* **2022**, *65*, 3002-3025.

[19] S. Chen, *et al.* Strong resistance of phosphorylcholine self-assembled monolayers to protein adsorption: Insights into nonfouling properties of zwitterionic materials. *J. Am. Chem. Soc.* **2005** *127*, 14473-14478.

[20] N. Nagahori, M. Abe, S. -I. Nishimura, Structural and functional glycosphingolipidomics by glycoblotting with an aminooxy-functionalized gold nanoparticle. *Biochemistry* **2009** *48*, 583-594.

[21] H. Hinou, M. Kurogochi, H. Shimizu, S.-I. Nishimura, Characterization of *Vibrio cholerae* neuraminidase by a novel mechanism-based fluorescent labeling reagent. *Biochemistry* **2005**, *44*, 11669-11675.

[22] S. H. Chen, *et al.*, Development of a Gd(III)-based receptor-induced magnetization enhancement (RIME) contact agent for b-glucuronidase activity profiling. *Inorg. Chem.* **2012**, *51*, 12426-12435.

[23] R. S. Tan, et al. Rapid endolysosomal escape and controlled intracellular trafficking of cell surface mimetic quantum-dots-anchored peptides and glycopeptides. *ACS Chem. Biol.* **2015** *10*, 2073-2085.

[24] Harless, Q., et al., Novel molecular mechanism of aspirin and celecoxib targeting mammalian neuraminidase-1 impedes epidermal growth factor receptor signaling axis and induces apoptosis in pancreatic cancer cells. *Drug Des. Devel. Ther.* **2020**, *14*, 4149-4167.

2-6. Supporting Information

Table S2-1. Nanosomes carrying mechanism-based glycoside inhibitors.

Nanosomes (PC/cargo)	Surface Coverage[a)]	Zeta potential[b)] [mV]	HD diameter[b)] [nm]
NS (control)	67.1 PC/nm^2	-21.4	16.1 ± 4.2
NS-8103 (2/1)	44.7 PC/nm^2 22.4 **103**/nm^2	-19.3	33.4 ± 1.8
NS-8104 (2/1)	44.7 PC/nm^2 22.4 **104**/nm^2	-16.6	22.5 ± 0.3
NS-8105 (2/1)	44.7 PC/nm^2 22.4 **105**/nm^2	-19.6	26.8 ± 1.2

a) Surface coverage was calculated using the density of PC linkers on the surface of NS (control, PCSAM NS) having an average diameter of 10 nm, which is estimated to be 67.1 PC linkers/nm^2 (0.0149 nm^2/PC linker).[20,21]

b) Zeta potential and hydrodynamic diameter of nanosomes

Table S2-2. IC_{50} (nM) values showing antitumor activities of nanosomes.

Nanosomes	Cancer cell line		
	A549	HepG2	HT-29
		IC_{50} (nM)	
NS (control)	-	-	-
NS-8101	67.0	10.7[a)]	32.3
NS-8102	-	59.3[a)]	26.5
NS-8103	9.57	13.5	11.1
NS-8104	71.8	36.9	23.0
NS-8105	-	44.7	16.0

a) These values were reported in the previous paper.[9] -: No significant antitumor effect.

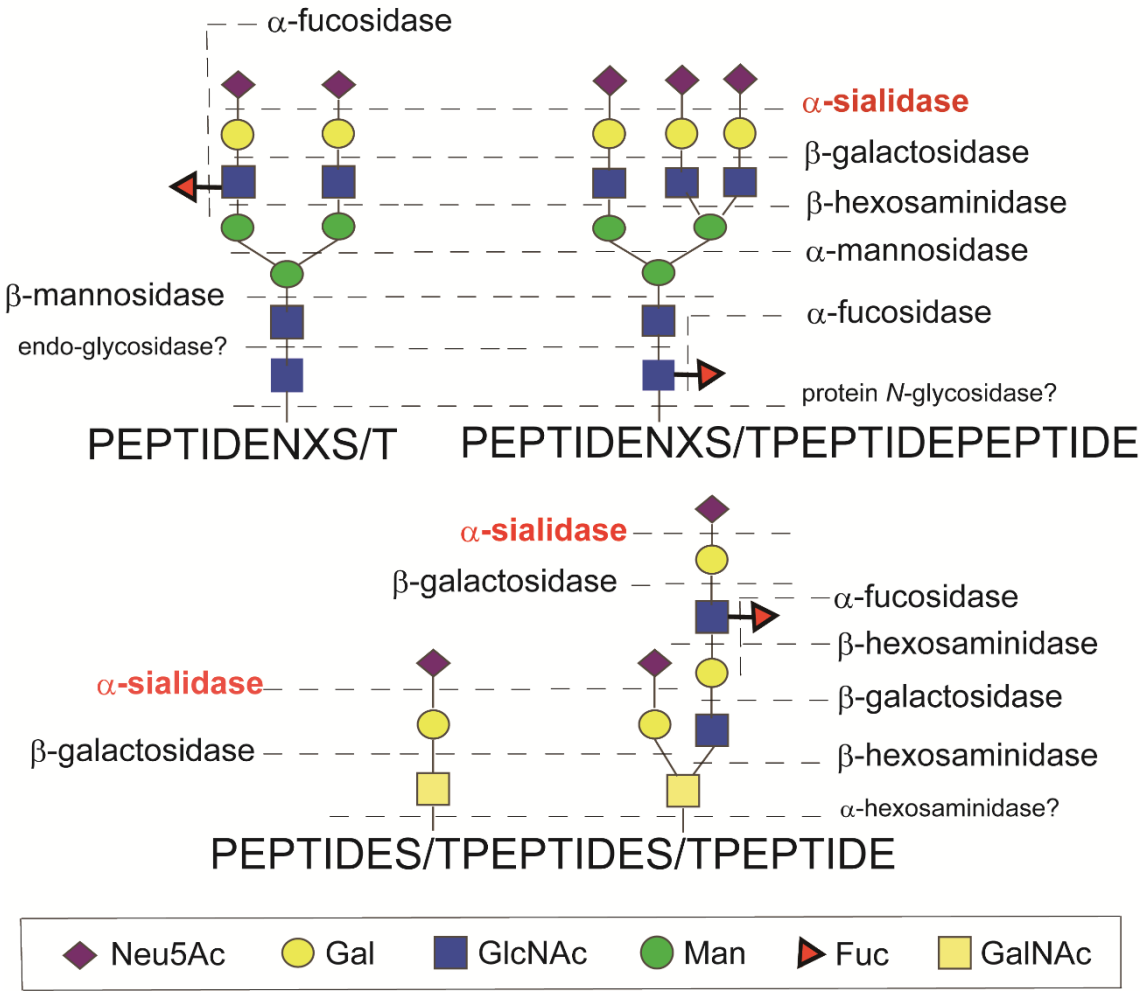

Figure S2-1. Neuraminidase (sialidase) is a key lysosomal glycosidase for the degradation of *N*- and *O*-glycans attached to glycoproteins. Neuraminidase (sialidase), encoded by the

NEU1 gene in the major histocompatibility complex locus catalyzes intralysosomal degradation of sialylated glycoproteins. Hydrolytic reaction catalyzed by sialidase is a critical step for the metabolic pathway of glycoproteins because removal of the non-reducing terminal Neu5Ac residues initiates further degradation of glycans by other lysosomal glycosidases such as b-galactosidase, b-hexosaminidase, and a-mannosidase.

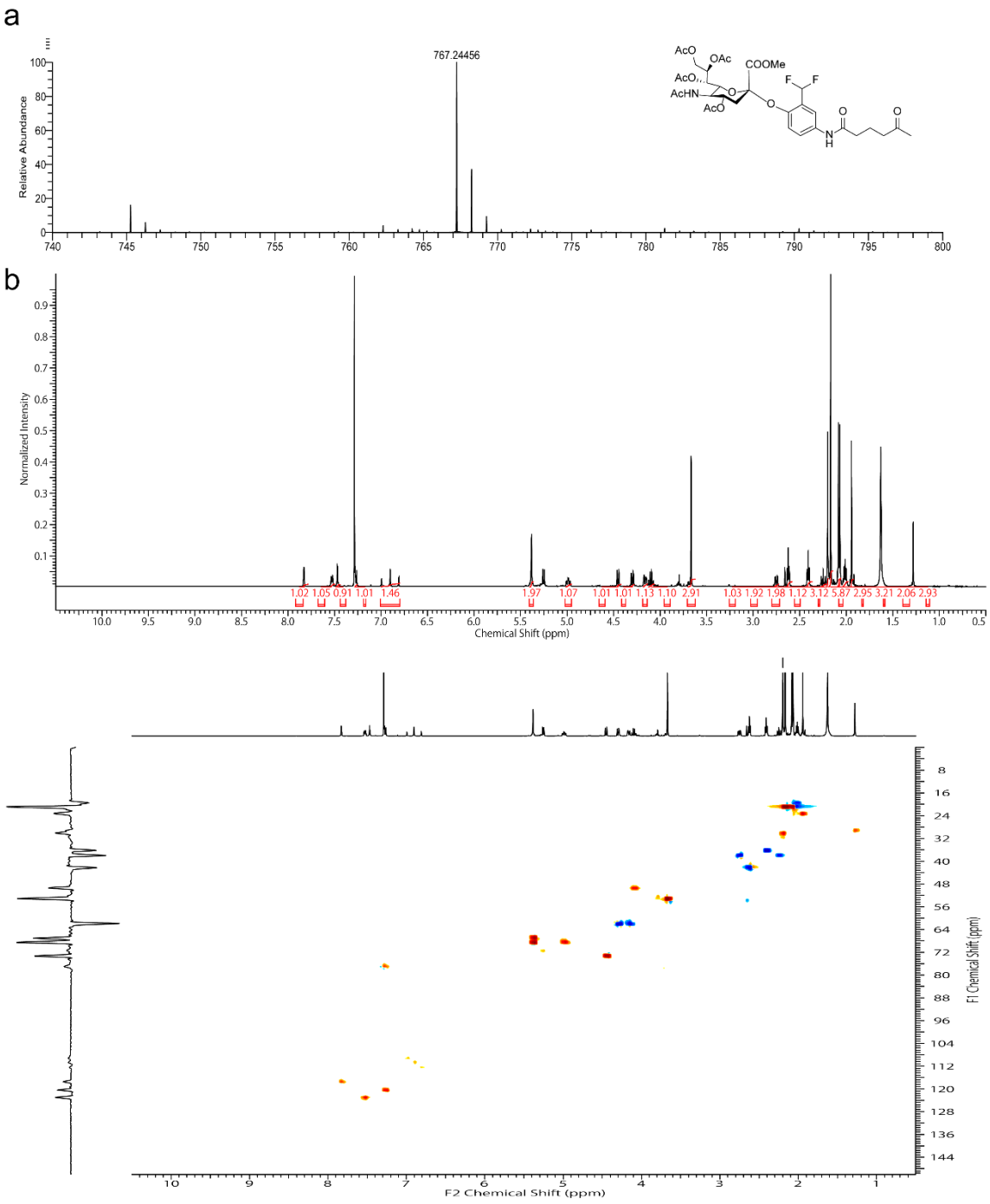

Figure S2-2. HR-MS and NMR of compound **2**.

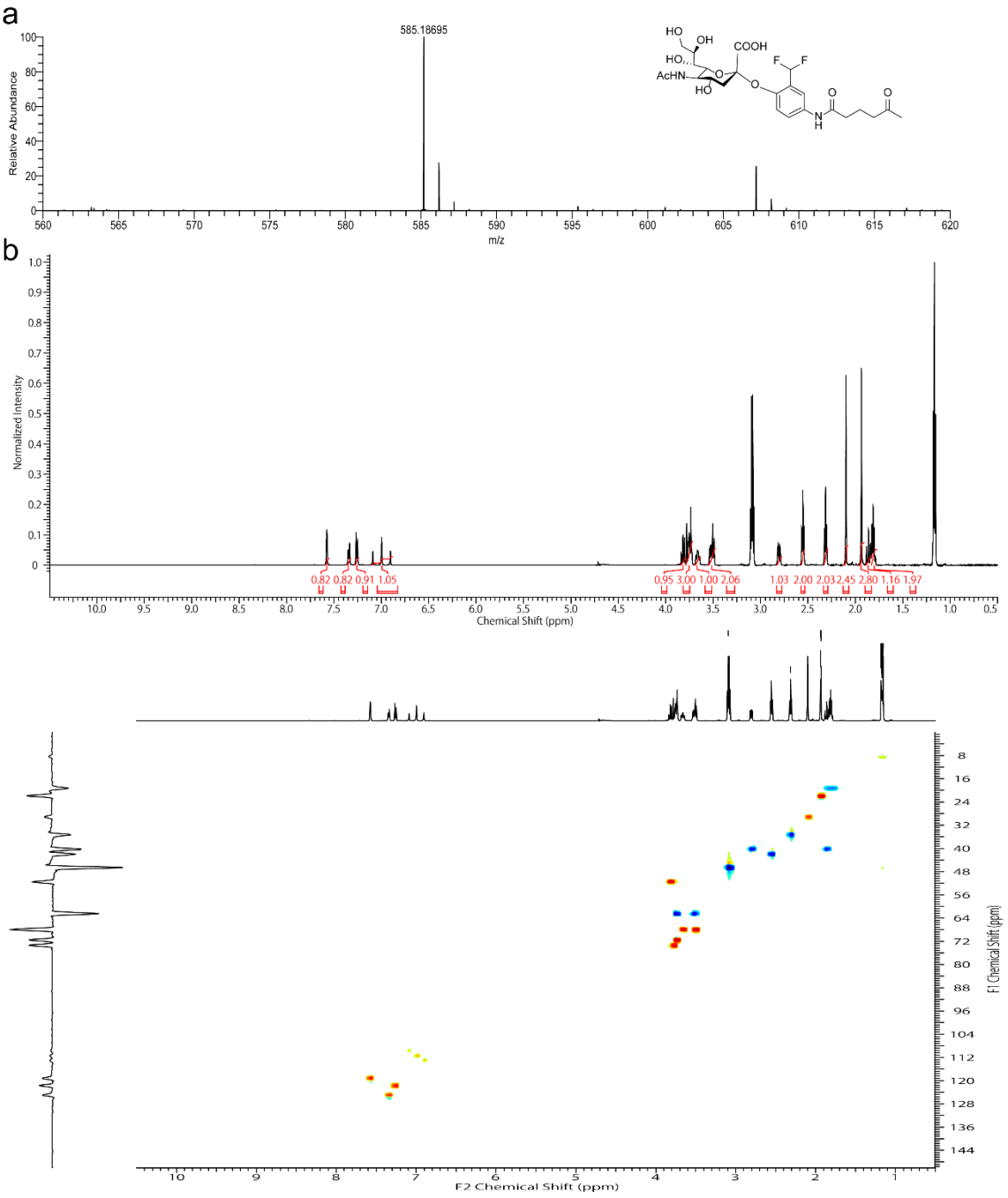

Figure S2-3. HR-MS and NMR of compound **103**.

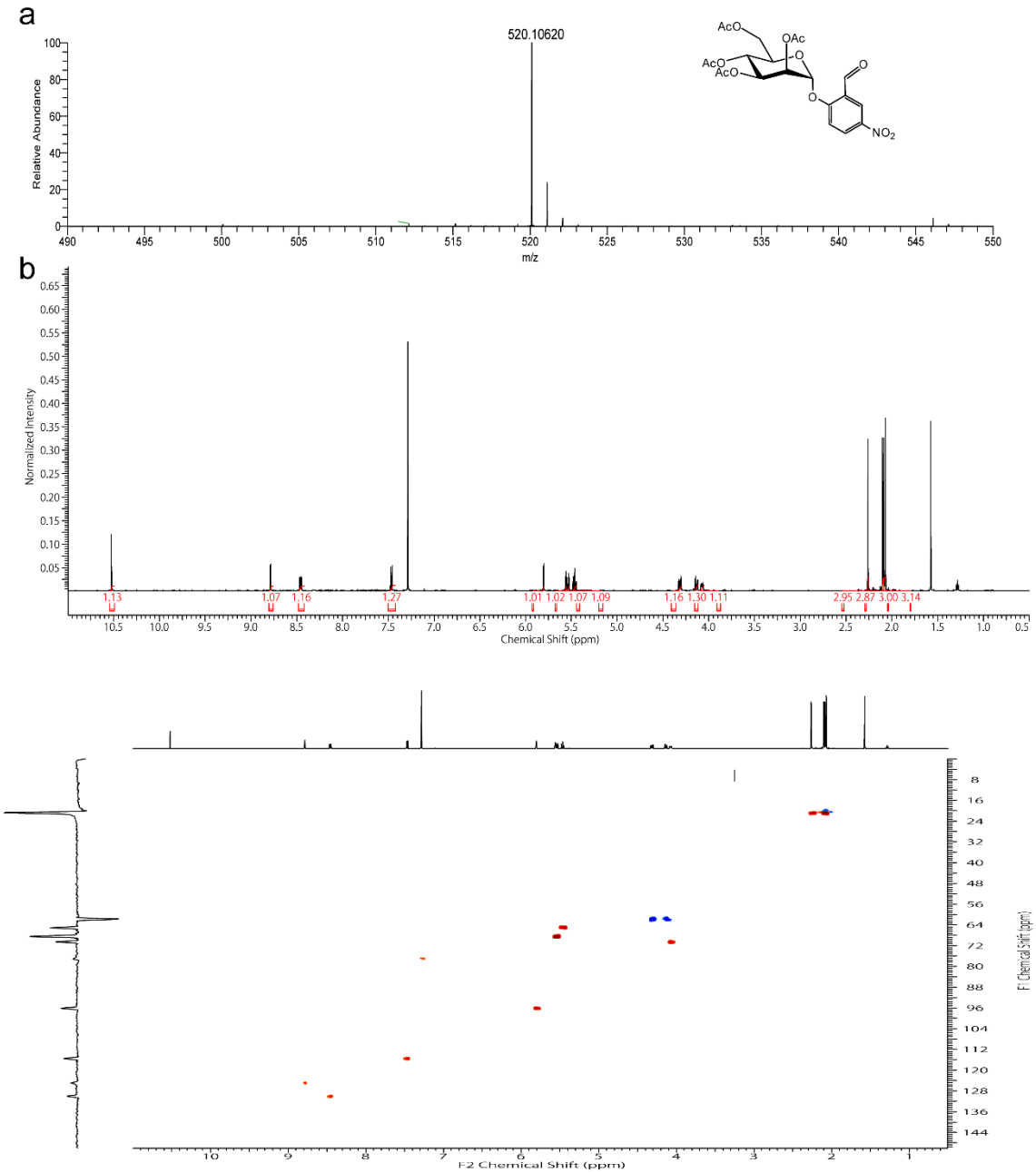

Figure S2-4. HR-MS and NMR of compound **4**.

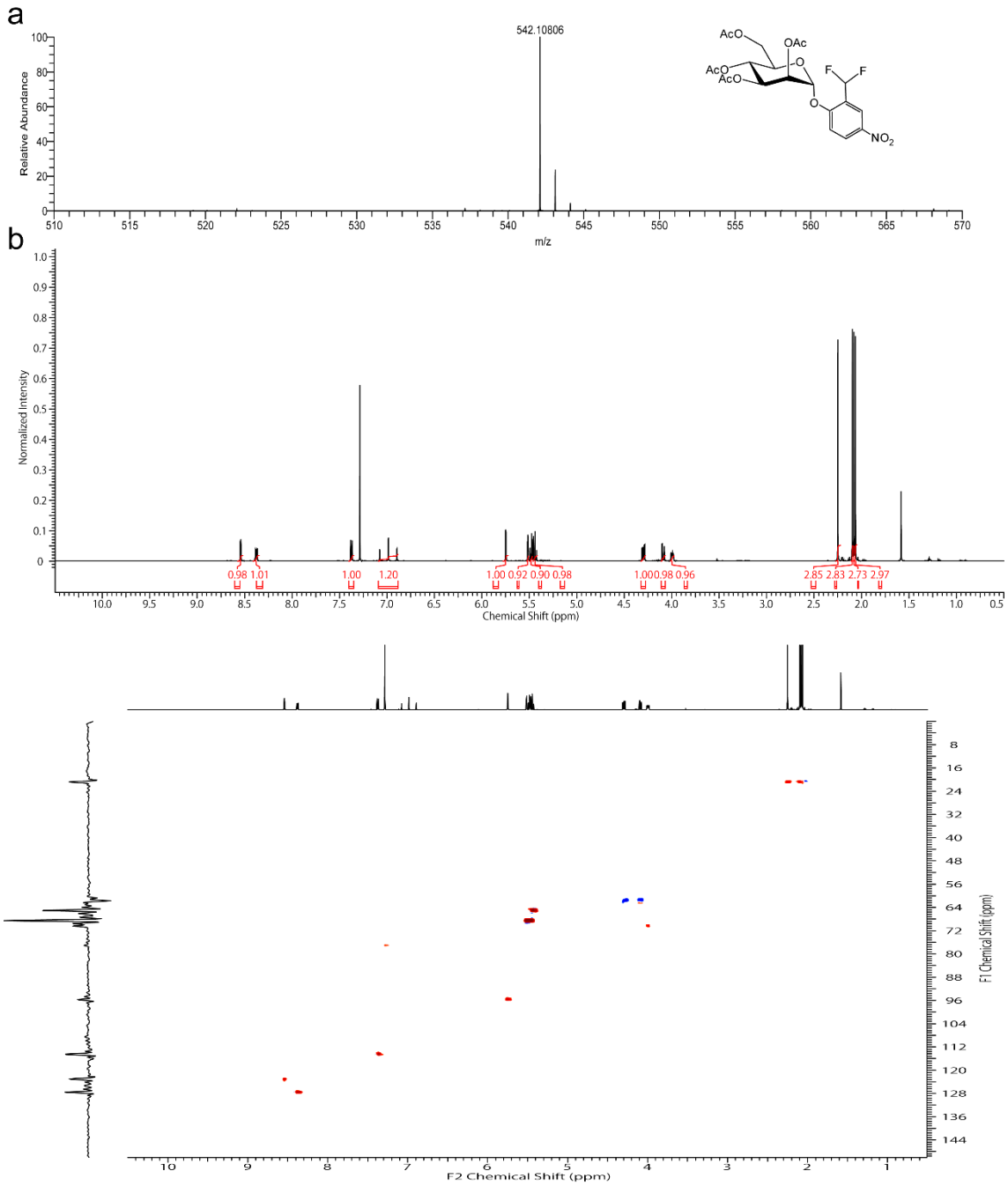

Figure S2-5. HR-MS and NMR of compound **5**.

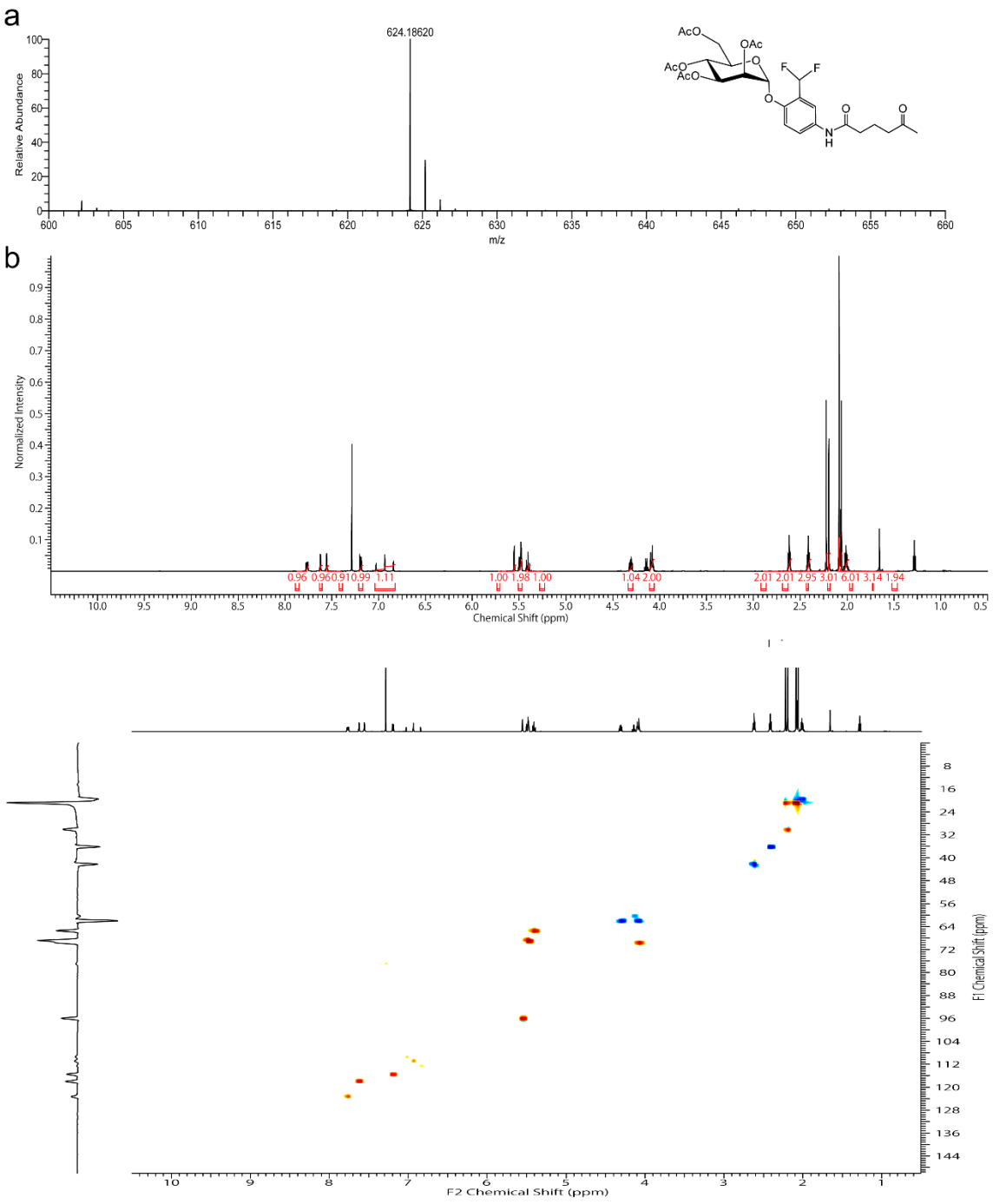

Figure S2-6. HR-MS and NMR of compound **6**.

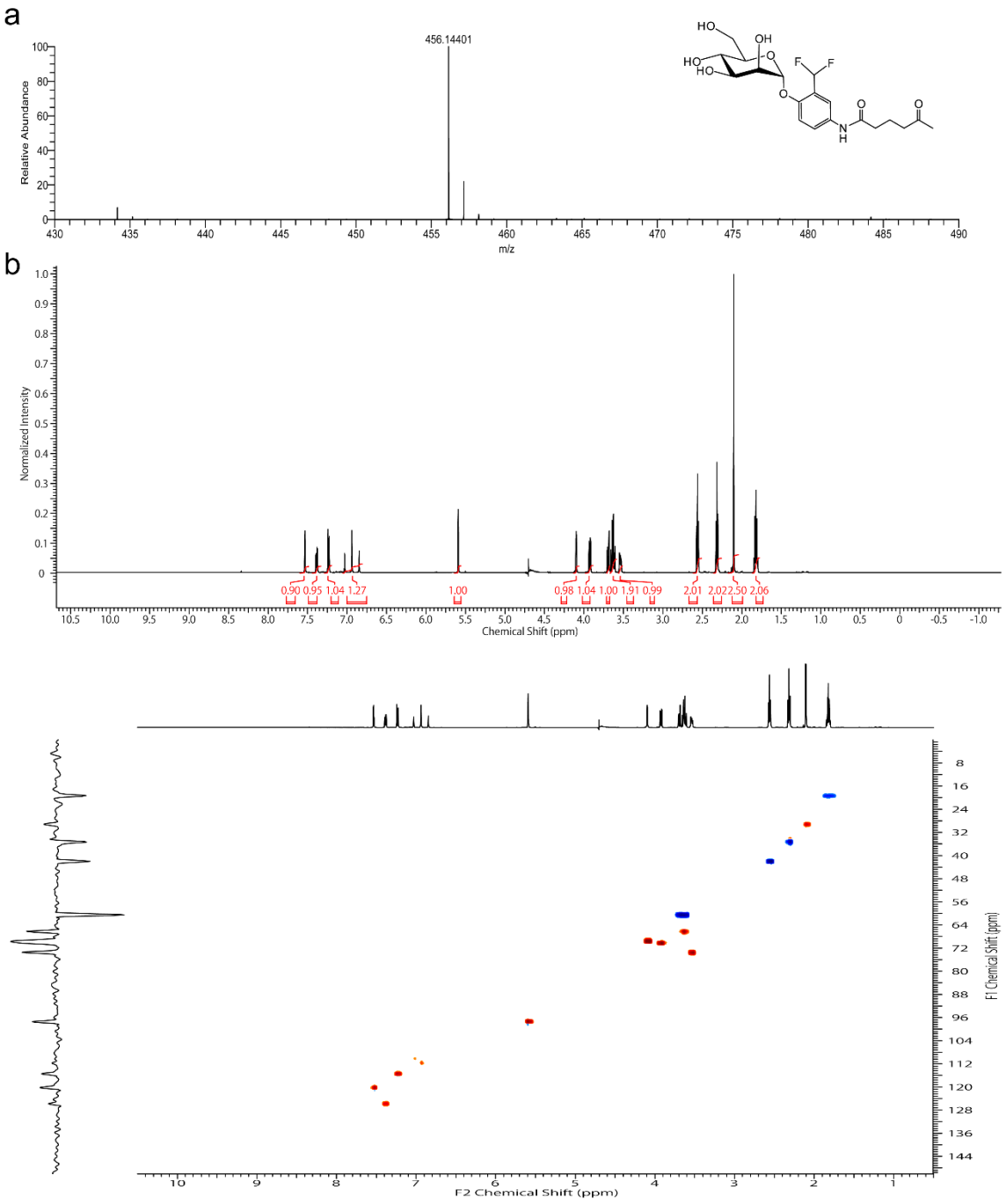

Figure S2-7. HR-MS and NMR of compound **104**.

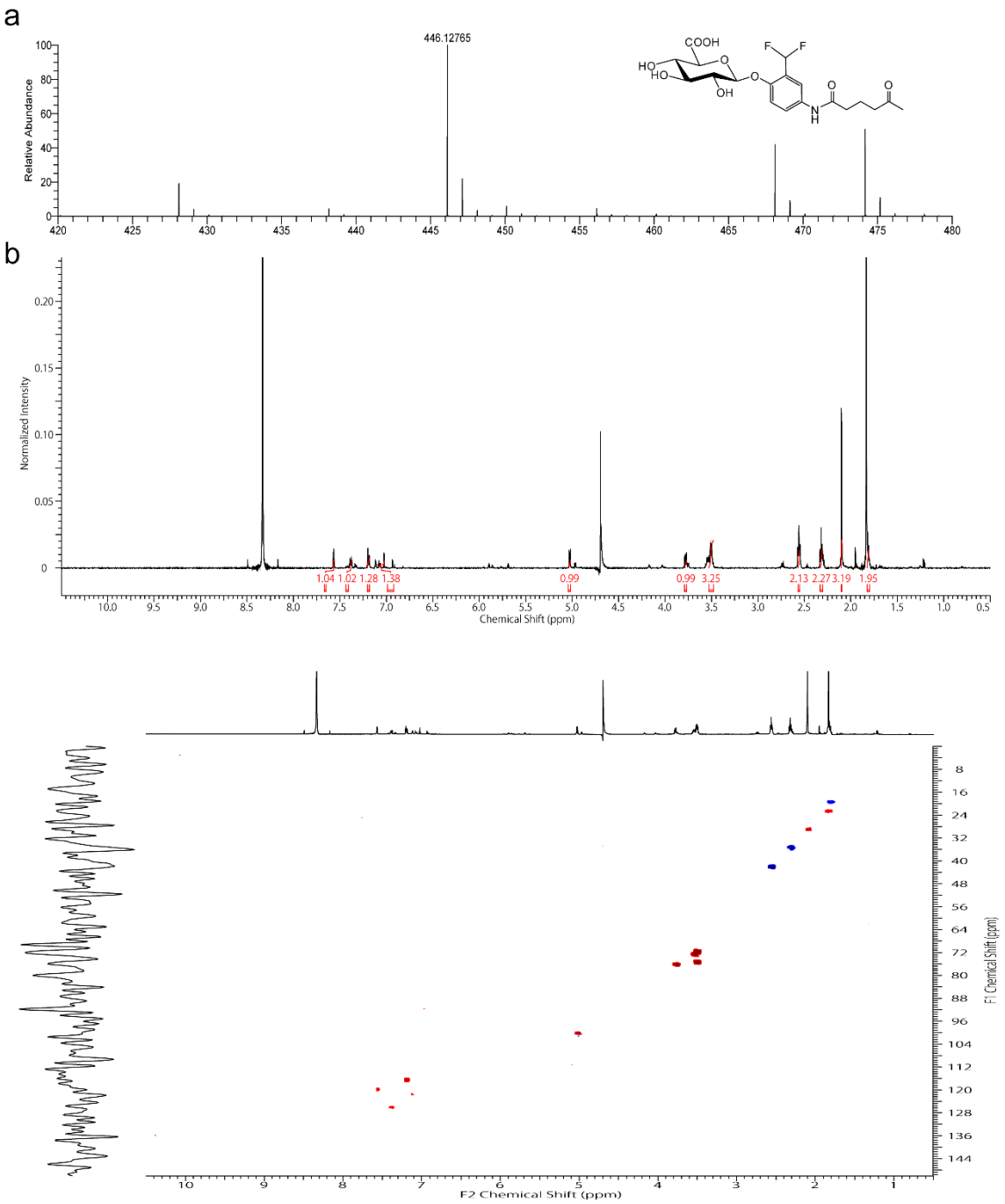

Figure S2-8. HR-MS and NMR of compound **105**.

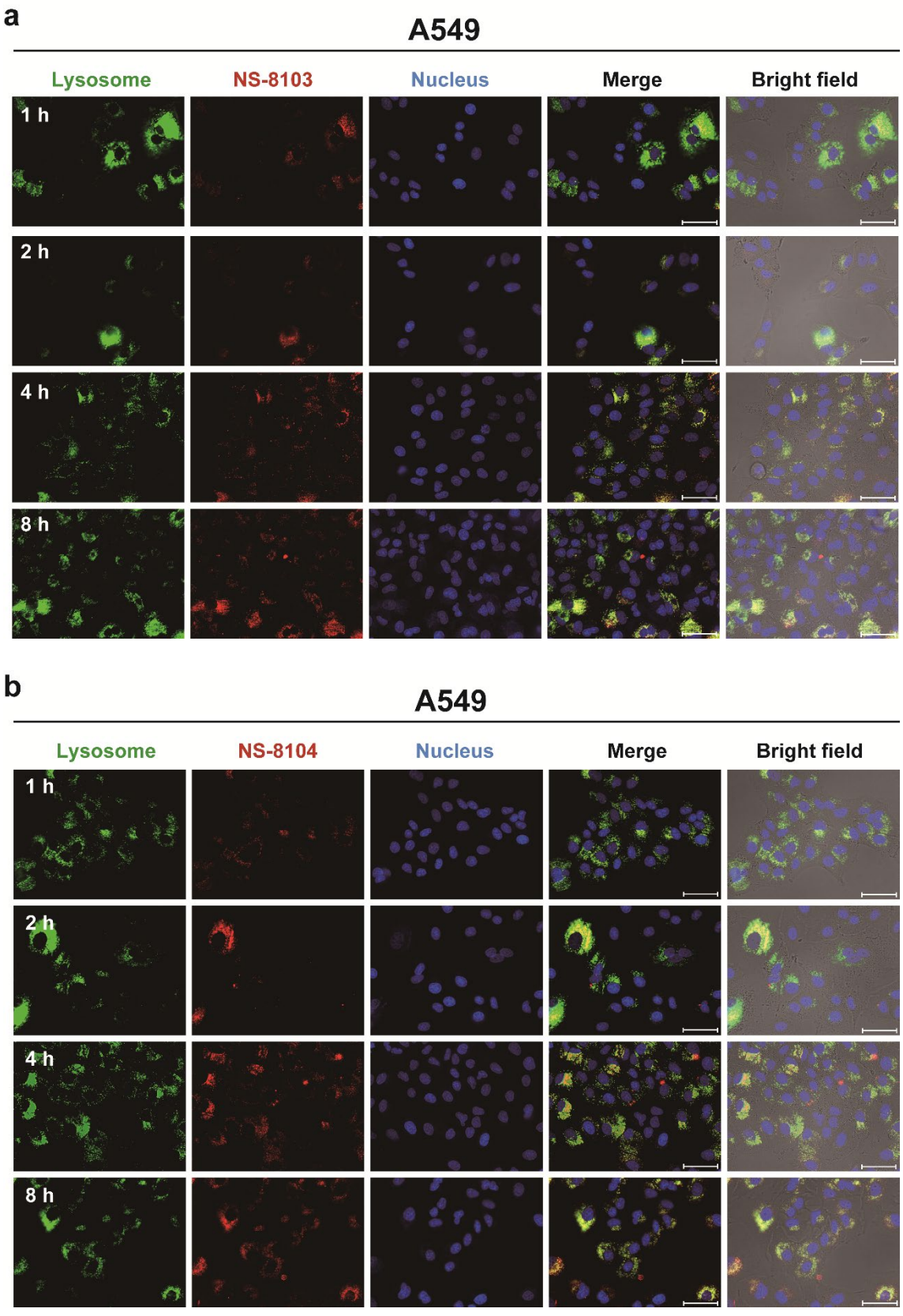
a
A549
Lysosome
NS-8103
Nucleus
Merge
Bright field
1 h
2 h
4 h
8 h
b
A549
Lysosome
NS-8104
Nucleus
Merge
Bright field
1 h
2 h
4 h
8 h

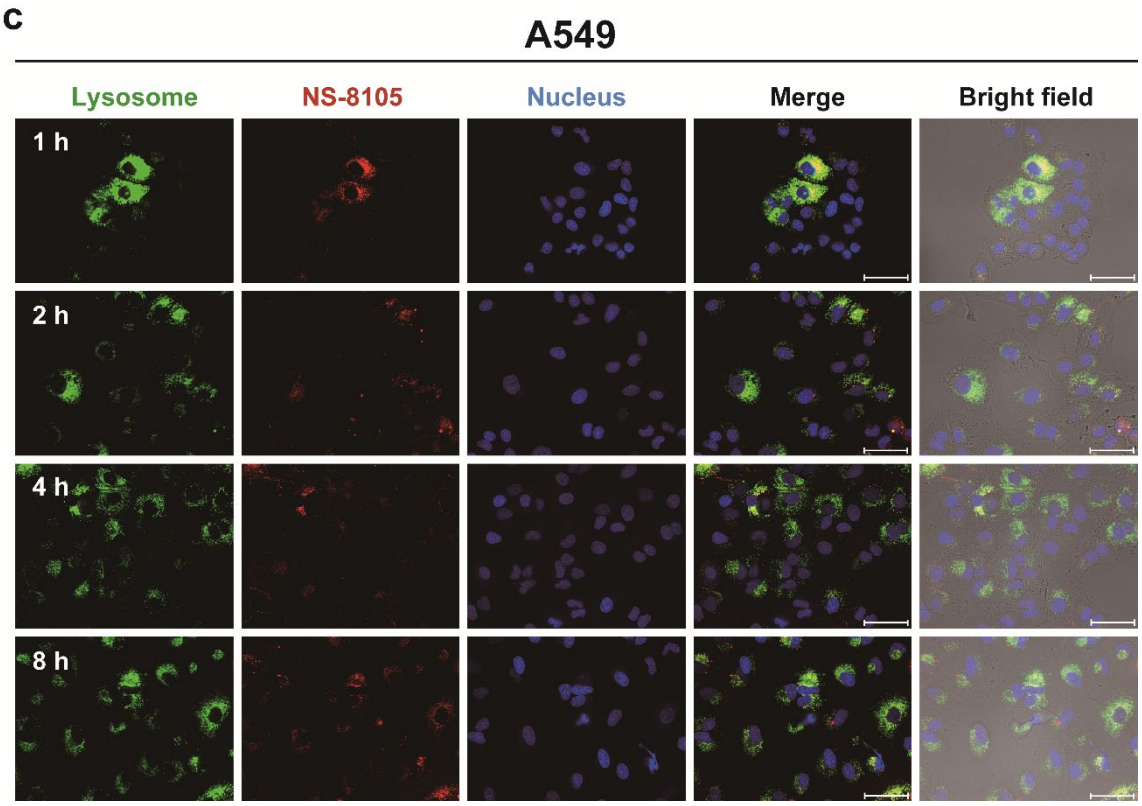
c
A549
Lysosome
NS-8105
Nucleus
Merge
Bright field
1 h
2 h
4 h
8 h

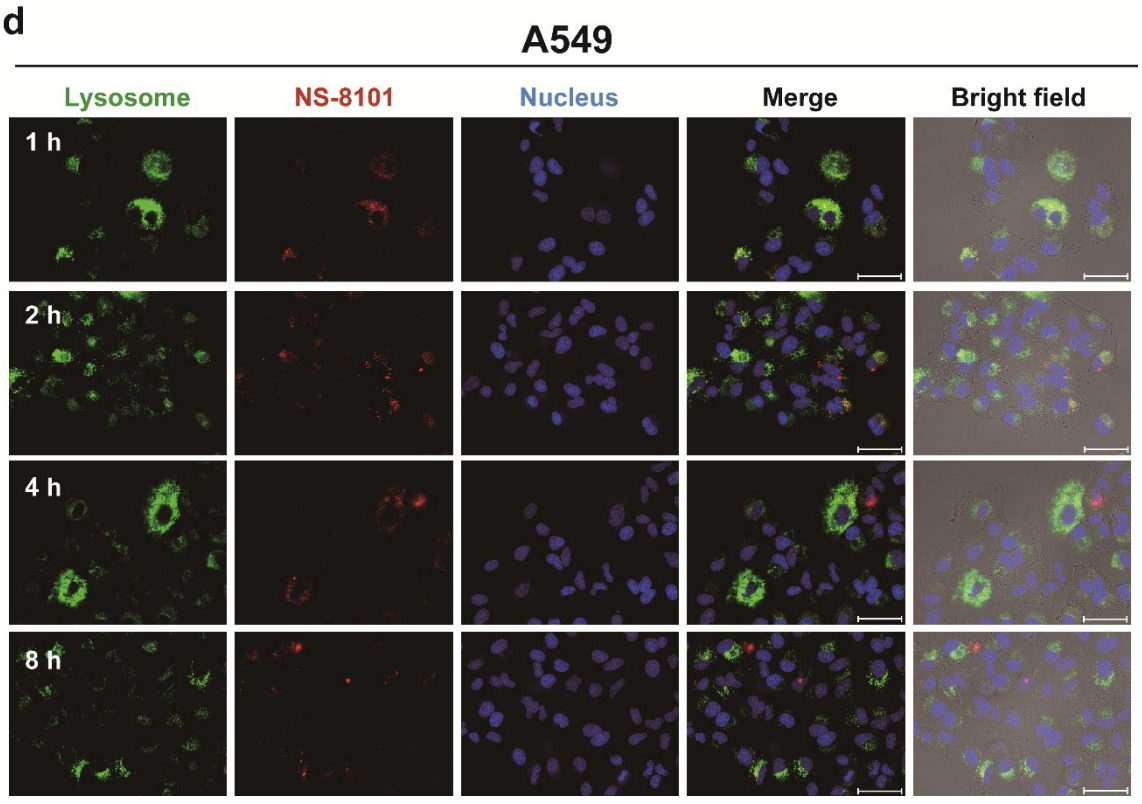
d
A549
Lysosome
NS-8101
Nucleus
Merge
Bright field
1 h
2 h
4 h
8 h

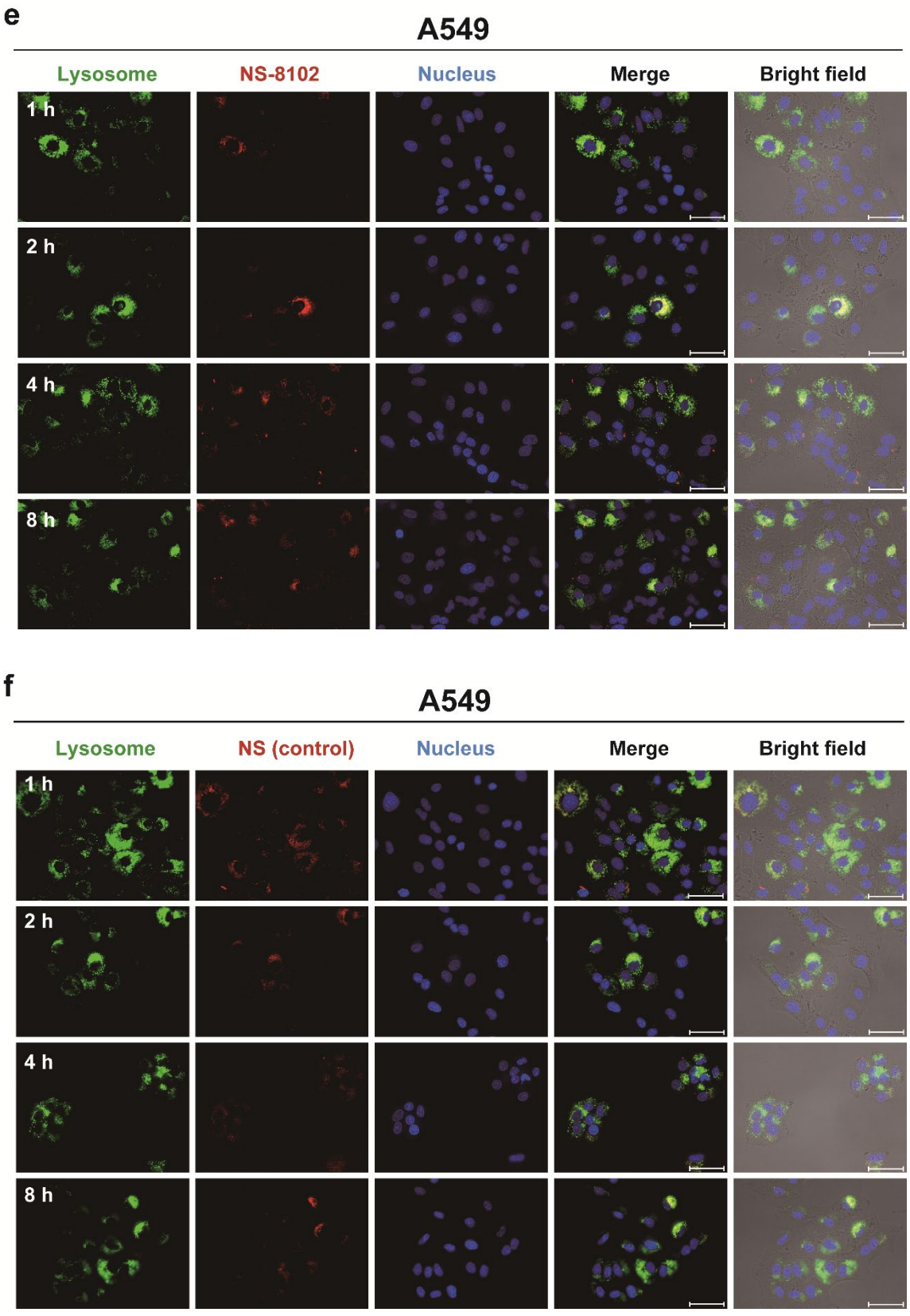

Figure S2-9. Representative cell images showing intracellular distribution of NSs for different

times after exposure of A549 cells to 10 nM NSs. Scale bar, 50 μm. Cells were co-incubated with NSs (red) for 1, 2, 4, and 8 h and fixed, respectively. Lysosomes were stained with LysoTracker Green DND-26 (green), while the nuclei were stained with Hoechst 33342 (blue). (a) Merged pictures in cases of 10 nM **NS-8103** indicate their distinct escape from endosomal entrapment at 4 and 8 h after exposure to A549 cells while yellow color area showing their endosomal colocalization can be detected dominantly in cases of other nanosomes (b)~(e). (f) The control NSs (PCSAM-QDs) were entirely accumulated in the endolysosome.

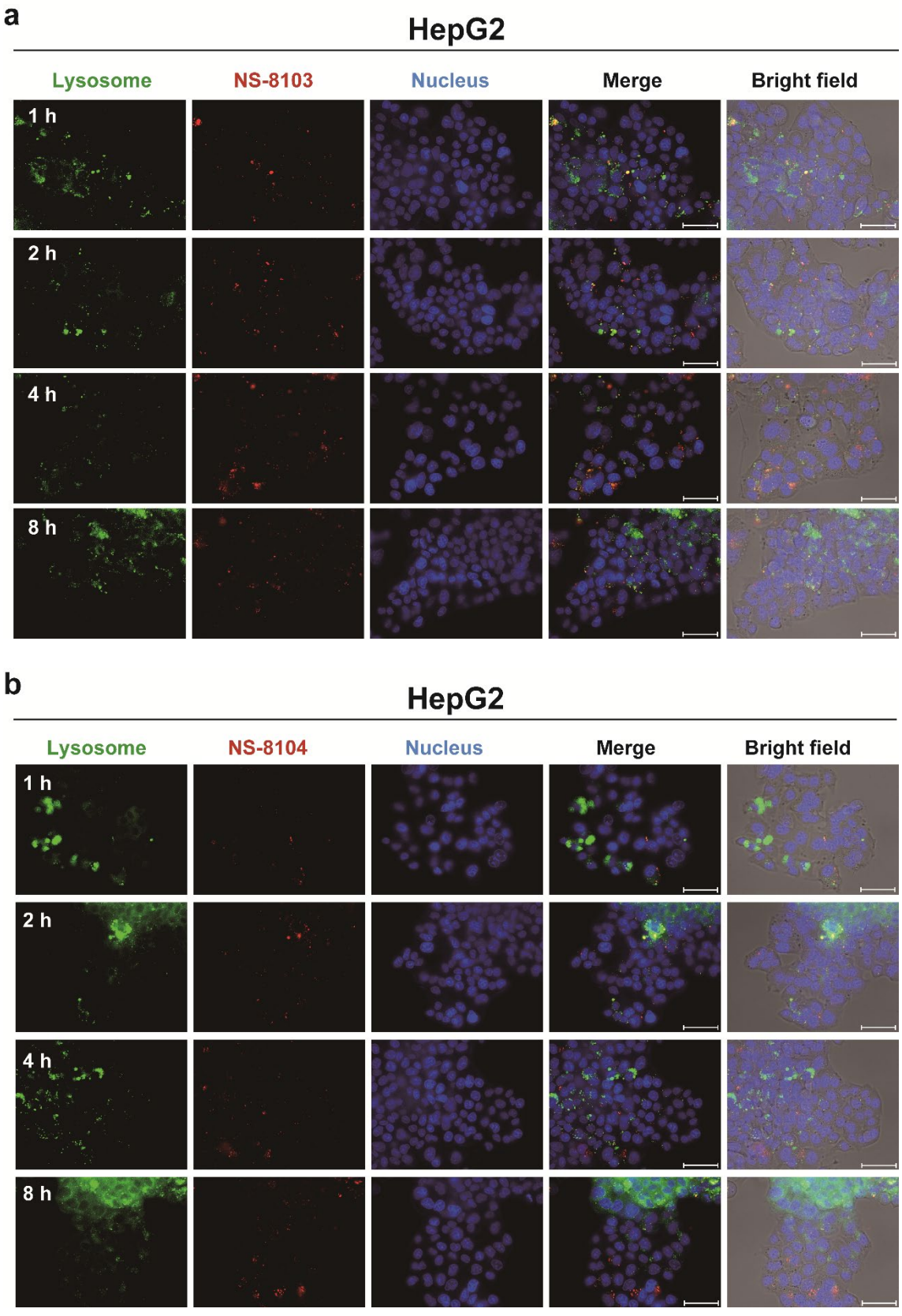
a
HepG2
Lysosome
NS-8103
Nucleus
Merge
Bright field
1 h
2 h
4 h
8 h
b
HepG2
Lysosome
NS-8104
Nucleus
Merge
Bright field
1 h
2 h
4 h
8 h

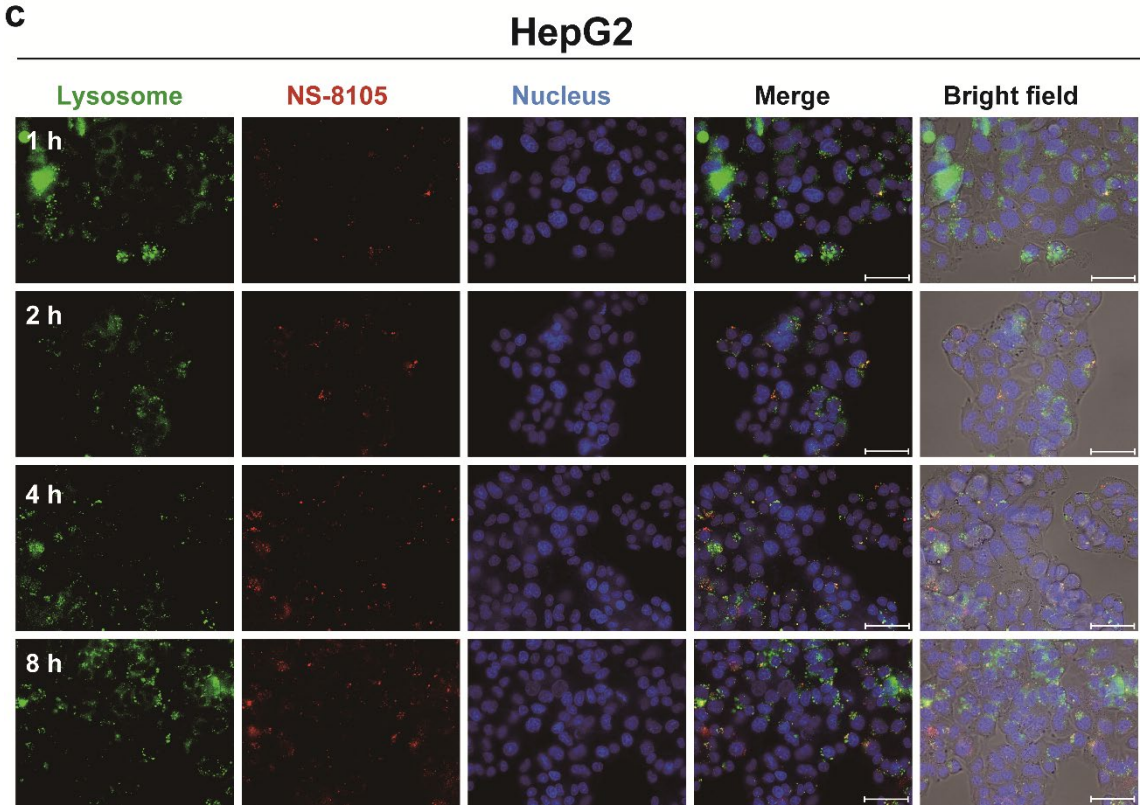

Figure S2-10. Representative cell images showing intracellular distribution of NSs for different times after exposure of HepG2 cells to 10 nM NSs. Scale bar, 50 μm. Cells were co-incubated with NSs (red) for 1, 2, 4, and 8 h and fixed, respectively. Lysosomes were stained with LysoTracker Green DND-26 (green), while the nuclei were stained with Hoechst 33342 (blue). Merged pictures for **NS-8103** (a) indicate their rapid distinct escape from endosomal entrapment at 1, 2, 4 and 8 h after exposure to HepG2 cells In contrast, **NS-8104** (b) and **NS-8105** (c) seem to escape partly from endosomal entrapment at 4 and 8 h after exposure to HepG2 cells and yellow color area showing their endosomal colocalization can also be detected significantly. The images of intracellular distribution for **NS-8101**, **NS-8102**, and control NSs (PCSAM-QDs) after exposure to HepG2 cells were reported previously.[9]

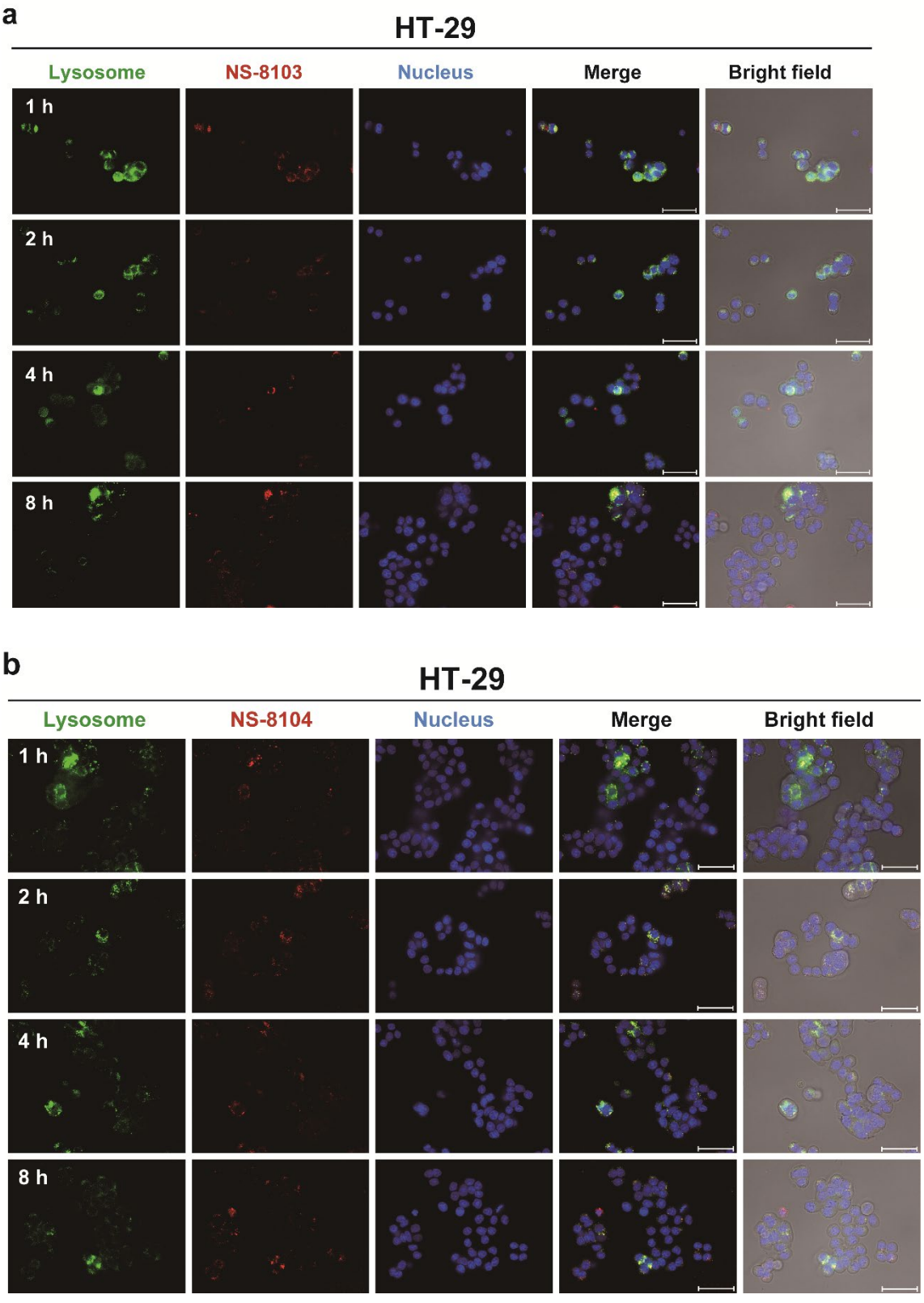
a
HT-29
Lysosome
NS-8103
Nucleus
Merge
Bright field
1 h
2 h
4 h
8 h
b
HT-29
Lysosome
NS-8104
Nucleus
Merge
Bright field
1 h
2 h
4 h
8 h

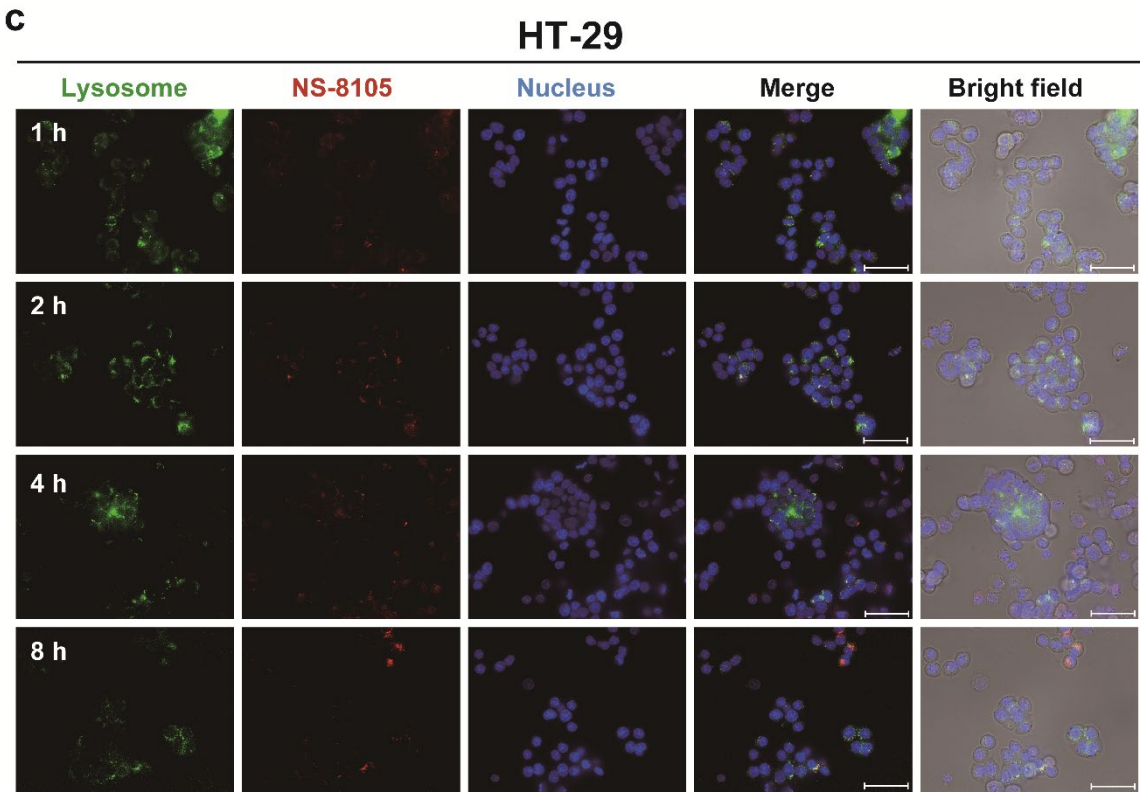
c
HT-29
Lysosome
NS-8105
Nucleus
Merge
Bright field
1 h
2 h
4 h
8 h

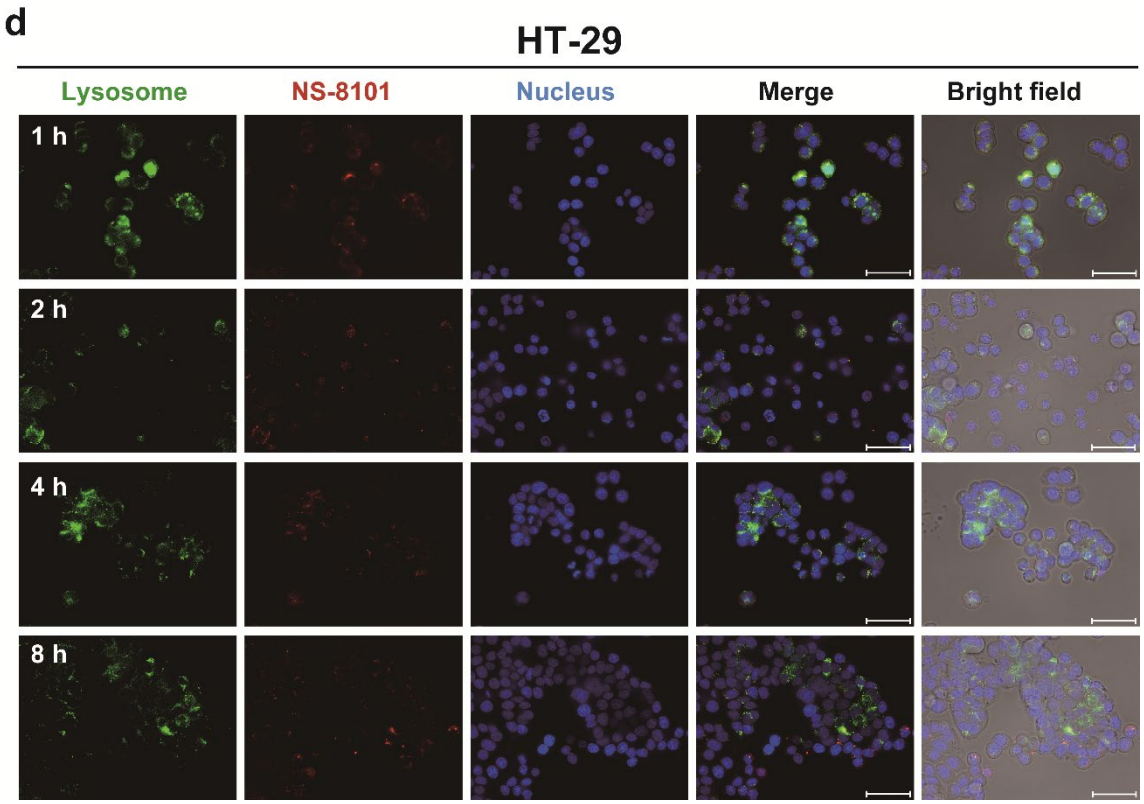
d
HT-29
Lysosome
NS-8101
Nucleus
Merge
Bright field
1 h
2 h
4 h
8 h

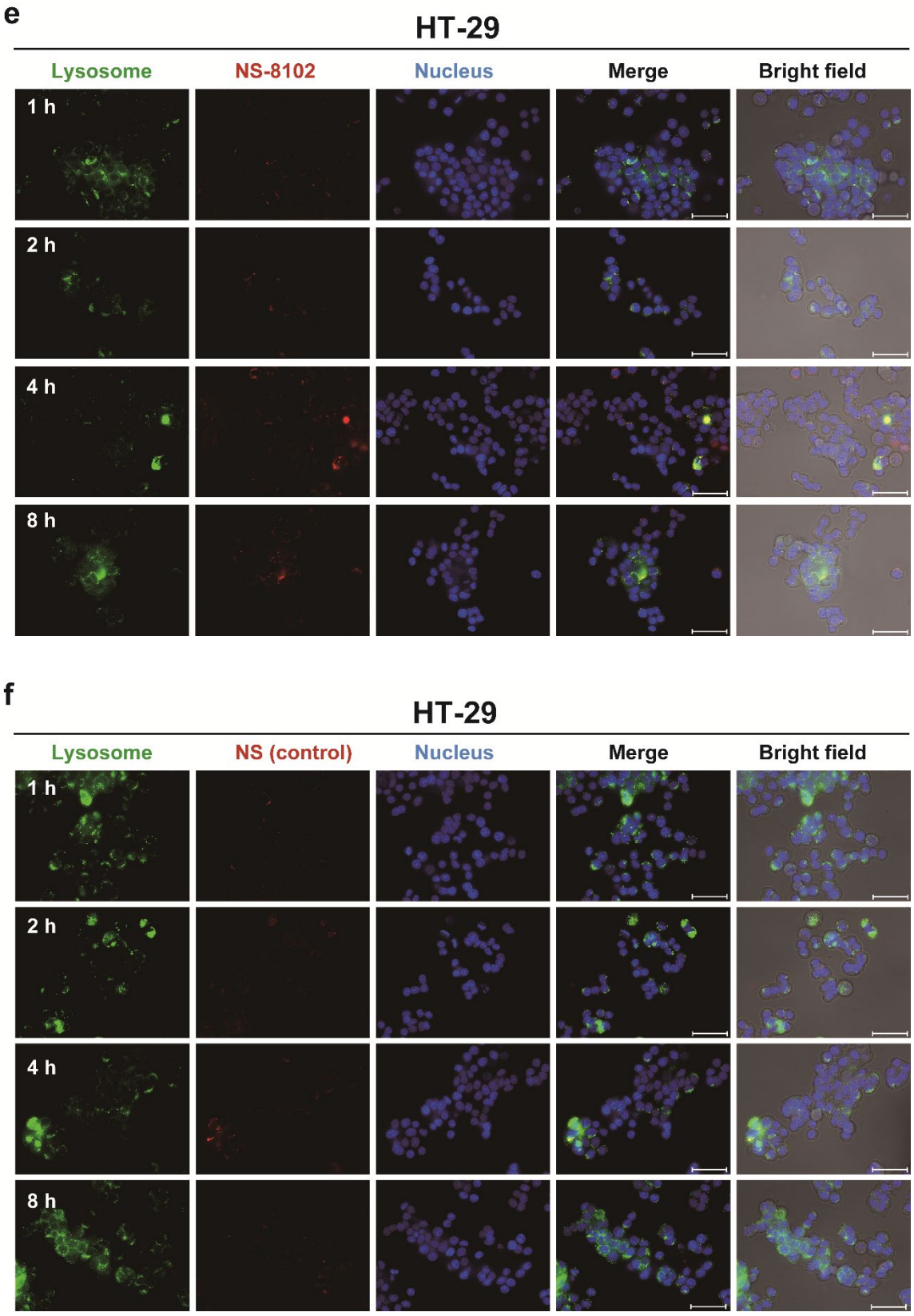

Figure S2-11. Representative cell images showing intracellular distribution of NSs for

different times after exposure of HT-29 cells to 10 nM NSs. Scale bar, 50 μm. Cells were co-incubated with NSs (red) for 1, 2, 4, and 8 h and fixed, respectively. Lysosomes were stained with LysoTracker Green DND-26 (green), while the nuclei were stained with Hoechst 33342 (blue). (a)~(e) Merged pictures in cases of 10 nM **NS-8101~NS8105** indicate quite similar intracellular distribution after exposure to HT-29 cells, while NSs seem to escape partly from endolysosomal compartment at 4 and 8 h after co-incubation. In contrast, the control NSs (PCSAM-QDs) were entirely accumulated in the endolysosome (f).

Chapter 3 Nanosomes loaded with hydrophobic drugs

3-1. Introduction

In Chapter 3, we decided to load clinically approved hydrophobic anticancer drugs onto nanosomes. The finding that membrane tethered NEU1-mediated endocytosis facilitates trafficking of nanomedicine to the intracellular space encouraged us to examine feasibility of **NS-8103** in the active delivery of small antitumor reagents into the cytosol of cancer cells. Unfavorable physicochemical properties such as poor solubility and high-level serum protein adsorption of many small-molecular-weight drugs lead to a dichotomy between concentrations active in the 10% serum concentrations generally used for in vitro testing and concentrations active in plasma, notably the clinically relevant concentrations.[1] For example, sorafenib, a potent multi-targeted kinase inhibitor of RAF/MEK/ERK signaling and the RTKs, has been recognized as a standard systemic treatment for patients with advanced hepatocellular carcinoma (HCC).[2] However, it seems likely that failure to recognize this distinction often leads to inappropriate claims of antitumor activity for sorafenib based on the micromolar concentrations commonly used for in vitro examinations in 10% serum conditions. Given that the dichotomy in the active concentrations unveiled between in vitro low serum conditions and in vivo clinical testing depends strongly on the poor solubility and heavy protein adsorption in plasma due to hydrophobic nature of sorafenib, we conceived that loading sorafenib to antiadhesive NSs could improve solubility in plasma, cellular uptake, intracellular trafficking, and anticancer activity of sorafenib directly affecting clinically relevant concentrations.

Pancreatic ductal adenocarcinoma (PDAC) is an emerging incidence and is one of the most lethal malignancies.1 Notably, PDAC is expected to surpass breast cancer before 2030[3] and colorectal cancer before 2040,[4] becoming the second leading cause of cancer-related deaths after lung cancer. PDAC is lethal because it cannot be detected early, often being discovered only after distant metastasis has occurred.[6] Most patients present with nonspecific symptoms at an advanced stage that can't be cured with surgery. Even in cases where surgical resection is performed, it is likely that most patients will develop recurrence within 2 years. Importantly, disseminated PDAC cells can be observed in circulation before localized invasion is readily visualized in primary tumors[5,6] indicating that PDAC cells as well as exosomes released from PDAC cells have escaped from the primary tumor, prior to or during surgical resection.

Until now, two major combination regimens have emerged as the first-line therapy in most patients with advanced PDAC, regardless of surgical eligibility: (a) a combination of 5-fluorouracil (5-FU), leucovorin, irinotecan, and oxaliplatin, namely FOLFRINOX,[7] and (b) the combination of gemcitabine and an albumin nanoparticle conjugate of paclitaxel (nab-paclitaxel).[8] In 2024, “NALIRIFOX”, a liposomal formation of irinotecan (ONIVYDE)[9-11] in

combination with 5-FU, was also approved as a new first-line treatment of metastatic PDAC by Food and Drug Administration of the United States.[37] Despite substantial advancements in pancreatic cancer therapy that extend patients' life expectancies, there have unfortunately been no appreciable changes in survival rates. On the other hand, accumulated evidence that one of the most specific features of the PDAC tumor microenvironment (TME) is the lack of infiltration by cytotoxic CD8+ T cells, demonstrating why therapies by immune checkpoint inhibitors have proven difficult in the PDAC TME.[12] Notably, immune checkpoint inhibitors have been approved to treat many patients with a variety of cancer types such as breast cancer, bladder cancer, cervical cancer, colon cancer, head and neck cancer, Hodgkin lymphoma, liver cancer, lung cancer, renal cell cancer, skin cancer, including melanoma, stomach cancer, and rectal cancer.[13] It should be emphasized that translating knowledge regarding the specific biology and pathophysiology of PDAC to the clinic to improve patient outcomes has been challenging.

We have established a facile and efficient method for the preparation of an antiadhesive nanoparticle platform, namely "nanosome", exhibiting excellent water solubility, long term stability in the stock solution, pH resistance, and a capacity to prevent non-specific serum/tissue protein adsorption, termed as "protein corona" of nanoparticles.[14,15] Nanosome is made of hard/high density-core materials such as semiconductor quantum dots (QDs) and gold nanoparticles (AuNPs), and soft-shell mixed self-assembled monolayer (SAM) membrane of 11-mercaptoundecylphosphorylcholine (PC linker)[13,16] and alkanethiol having an aminooxy-functional headgroup, 11,11'-dithio bis[undec-11-yl 12-(aminooxyacetyl)amino hexa(ethyleneglycol)] (AO linker)[17] (Figure 3-1a). Oxime-based surface loading of the aldehyde/ketone auxiliary[18] enabled multimodal design of antiadhesive nanoparticles carrying various payloads in a designated avidity (Figure 3-1b and 3-1c).[14,15,19,20] Our Chapter 2 results uncovered that neuraminidase-1 (NEU1) sialidase distributed specifically in cancer cell surfaces is highly potential target molecule for the development of universal anticancer nanomedicines among common lysosomal glycosidases expressed dominantly in cancer cells (Figure 3-1d).[15,21] We demonstrate potential benefits of nanosomes targeting NEU1 sialidase to maximize therapeutic efficacy and minimize off-target toxicity of the irinotecan used as one of the most efficient payloads for the first-line anti-pancreatic cancer chemotherapy.

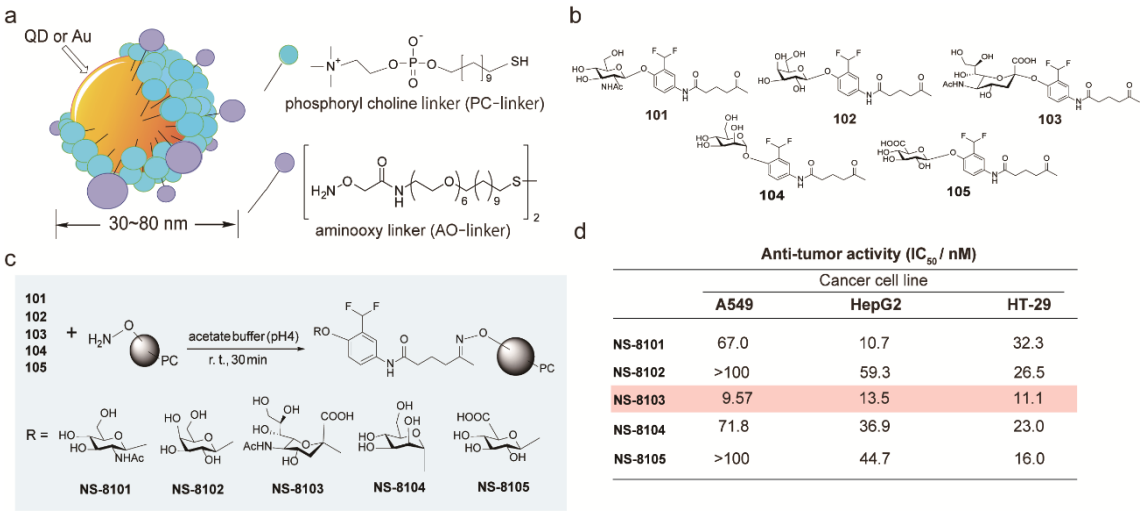

	Cancer cell line		
	A549	HepG2	HT-29
NS-8101	67.0	10.7	32.3
NS-8102	>100	59.3	26.5
NS-8103	9.57	13.5	11.1
NS-8104	71.8	36.9	23.0
NS-8105	>100	44.7	16.0

Figure 3-1. NEU1 sialidase is a promising target for the development of universal anti-cancer nanomedicines. (a) Nanosome is antiadhesive nanoparticle platform made of hard/high density-core materials such as semiconductor monocrystal quantum dots (QDs) and gold nanoparticles (AuNPs), and soft-shell mixed self-assembled monolayer (SAM) membrane of 11-mercaptoundecylphosphorylcholine (PC-linker) and an aminooxy-functional headgroup, 11,11'-dithio bis[undec-11-yl 12-(aminooxyacetyl)amino hexa(ethyleneglycol)] (AO-linker). (b) Chemical structures of irreversible mechanism-based covalent inhibitors for hexosaminidase **101**, galactosidase **102**, sialidase **103**, mannosidase **104**, and glucuronidase **105**, respectively. (c) The general method and chemical structures of nanosomes **NS-8101~NS-8105** displaying individual irreversible mechanism-based glycosidase inhibitors **101~105**. (d) In vitro anti-tumor effects of nanosomes displaying "suicide substrates" **NS-8101~NS-8105** on the proliferation of lung (A549), liver (HepG2), and colon cancer cells (HT-29), respectively.[15,21]

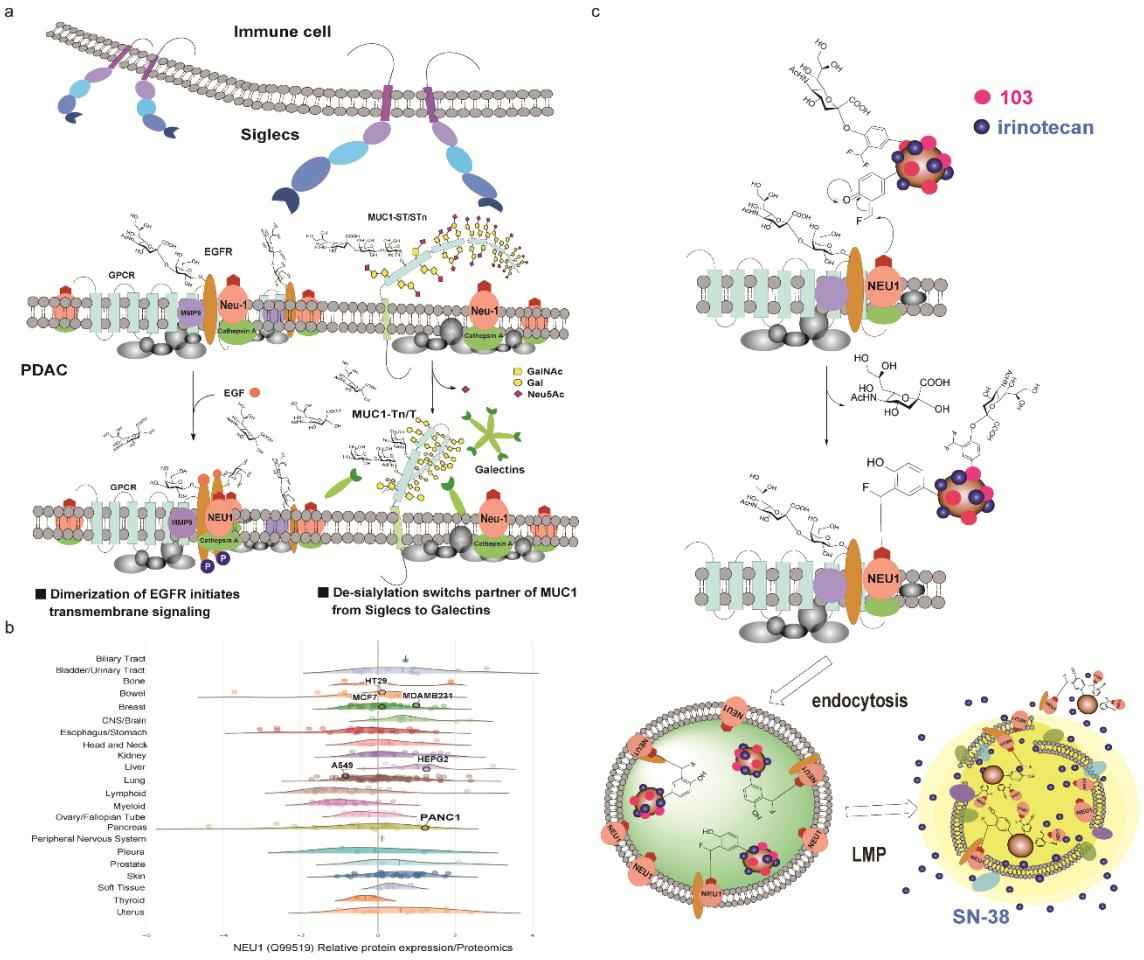

Figure. 3-2 PDAC cell surface NEU1 sialidase is an ideal target molecule. (a) Cancer NEU1 sialidase has emerged as a key player involved in the regulation of transmembrane signaling at the cell surface through modulation of the functions of cell surface various receptors such as epithelial growth factor receptor (EGFR)[22,23] and mucin glycoprotein MUC1[24,25,26] as the results of removal of the terminal sialic residues. (b) Relative expression levels revealed by proteomics of cancer cell NEU1 sialidase (This cartoon was made by modification of an original data presented in the database linked by, https://depmap.org/portal/gene/NEU1?tab=characterization&characterization=proteomics_283458). Relative expression levels of NEU1 in Panc-1 cells of pancreatic cancer and a few examples, HepG2 of liver, A549 of lung, MCF7 and MDA-MB-231 of breast, and HT-23 cells of colon cancer were represented. (c) Proposed mechanism of active targeting delivery of irinotecan by endocytic internalization of nanosomes displaying suicide substrate **103** and irinotecan prodrug, concurrently. Nanosomes displaying multiple "suicide substrates" produce large aggregates of nanoparticles by irreversible inactivation of lysosomal NEU1 sialidases and induce apoptotic lysosomal membrane permeabilization (LMP), resulting in

the release of SN-38 derived from nanosomes to the intracellular space.

3-2. Results and Discussion

3-2-1. Sorafenib

A sorafenib derivative (**201**) with an external ketone auxiliary group on the pyridine ring was synthesized based on the binding mode to vascular endothelial growth factor receptor 2 (VEGFR2). This modification enabled the formation of an oxime bond with aminooxy-functionalized NS, and **NS-8201** (PC/**201** = 16/1, 32/1, 128/1) and **NS-8103/8201** (PC/**103**/**201** = 4/1/1) were generated. Fluorescence correlation spectroscopy (FCS) in 100% fetal bovine serum (FBS) confirmed the non-fouling properties of **NS-8201** and showed that the PC-coated surface significantly improved solubility while maintaining anti-tumor activity.

The IC_{50} of sorafenib derivative **201** (DMSO) after 96 hours of co-culture with HepG2 cells was 2.1 μM, which was consistent with the previously reported activity of sorafenib (IC50 = 4.5 μM). It is worth noting that when **NS-8201** (PC/**201** = 32/1) was dissolved in aqueous solution, it showed anti-cancer activity that greatly exceeded that of **201** and sorafenib, with an IC_{50} of 33.5 nM. The antitumor effect of **NS-8201** was not affected by changing the payload density on the NS of sorafenib derivative **201**, suggesting that there is a threshold for surface density for the effective release of drugs in acidic endolysosomal environments.

Furthermore, **NS-8103/8201**, which is equipped with both irreversible NEU1 inhibitor **103** and sorafenib derivative **201**, showed potent and sustained anti-tumor activity against HepG2 cells over a variety of time periods (24, 48, 72, and 96 hours). Importantly, **NS-8103/8201** was found to be low cytotoxic to normal control cells, but toxic at high concentrations (50 nM or more) in long-term culture (96 hours or more). Live cell imaging revealed that **NS-8103/8201** was efficiently taken up by HepG2 cells, rapidly escaped from the lysosomal compartment, and underwent intracellular transport like that observed with **NS-8103**. In contrast, **NS-8201** was slowly taken up and tended to accumulate in the lysosome.

The rapid release of the **NS-8103/8201** from the lysosome is due to the presence of multiple NEU1 inhibitors, which allows for effective lysosomal membrane permeabilization (LMP) and the release of the active portion of sorafenib into the cytoplasm. This release occurs in response to the acidic environment of the lysosome (pH 5), which is different from that of the early endosome (pH 6.5). Interestingly, the released sorafenib fragments may inhibit the phosphorylation of the C-terminal tetrapeptide of NEU1, thereby promoting endocytosis and further amplifying the therapeutic effect.

These findings suggest that NEU1-mediated endocytosis could be an effective platform for

the delivery of small-molecule anti-tumor agents. The dual-function system of NS-8103/8201 highlights the potential for the simultaneous delivery of other targeted anti-cancer agents, but further research is needed to fully elucidate the mechanisms of NEU1-mediated endocytosis enhancement and its role in intracellular drug delivery.

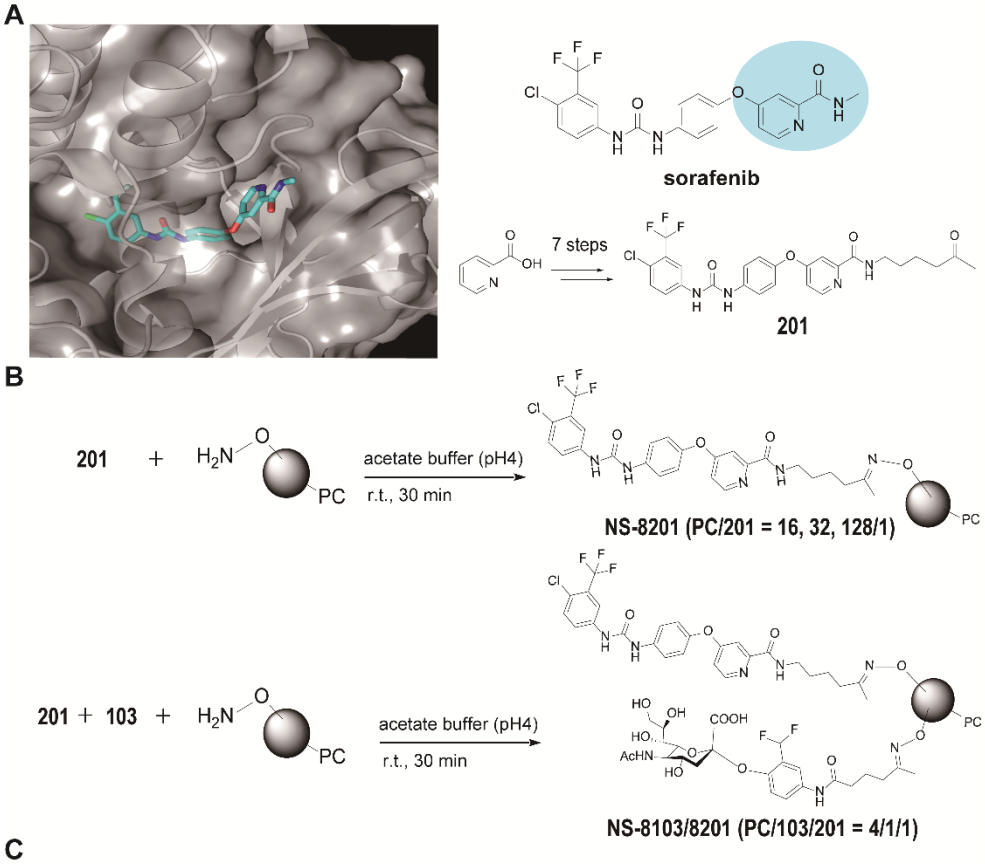
A
sorafenib
7 steps
201
B
201 + H2N PC
acetate buffer (pH4)
r.t., 30 min
NS-8201 (PC/201 = 16, 32, 128/1)
201 + 103 + H2N PC
acetate buffer (pH4)
r.t., 30 min
NS-8103/8201 (PC/103/201 = 4/1/1)
C
NS (PC/AO)
Normalized Intensity
Chemical Shift (ppm)
NS-8103/8201
Normalized Intensity
Chemical Shift (ppm)

Figure 3-3. Nanomedicine carrying sorafenib derivative. (A) Design and synthesis of sorafenib derivative 201 based on the X-ray crystallographic structure of VEGFR2 in complex with sorafenib (PDB ID: 4ASD). (B) Surface loading of sorafenib derivative **201** to AO/PC-NSs for the preparation of **NS-8201** and **NS-8103/8201**. (C) Proton NMR spectra (600 MHz) of NS (PC/AO=2/1) and isolated **NS-8103/8201** (2 M in D_2O) derived by the protocol established herein.

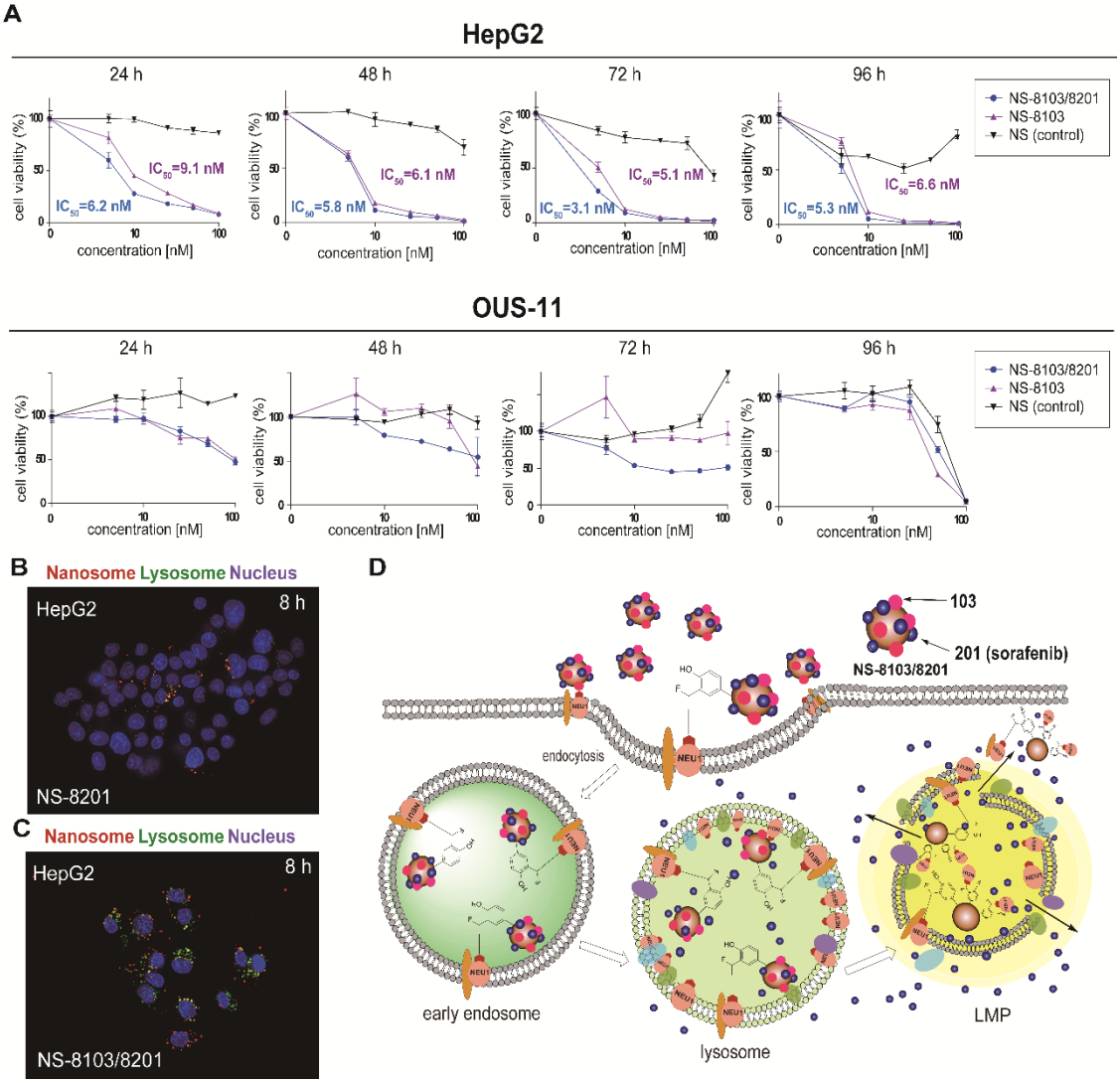

Figure 3-4. NEU1-mediated endocytosis of nanomedicine facilitates intra-cellular delivery of sorafenib derivative. (A) Antitumor activity of **NS-8201** and **NS-8103/8201** represented by loss of viability determined by the MTT assay of human liver cancer HepG2 cells and OUS-11 (control normal cells) after 24, 48, 72, and 96 h coincubation with 1~100 nM NSs. Intracellular distribution of **NS-8201** (B) and **NS-8103/8201** (C) at 8 h after co-culturing with HepG2 cells. Nuclei and lysosomes were stained with Hoechst 33342 (blue) and LysoTracker Green DND-26 (green). (D) Proposed mechanism of the up-take and

intracellular trafficking of **NS-8103/8201** through membrane tethered NEU1-mediated endocytosis.

3-2-2. Design and synthesis of anti-pancreatic cancer nanosomes targeting cell surface NEU1 sialidase

Human neuraminidase 1 (NEU1) plays a much more profound functional role, especially in cancer cells, than previously considered. It regulates ligand-receptor interactions on plasma membranes, as well as subsequent transmembrane signaling, metabolism, remodeling, and transportation of endocytosed glycoproteins between intracellular spaces and the plasma membrane.[22,24,27,28] As represented in Figure 3-5a, removal of the non-reducing terminal sialic acid (Neu5Ac) residues from epithelial growth factor receptor (EGFR) by cancer cell surface NEU1 sialidase facilitates dimerization of EGFR and initiates transmembrane signaling to activate tumor proliferation.[23] On the other hand, it seems likely that cancer cell surface NEU1 sialidase has a pivotal function to control key partner molecules of cell surface glycoproteins between Siglec and Galectin families.[29] Accumulated results demonstrated that cancer cell membrane tethered mucin MUC1 bearing sialyl-glycoforms interacts dominantly with Siglecs of M2-like macrophage (Mϕ) and other immune suppressive cancer associated fibroblast cells (CAFs) in the anti-inflammatory state,[30,31] whereas formation of galectin-lattice by MUC1 bearing asialo-O-glycans derived after removal of the terminal sialic acids may be crucial for tumor proliferation during a pro-inflammatory state of TME.[24,25,26]

As summarized in Figure 3-5d, we recently assessed the in vitro anti-tumor activity of nanosomes with designated "suicide substrates" that target five major lysosomal exoglycosidases. Endocytosis is mediated by the cancer cell surface sialidase (NEU1) of liver (HepG2), lung (A549), and colon (HT-29) cancers can serve as a novel mechanism for developing a universal anti-cancer chemotherapeutic drug delivery strategy.[15,21] These results greatly encouraged us to expand this concept to the active drug delivery system (DDS) to the PDAC cells. Indeed, higher level expression of NEU1 sialidase in Panc-1 cells has been reported by comparing with those of other human cancer cell lines (Figure 3-5b), suggesting that NEU1 sialidase of PDAC cell surface is a promising target and gate keeper for active DDS by nanomedicines. We hypothesized that NEU1 mediated endocytosis of nanosomes carrying an irreversible mechanism-based covalent inhibitor **103**[21] and an irinotecan analog will enhance dramatically therapeutic efficacy of intracellular inhibitory activity and safety of an active metabolite SN-38 released from a prodrug irinotecan analog against intracellular DNA topoisomerases (Figure 3-5c).

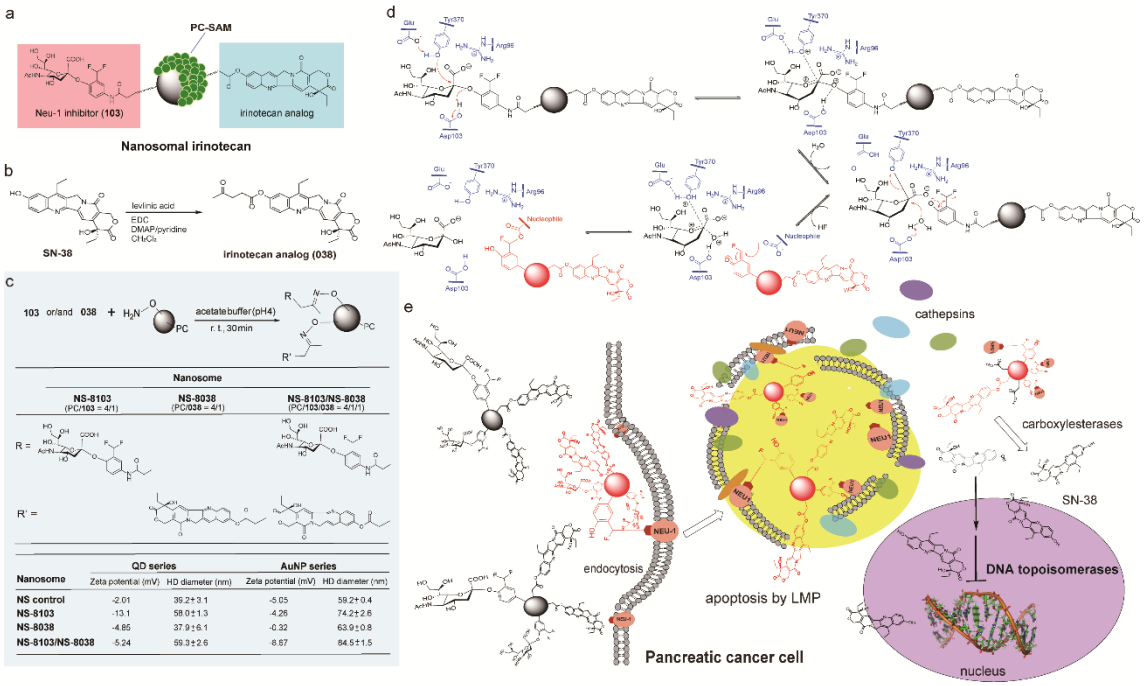

Figure 3-5. Design and synthesis of nanosomal irinotecan targeting NEU1 sialidase of PDAC cell surface. (a) Cartoon representation of the structure and compositions of nanosomal irinotecan. (b) Synthesis of an irinotecan analog from SN-38, (S)-4,11-diethyl-4-hydroxy-3,14-dioxo-3,4,12,14-tetrahydro-1H-pyrano [3',4':6,7] indolizino [1,2-b] quinolin-9-yl 4-oxopentanoate (**038**). (c) Conjugation of 103 or/and **038** with AO/PC-nanosome derived from QD core and AuNP core materials allows for the preparation of **NS-8103**, **NS-8038**, and **NS-8103/8038**, respectively. (d) Catalytic mechanism of the hydrolytic NEU1 sialidase with net retention of the anomeric configuration and subsequent irreversible mechanism-based covalent inhibition of NEU1 sialidase by nucleophilic addition reaction in the aglycone moiety, resulting in the nanoparticles immobilizing NEU1 (red). (e) Proposed endocytic mechanism of pancreatic cancer membrane-tethered NEU1 covalently anchored with nanosomes (red), in which internalized materials from plasma membrane are delivered into lysosomes and metabolized in a content dependent manner. Aggregation of nanoparticles by inactivation of multiple NEU1 sialidases in lysosomal compartment induces apoptotic lipid membrane permeabilization by large nanosome-NEU1 aggregates, releasing cathepsins to the intracellular space. Consequently, active metabolite SN-38, a potent inhibitor of DNA topoisomerases, is generated by hydrolysis of prodrug irinotecan analog with intracellular non-specific carboxylesterases.

To establish a facile procedure for the preparation of a novel modality of the nanosomal irinotecan illustrated in Figure 3-5a, a ketone auxiliary of SN-38 as an irinotecan analog, (S)-

4,11-diethyl-4-hydroxy-3,14-dioxo-3,4,12,14-tetrahydro-1H-pyrano [3',4':6,7] indolizino [1,2-b] quinolin-9-yl 4-oxopentanoate (**038**), was synthesized simply by coupling of SN-38 with levlinic acid by using 1-ethyl-3-(3-dimethylaminopropyl)-carbodiimide in the presence of DMAP/pyridine (Figure 3-5b). Based on the general procedure,[15,21] nanosomes, control NS, **NS-8103**, **NS-8038**, and **NS-8103/8038**, composed both of QD core for in vitro examinations using cultured tumor cells and in vivo live animal imaging analysis, and AuNP core for further non-clinical/preclinical studies were prepared and characterized, respectively. Covalent immobilization of the irinotecan analog **038** through an oxime-bond formation with aminooxy functional groups of AO/PC-mixed SAM surface of nanosomes enhanced dramatically water-solubility of highly hydrophobic SN-38, an active metabolite liberated from **038**. Importantly, all nanosomes prepared herein exhibited quite similar physical and chemical properties such as antifouling nature due to amphoteric PC-dominant mixed SAM surface, an exosome-like hydrodynamic diameter in a range from 30 to 80 nm (38 ~ 59 nm for QD core nanosomes, and 59 ~85 nm for AuNP core nanosomes, respectively), and their negative Zeta potential in a range from -0.32 to -13.1 mV. It should be emphasized that nanosomal platform enables simple and highly flexible ligand/payload design as a ketone/aldehyde auxiliary, facile and efficient protocols to display, and quality control of the antiadhesive nanomedicines.[14,15] Importantly, the pharmacokinetics, biodistribution, metabolism, and mechanism of the anticancer activity of the nanosomes depend strongly on the surface chemistry including contents and avidity of cargos, notably ligands targeting cancer cell surface receptors and cytotoxic chemotherapeutics. Figure 3-5d represents mechanism of the irreversible inhibition by nanosomes bearing “suicide substrate 103” against NEU1 sialidase of the pancreatic cancer cells, resulting in a product of NEU1 inactivated by the nucleophilic addition reaction between some nucleophiles of NEU1 sialidase and Michael acceptor of the aglycon moiety elaborated after hydrolysis of a sialic acid residue in 103 of a single nanosome.[21,32,33] Based on this mechanism, we thought that endocytosis of pancreatic cancer cell membrane-tethered NEU1 sialidase covalently anchored with nanosomes can deliver efficiently payloads to the intracellular space. Subsequently, aggregation of nanosomes formed by inactivating multiple NEU1 sialidases residing in the lysosomal compartment rapidly apoptotic lipid membrane permeabilization.[21] Consequently, active metabolite SN-38, a potent inhibitor of DNA topoisomerases, is generated by hydrolysis of prodrug irinotecan analog 038 displayed on the nanosome with intracellular non-specific carboxylesterases.

3-2-3. Nanosomes targeting NEU1 sialidase-mediated endocytosis enhances cellular uptake and anti-pancreatic cancer activity of cargo irinotecan in vitro

To test our hypothesis, we evaluated the efficiency with which cultured human Panc-1 cells took up fluorescent nanosomes prepared from semiconductor monocrystal QD-core into their cytoplasm. Fluorescence microscopic images showed that endocytic uptake of nanosomes by Panc-1 cells depends strongly on payloads displayed on the nanosomes. As expected, the uptake of nanosome **NS-8103** carrying multiple "suicide substrate" of NEU1 sialidase **103** by Panc-1 cells was observed distinctly at 8 h after incubation as large aggregations of red nanoparticles (Figure 3-6), leading to the apoptotic lipid membrane permeabilization (LMP).[24] In contrast, the uptake of the nanosome **NS-8038** carrying irinotecan analog **038** by Panc-1 cells was detected in endo-lysosomes as yellow merged area at 24 h after incubation without induction of LMP. It is important to note that, after 8 and 24 hours of incubation, Panc-1 cells incorporated nanosomes **NS-8103/8038** that co-displayed the "suicide substrate" of NEU1 and the irinotecan analog **038**. Multiple large nanosome aggregates were also observed in a manner similar to **NS-8103**. Apparently, the results demonstrate that attachment of suicide substrate 103 converts "NEU1 non-sensitive" nanosome **NS-8038** into "NEU1 targeting" nanosome **NS-8103/8038**, in which NEU1-mediated endocytosis promotes uptake of nanosomes by Panc-1 cells and anti-tumor effect of the active metabolite SN-38 generated as a result of apoptotic LMP and subsequent hydrolysis of payload irinotecan analog by intracellular non-specific carboxylesterases (Figure 3-6). On the other hand, normal control cells (human lung OUS-11) did not incorporate any nanosomes tested herein at 8 h after co-incubation, while non-specific endocytosis by OUS-11 cells of **NS-8038** and other nanosomes can be detected partly as yellow overlapped area in the endo-lysosomes at 24 h after co-culture. Importantly, nanosomes **NS-8103** and **NS-8103/8038** carrying multiple "suicide substrate" of NEU1 sialidase 103 did not produce any large red aggregates of nanoparticles in the endo-lysosomes of OUS-11 even at 24 h after co-incubation, demonstrating significantly lower level-expression of NEU1 sialidase in the normal mature human cells than cancer cells. It was conceivable that targeting PDAC cell surface NEU1 sialidase enables active delivery of cytotoxic chemotherapeutics to the intracellular space of pancreatic cancer cells without off-target toxicity in normal cells.

Our attention was next directed toward in vitro anti-tumor activity of nanosomes targeting NEU1 sialidase of Panc-1 cell surface. The inhibitory effects of nanosomes (control NS, **NS-8103**, **NS-8038**, and **NS-8103/8038**) on the Panc-1 cell proliferation were assessed by determining cancer cell viability in the presence of 1~100 nM nanosomes using the MTT

assay. As shown in Figure 3-6c, the results clearly uncovered beneficial significance of NEU1-mediated endocytosis in the development of smart nanomedicines by enabling active drug delivery to pancreatic cancer cells. It was demonstrated for the first time that co-displaying the irinotecan analog **038** and the suicide substrate of NEU1 **103** (**NS-8103/8038**) exhibits synergistically enhanced anti-PDAC activity in vitro (IC50=8.07 nM, equivalent to IC50 = 2.02 nM of **038**) when compared with the effects by **NS-8103** (IC50=12.4 nM) or **NS-8038** (IC50=71.5 nM), respectively. Given the significantly enhanced anti-tumor activity of **NS-8038** (equivalent to IC50 = 17.9 nM of **038**), the nanosomal platform might improve efficacy of various cytotoxic chemotherapeutics and off-target toxicity by the unique physical property and surface chemistry, even without cancer-specific targeting. These results clearly implicate the merit and versatility of nanosomal platforms in the development of new class and high-performance DDS, especially by targeting the cancer relevant NEU1 sialidase-mediated endocytic pathway. We considered that NEU1 mediated endocytosis enables active delivery of irinotecan-like small drugs with beneficial potentials to overcome a limitation due to off-target toxicity of cytotoxic chemotherapeutics for the patients with advanced PDAC.

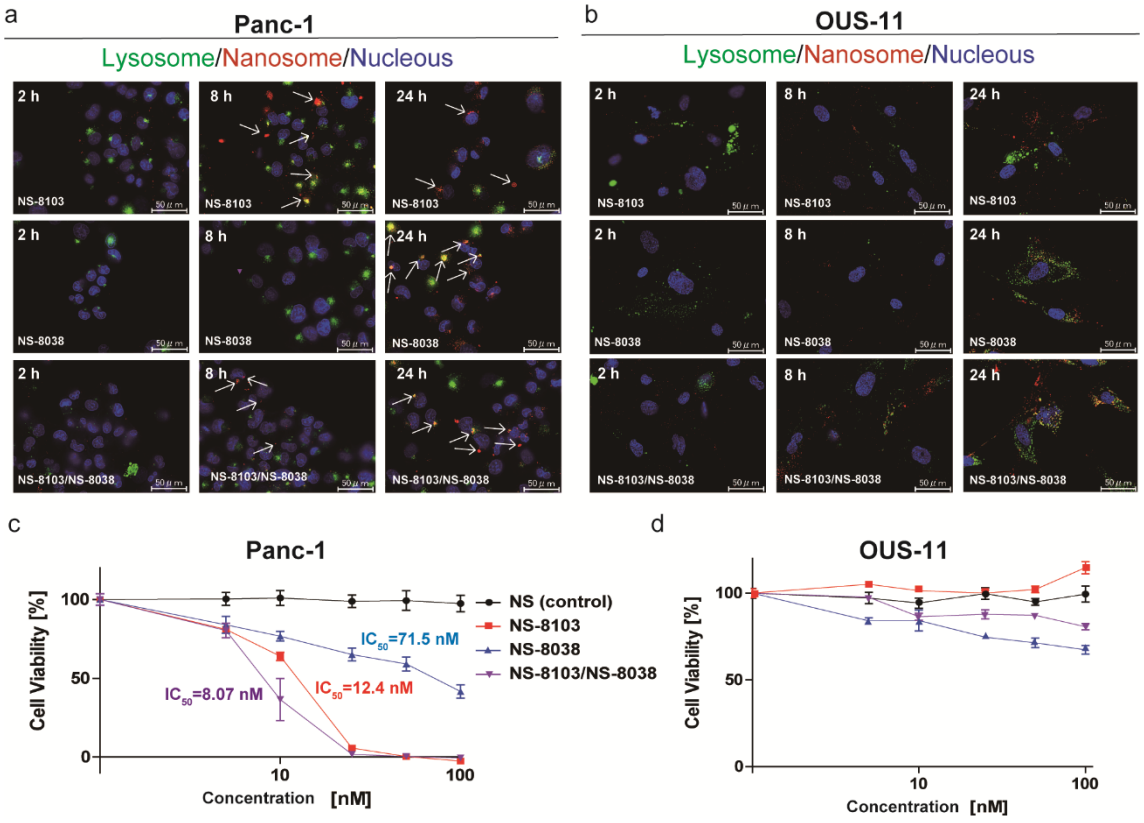

Figure 3-6. Cellular uptake and *in vitro* anti-pancreatic cancer activity of nanosomes. Intracellular distribution of 10 nM QD-core nanosomes, **NS-8103**, **NS-8038**, and **NS-8103/8038** (red) at 2, 8, and 24 h after co-culture with Panc-1 cells (a) and OUS-11 cells (b),

respectively (see, also Supplementary Information, Figure S3-9). Scale bar: 50 μm. Nuclei and lysosomes were stained with Hoechst 33342 (blue) and LysoTracker Green DND-26 (green). (c) Antitumor activity of nanosomes, NS (control), **NS-8103**, **NS-8038**, and **NS-8103/8038** represented by loss of viability determined by the MTT assay of human pancreatic cancer Panc-1 cells after 24 h coincubation with 1~100 nM nanosomes. (d) The effects of nanosomes, NS (control), **NS-8103**, **NS-8038**, and **NS-8103/8038** on cell viability of the normal human lung OUS-11 cells examined by the MTT assay after 24 h coincubation with 1~100 nM nanosomes.

3-3. Conclusion

This study reports for the first time that NEU1 distributed widely in cancer cell surfaces is a promising molecular target for creating an innovative anticancer therapeutic nanomedicine exhibiting potent and universal inhibitory effect on the proliferation of various cancer cells, and concurrently a desired "gatekeeper" for enabling transport of small molecular drugs to the intracellular space via specifically NEU1-mediated endocytic pathway. Our results demonstrate that antiadhesive nanomedicines displaying multiple suicide substrates of sialidase, such as **NS-8103** and **NS-8103/8201**, can inactivate irreversibly cancer cell surface-NEU1, internalize endocyticly into the cytoplasm, traffic to the endolysosomal compartments, perturb integrity in the lysosomal membranes, ultimately induce cell death. The rationale for targeting NEU1 is justified by its proven pivotal roles in the regulation of multistage tumorigenesis, particularly it should be emphasized that NEU1 and MMP9 cross-talk in alliance with GPCR controls ubiquitously activity of cancer cells EGFRs (RTKs) and subsequent downstream signaling cascade.[3-5] Merit of the present strategy to new generation nanocarrier based on the membrane tethered NEU1-mediated endocytosis is evident because **NS-8103/8201** bearing both irreversible NEU1 inhibitor **103** and sorafenib derivative **201** exhibits an enhanced higher anticancer activity to HepG2 cell growth (IC_{50}=3.1~6.2 nM) than **NS-8201** and **NS-8103** after 24~96 h co-incubation. The result clearly shows that antiadhesive nanosomal platform enables targeted delivery of hydrophobic sorafenib derivative **201** into the cancer cells cytoplasm by the NEU1-mediated endocytosis conducted through irreversible inactivation with suicide substrate **103** on **NS-8103/8201**, while precise molecular mechanisms in the enhanced inhibitory effect of the sorafenib fragments released from the NSs and feasibility of this concept in DDS to the targeted cancer tissues in vivo remain to be elusive. However, our previous results based on NS-based exosome models uncovered that glycocalyx, in particular, expression levels of sialic acidcontaining glycans of the surface glycoproteins determines long term circulation and delocalized biodistribution of the NSs displaying cancer cells N-glycans after intravenous injection to mice.[34,35] Therefore, antiadhesive NSs having multiple irreversible NEU1 inhibitor **103** would be an ideal nanocarrier allowing for in vivo targeting of cancer tissue/organ cell surface-NEU1 and subsequent endocytic intracellular delivery of various small antitumor reagents modified with a suited ketone/aldehyde auxiliary. More importantly, the concept and chemistry of the antiadhesive nanomedicine targeting endocytosis mediated by cancer cell surface-NEU1 can be expanded widely to other nanoparticular modalities such as gold nanoparticles, dendrimers, small exosome-like liposomes as well as new class non-toxic Cd-free QDs,[29] while the present results communicate preliminary data obtained by employing NSs synthesized from

commercially available fluorescent light-emitting QD core.

In conclusion, our results indicate that multifunctional nanosomes promote the delivery and intracellular transport of target molecules via the endocytosis pathway. Our results show that the anti-adhesion nanomedicines NS-8103 and NS-8103/8038, which are multiple suicide substrates of sialidase, irreversibly inactivate NEU1 on the surface of pancreatic cancer cells, are internalized into the cytoplasm by endocytosis, transported to the endolysosomal compartment, disrupt the integrity of the lysosomal membrane, and ultimately induce cell death. This innovative new anticancer nanomedicine has demonstrated the potential to be highly effective in pancreatic cancer, which still has a poor five-year survival rate.

3-4. Experimental Section

General methods and materials

All solvents and reagents were purchased from Aldrich Chemical Co. (Milwaukee, WI), Tokyo Chemical Industry Co. Inc. (Tokyo, Japan), Wako Pure Chemical Industries Co. Inc. (Tokyo, Japan), Funakoshi Co., Inc. (Japan, Tokyo), ENU Pharma, Co., Inc. (Hokkaido, Japan), Thermo Fisher Scientific K. K. Co. Inc. (Tokyo, Japan), Kanto Chemical Co. Inc. (Tokyo, Japan) and used without further purification. TOPO-coated QDs (655 nm and 800 nm) were purchased from Thermo Fisher Scientific K. K. Co. Inc. (Tokyo, Japan). Microcon YM50 was purchased from Millipore Co. Inc (Tokyo, Japan). 11-Mercaptoundecylphosphorylcholine (PC linker) was synthesized according to the procedure reported previously.1 11,11'-dithio bis [undec-11yl 12-(aminooxyacetyl) amino hexa (ethyleneglycol)] (AO linker) was synthesized by the method reported previously. Proton and carbon NMR were recorded at 25 °C on BRUKER AVANCE 600 MHz (1H: 600 MHz, 13C: 150 MHz) Bruker AVANCE (Bruker Biospin Co., Germany). Chemical shifts are indicated by ppm. Electro-spray ionization mass (ESI-MS) spectra were obtained with a JMS-T100LP mass spectrometer (JEOL Co. Inc., Tokyo, Japan). Matrix Assisted Laser Desorption Ionization time-of-flight mass (MALDI-TOFMS) spectra were obtained with an Ultraflex III TOF mass spectrometer (Bruker Daltonik GmbsH Co. Inc, Germany) equipped with a reflector and controlled by the Flexcontrol 3.0 software package. Reactions were monitored by thin layer.

Synthesis

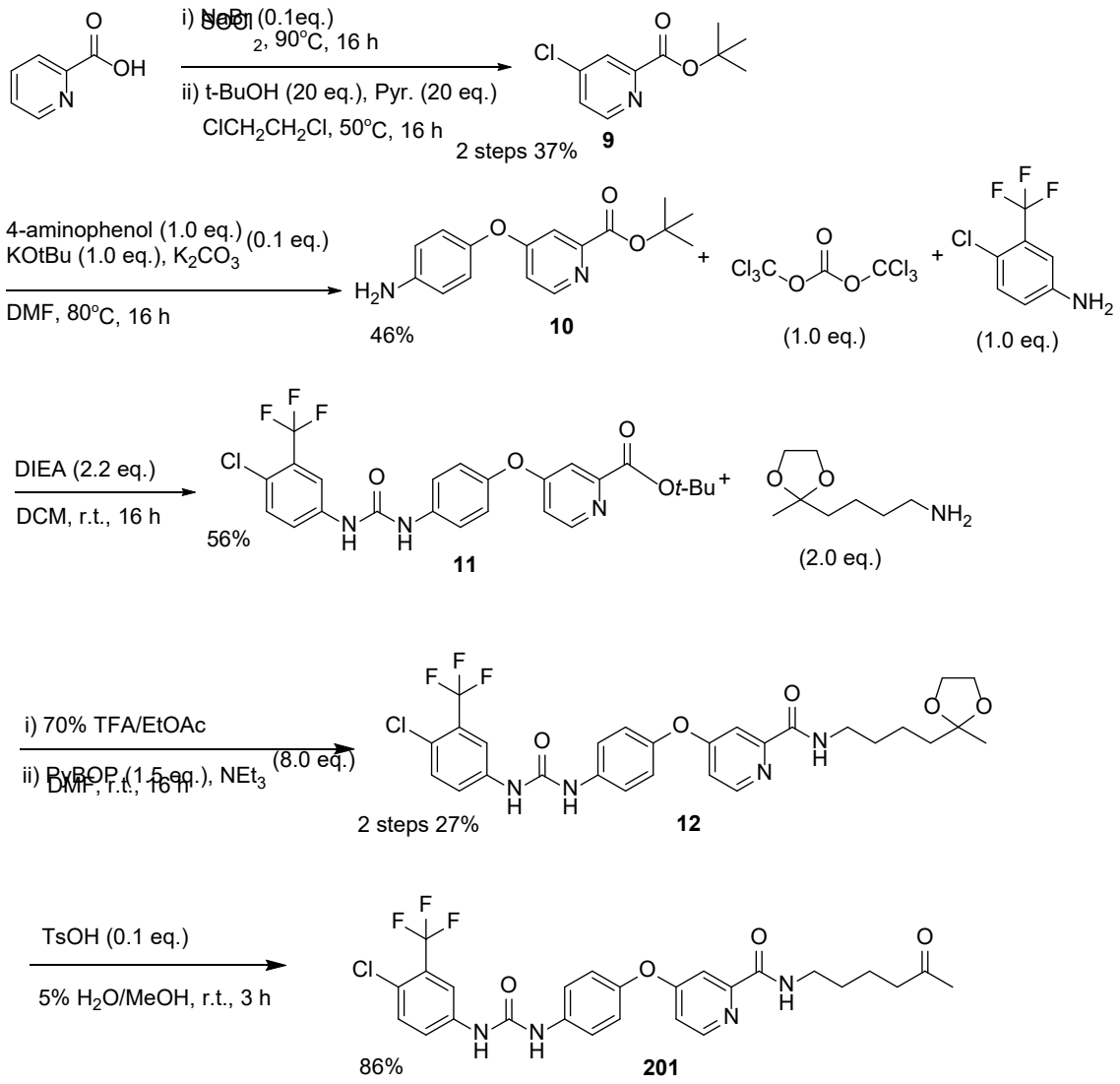

Scheme S3-1 Synthetic procedure of compound 201, partly according to the protocols reported previously.[36]

Tert-Butyl 4-chloropicolinate (**9**). To thionyl chloride (40 mL) was added picolinic acid (4.94 g, 40 mmol) followed by sodium bromide (412 mg, 4 mmol) at room temperature. The reaction mixture was warmed up to 90℃ and stirred overnight. After cooling, thionyl chloride was removed in vacuo. The crude product was used for further reaction without purification. To a solution of t-BuOH (76.0 mL), pyridine (64.0 mL) and 1,2-dichloroethane (150 mL) was added a solution of crude 4-chloropicolinyl chloride obtained above in 1,2-dichloroethane (60 mL) at 0 ℃. The reaction mixture was heated at 50 ℃ for 48 h. The reaction mixture was diluted with 1,2-dichloroethane and then washed with 5% citric acid several times. The

organic layer was dried over $MgSO_4$ and concentrated. The residue was purified by column chromatography on silica gel (25% EtOAc in hexane) to give a white solid (4.2 g, 49%). HR-ESI-MS: $C_{10}H_{12}ClNO_2Na$ [M+Na]+ calcd. 236.04488, found 236.04434 (Figure S3-3a). 1H NMR (500 MHz, CDCl3) δ ppm 8.63 (d, 1 H, J=5.37 Hz), 8.02 (d, 1 H, J=1.95 Hz), 7.43 (dd, 1 H, J=5.37, 1.95 Hz), 1.63 (s, 9 H). 13C NMR (125 MHz, $CDCl_3$) δ ppm 150.77, 126.09, 124.22, and 26.90 (Figure S3-3).

Tert-Butyl 4-(4-aminophenoxy)picolinate (**10**). To a solution of 4-aminophenol (2.7 g, 19 mmol) in DMF (40 mL) were added potassium tert-butoxide (2.13 g, 19 mmol). The reaction mixture warmed up to room temperature and stirred 30 min. Added compound 9 (4.0 g, 19 mmol) and potassium carbonate (262 mg, 1.9 mmol) was dissolved in DMF (60 mL). The reaction mixture was warmed up to 80℃ and stirred overnight. The reaction mixture was diluted with EtOAc and then washed with 5% citric acid several times. The organic layer was dried over $MgSO_4$ and concentrated. The residue was purified by silica gel column chromatography (50 % EtOAc in hexanes) to give a yellow oil (1.9 g, 35 %). HR-ESI-MS: $C_{16}H_{18}N_2O_3Na$ [M+Na]+ calcd. 309.12096, found 309.12035 (Figure S3-4a). 1H NMR (500 MHz, $CDCl_3$) δ ppm 8.52 (d, 1 H, J=5.37 Hz), 7.58 (d, 1 H, J=2.44 Hz), 6.87-6.92 (m, 3 H), 6.70-6.75 (m, 2 H), 3.54-3.85 (m, 2 H), 1.62 (s, 9 H). 13C NMR (125 MHz, $CDCl_3$) δ ppm 151.23, 121.89, 116.31, 113.05, 112.58, and 27.36 (Figure S3-4).

Tert-Butyl 4-(4-(3-(4-chloro-3-(trifluoromethyl)phenyl)ureido)phenoxy)picolinate (**11**). To a solution of triphosgene (110 mg, 0.37 mmol) in DCM (70 μL) was added 4-chloro-3-(trifluoromethyl)aniline (72 mg, 0.37 mmol) in DIEA/DCM (105mg, 0.407 mmol) drop wisely. The reaction mixture was stirred for 15 min. To this mixture was added compound 10 (106 mg, 0.37 mmol) in DIEA/DCM (105mg, 0.407 mmol) dropwise. The reaction mixture was stirred overnight. The reaction mixture was diluted with DCM and then washed with 5 % citric acid several times. The organic layer was dried over $MgSO_4$ and concentrated. The residue was purified by silica gel column chromatography (75 % EtOAc in hexanes) to give orange oily product **11** (47 mg, 25 %). HR-ESI-MS: $C_{24}H_{21}ClF_3N_3O_4Na$ [M+Na]+ calcd. 530.10649, found 530.10626 (Figure S3-5a). 1H NMR (500 MHz, DMSO-d6) δ ppm 9.17-9.20 (m, 1 H), 8.95-8.99 (m, 1 H), 8.51-8.54 (m, 1 H), 8.08-8.11 (m, 1 H), 7.57 (d, 4 H, J=8.79 Hz), 7.37-7.41 (m, 1 H), 7.16 (s, 2 H), 7.08-7.12 (m, 1 H), 1.51 (s, 9 H). 13C NMR (125 MHz, DMSO-d6) δ ppm 151.67, 151.158, 132.21, 123.25, 121.46, 120.69, 116.855, 114.79, 111.90, 40.17, and 27.66 (Figure S3-5).

4-(4-(3-(4-Chloro-3-(trifluoromethyl)phenyl)ureido)phenoxy)-N-(4-(2-methyl-1,3-

dioxolan-2-yl)butyl)picolinamide (**12**). To a solution of compound 11 (47 mg, 0.09 mmol) in EtOAc (6 mL) was added trifluoroacetic acid (14 mL) at room temperature and the solvent was removed in vacuo. To a solution of PyBOP (70 mg, 0.135 mmol) and triethylamine (100 μL, 0.72 mmol) in DMF (10 mL) prepared at 0°C was added above deprotected intermediate derived from 11 dropwise at room temperature and kept for 16 h. The reaction mixture was diluted with EtOAc and then washed with $NaHCO_3$ aq. several times. The organic layer was dried over $MgSO_4$ and concentrated. The residue was purified by silica gel column chromatography (25% EtOAc in hexane) to give orange oily compound **12** (31 mg, 58 %). This compound was used directly for the next step without further purification.

4-(4-(3-(4-Chloro-3-(trifluoromethyl)phenyl)ureido)phenoxy)-N-(5-oxohexyl)picolinamide (**201**). To a solution of compound 12 in MeOH (19 mL) and H2O (1 mL) was added p-toluenesulfonic acid (0.95mg, 0.005 mmol) and the mixture was stirred at room temperature for 3 h. The reaction mixture was diluted with EtOAc and then washed with $NaHCO_3$ aq. several times. The organic layer was dried over $MgSO_4$ and concentrated. The residue was purified by silica gel column chromatography (25% EtOAc in hexane) to give white solid product **201** (20 mg, 73 %). HR-ESI-MS: $C_{26}H_{24}ClF_3N_4O_4Na$ [M+Na]+ calcd. 571.13304, found 571.13209 (Figure S3-6a). 1H NMR (500 MHz, DMSO-d6) δ ppm 9.24-9.35 (m, 1 H), 9.03-9.13 (m, 1 H), 8.77-8.83 (m, 1 H), 8.52 (d, 1 H, J=5.86 Hz), 8.13 (d, 1 H, J=2.44 Hz), 7.66-7.70 (m, 1 H), 7.58-7.65 (m, 3 H), 7.38 (d, 1 H, J=2.44 Hz), 7.14-7.21 (m, 3 H), 3.22-3.28 (m, 2 H), 2.45 (s, 2 H), 2.07 (s, 3 H), 1.46 (d, 4 H, J=1.95 Hz). 13C NMR (125 MHz, DMSO-d6) δ ppm 150.46, 132.08, 123.38, 121.41, 120.56, 116.89, 114.34, 108.97, 41.49, 38.61, 29.48, 28.52, and 20.36 (Figure S3-6).

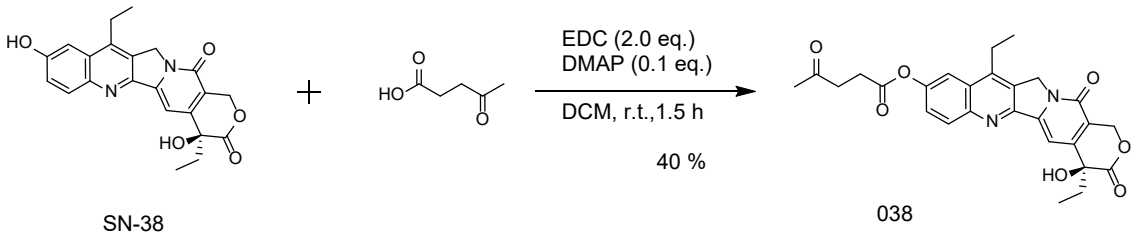

Scheme S3-2

(S)-4,11-diethyl-4-hydroxy-3,14-dioxo-3,4,12,14-tetrahydro-1H-pyrano [3',4':6,7] indolizino [1,2-b] quinolin-9-yl 4-oxopentanoate

SN-38 (500 mg, 1.27 mmol) was dissolved in CH_2Cl_2 (60 mL) and then levlinic acid (147 mg, 1.2 mmol), 1-ethyl-3-(3-dimethylaminopropyl)-carbodiimide (EDC, 485 mg, 2.53 mmol), DMAP (15.5 mg, 0.127 mmol) and Pyridine (150 μL) were added at room temperature.

After stirring for 3h, the reaction mixture was extracted by CH_2Cl_2. The organic layer was washed with H_2O and BRINE. The solution was dried with $MgSO_4$, filtered with filter, and evaporated under reduced pressure. Silica-gel chromatography (Chloroform/MeOH, 30:1) of the crude product gave pure compound (249.1 mg, 0.508 mmol, 40%). HR-ESI-MS: $C_{27}H_{27}N_2O_7$ [M+H]+ calcd 491.18128, found 491.18127.
1H NMR (500 MHz, DMSO-d6) δ ppm 0.89 (t, J=7.33 Hz, 3 H) 1.30 (t, J=7.57 Hz, 3 H) 1.88 (d, J=7.33 Hz, 2 H) 2.51 (q, J=1.77 Hz, 3 H) 2.83 (dd, J=6.84, 5.37 Hz, 1 H) 2.93 (t, J=6.35 Hz, 1 H) 3.18 (q, J=7.65 Hz, 2 H) 5.33 (s, 2 H) 5.44 (s, 2 H) 6.53 (s, 1 H) 7.33 (s, 1 H) 7.62 (dt, J=6.84, 2.44 Hz, 1 H) 7.98 (d, J=2.44 Hz, 1 H) 8.21 (d, J=9.28 Hz, 1 H). 13C NMR (500 MHz, DMSO-d6) δ ppm 8.68, 14.25, 21.69, 27.26, 29.59, 37.02, 39.81, 48.64, 65.37, 96.97, 115.09, 125.78, 131.36 (Figure S3-2).

Cell culture

PANC-1 (ECACC, UK), human pancreatic cancer cell, HepG2 (RIKEN cell bank, Japan), human hepatocellular carcinoma, were cultured in D-MEM (Wako, Osaka, Japan) containing 10% fetal bovine serum at 37 ℃ with 5 % CO_2. Capan-1 (ATCC, USA), human pancreatic cancer cell, was cultured in Iscove's Modified Dulbecco's Medium (IMDM) (Wako, Osaka, Japan) containing 20 % fetal bovine serum at 37 ℃ with 5 % CO_2. OUS-11 cell (Health Science Research Bank), normal human cell line from lung cancer patient, was grown in Eagle's Minimum Essential Medium (EMEM, Wako, Osaka, Japan) supplemented with 10% fetal bovine serum at 37 ℃ with 5 % CO_2.

Live cell imaging

Cells were suspended in medium supplemented with 10% FBS and seeded into 8-well cover glass (Thermo Fisher Scientific) at a seeding density of 5 x 10^4 cells/well. Cells were allowed to attach overnight in an incubator at 5 % CO_2 and 37 ℃. A stock solution of nanosomes was diluted with autoclaved MillQ and added to the existing medium; QD-derived nanosomes were added to a final concentration of 10 nM and co-cultured with the cells. At the indicated time points, cells were washed three times with Opti-MEM (Gibco) to remove nanosomes, stained with the lysosomal marker LysoTracker Green DND-26 (200 μL, 5 nM/Opti-MEM), and incubated in an incubator at 37 ℃, 5 % CO_2 for 30 minutes. The nuclei were then stained with Hoechst 33342 (2 μL, 1 ng/μL/Opti-MEM) and incubated in an incubator at 37 ℃, 5 % CO_2 for 15 min. Stained cells were photographed using a BIOREV BZ-9000 series 2nd generation all-in-one fluorescence microscope (Keyence, Osaka, Japan) equipped with a 60

× objective. The captured images were analyzed using BZ-II Analyzer software (Keyence, Osaka, Japan).

Cell viability assay

Human pancreatic cancer cells PANC-1 were seeded in 96-well plate (Thermo Fisher, USA), at 5 x 10^3 cells/well/100 µL and incubated 37 ℃ with 5 % CO_2 for 24h. After incubation, medium was replaced by reagents (nanosomes in 0, 5, 10, 25, 50, and 100 nM concentrations, respectively) and incubated for 24 h at 37 ℃ with 5% CO_2. Cell viability assay was performed according to the procedure of a Cell Counting Kit-8 solution (Dojindo, Kumamoto, Japan). After 24 h incubation, cells were washed with medium (100 µL) and then replaced with new medium (100 µL). 10 µL Cell Counting Kit-8 solution was added to the medium and incubated at 37 ℃ with 5 % CO_2 for 1 h. The optical density was measured with microplate reader (spectraMax M5, Molecular Devices Japan, Tokyo). All values are expressed as means ± the standard error of the mean (SEM), and the assays were repeated three times. The error bar graphs in each picture were generated with Prism 4.0 (GraphPad Software, Inc., San Diego, CA).

At antitumor activity of free compounds experiences, HepG2, A549, HT-29, DLD-1 and Panc-1 cells were seeded in 96-well plate (Thermo Fisher, USA), at 5 x 10^3 cells/well/100 µL and incubated at 37 ℃ with 5 % CO_2 for 24 h. After incubation, medium was replaced by D-MEM containing reagents (free compounds in 0, 5, 10, 20, 40, 80 and 100 µM concentrations, respectively or 0, 5, 10, 20, 40, 80µM), and incubated for 48 h at 37 ℃ with 5 % CO_2. Cell viability assay was performed according to the procedure of a Cell Counting Kit-8 solution (Dojindo, Kumamoto, Japan).

3-5. Reference

[1] Smith, M. A., Houghton, P. A proposal regarding reporting of in vitro testing results. *Clin. Cancer Res.* 2013, *19*, 2828-2833.

[2] Liu, L. *et al.*, Sorafenib blocks the RAF/MEK/ERK pathway, inhibits tumor angiogenesis, and induces tumor cell apoptosis in hepatocellular carcinoma model PLC/PRF/5. *Cancer Res.* 2006, *66*, 11851-11858

[3] Rahib, L., Smith, B.D., Aizenberg, R., Rosenzweig, A.B., Fleshman, J.M., Matrisian, L.M., Projecting cancer incidence and deaths to 2030: the unexpected burden of thyroid, liver, and pancreas cancers in the United States. *Cancer Res.* **74**, 2913–2921 (2014)

[4] Rahib, L., Wehner, M.R., Matrisian, L.M., Nead, K.T., Estimated projection of US cancer incidence and death to 2040. *JAMA Netw. Open* **4**, e214708 (2021)

[5] Christopher J. Halbrook, Costas A. Lyssiotis, Marina Pasca di Magliano, Anirban Maitra, Pancreatic cancer: Advances and challenges. *Cell* **186**, 1729-1754 (2023)

[6] Jorg Kleeff, Murray Korc, Minoti Apte, Carlo La Vecchia, Colin D. Johnson, Andrew V. Biankin, Rachel E. Neale, Margaret Tempero, David A. Tuveson, Ralph H. Hruban, John P. Neoptolemos, Pancreatic cancer. N*at. Rev. Dis. Prim.* **2**, 1-22 (2016)

[7] Thierry Conroy, Françoise Desseigne, Marc Ychou, Olivier Bouché, Rosine Guimbaud, Yves Bécouarn, Antoine Adenis, Jean-Luc Raoul, Sophie Gourgou-Bourgade, Christelle de la Fouchardière, Jaafar Bennouna, Jean-Baptiste Bachet, Faiza Khemissa-Akouz, Denis Péré-Vergé, Catherine Delbaldo, Eric Assenat, Bruno Chauffert, Pierre Michel, Christine Montoto-Grillot, Michel Ducreux, FOLFIRINOX versus Gemcitabine. *N. Engl. J. Med.* **364**, 1817-1825 (2011)

[8] Daniel D. Von Hoff, Thomas Ervin, Francis P. Arena, E. Gabriela Chiorean, Jeffrey Infante, M.D., Malcolm Moore, M.D., Thomas Seay, M.D., Sergei A. Tjulandin, M.D., Wen Wee Ma, M.D., Mansoor N. Saleh, Marion Harris, Michele Reni, Scot Dowden, Daniel Laheru, Nathan Bahary, Ramesh K. Ramanathan, Josep Tabernero, Manuel Hidalgo, David Goldstein, Eric Van Cutsem, Xinyu Wei, Jose Iglesias, Markus F. Renschler, Increased Survival in Pancreatic Cancer with nab-Paclitaxel plus Gemcitabine. *N. Engl. J. Med.* **369**, 1691-1703

(2013)

[9] Drummond DC, Noble CO, Guo Z, Hong K, Park JW, Kirpotin DB., Development of a highly active nanoliposomal irinotecan using a novel intraliposomal stabilization strategy. *Cancer Res.* **66**, 3271-3277 (2006)

[10] Ashish V. Kalra, Jaeyeon Kim, Stephan G. Klinz, Nancy Paz, Jason Cain, Daryl C. Drummond, Ulrik B. Nielsen, and Jonathan B. Fitzgerald, Preclinical Activity of Nanoliposomal Irinotecan Is Governed by Tumor Deposition and Intratumor Prodrug Conversion. *Cancer Res.* **74**, 7003-7013 (2014)

[11] Andrea Wang-Gillam, Chung-Pin Li, György Bodoky, Andrew Dean, Yan-Shen Shan, Gayle Jameson, Teresa Macarulla, Kyung-Hun Lee, David Cunningham, Jean F Blanc, Richard A Hubner, Chang-Fang Chiu, Gilberto Schwartsmann, Jens T Siveke, Fadi Braiteh, Victor Moyo, Bruce Belanger, Navreet Dhindsa, Eliel Bayever, Daniel D Von Hoff , Li-Tzong Chen, Nanoliposomal irinotecan with fluorouracil and folinic acid in metastatic pancreatic cancer after previous gemcitabine-based therapy (NAPOLI-1): a global, randomised, open-label, phase 3 trial. *Lancet.* **387**, 545–557 (2016)

[12] Adham S. Bear, Robert H. Vonderheide, Mark H. O'Hara, Challenges and Opportunities for Pancreatic Cancer Immunotherapy. *Cancer Cell.* **38**, 788-802 (2020).

[13] Qian Sun, Zhenya Hong, Cong Zhang, Liangliang Wang, Zhiqiang Han, Ding Ma, Immune checkpoint therapy for solid tumours: clinical dilemmas and future trends. *Signal Trans. Targeted Ther.* **8**, 320 (2023)

[14] T. Ohyanagi, N. Nagahori, K. Shimawaki, H. Hinou, T. Yamashita, A. Sasaki, T. Jin, T. Iwanaga, M. Kinjo, S.-I. Nishimura, Importance of sialic acid residues illuminated by live animal imaging using phosphorylcholine self-assembled monolayers-coated quantum dots. *J. Am. Chem. Soc.* **133**, 12507-12517 (2011)

[15] R. Koide, S.-I. Nishimura, Antiadhesive nanosomes facilitate targeting of lysosomal GlcNAc salvage pathway through derailed cancer endocytosis. *Angew. Chem. Int. Ed.* **58**, 14513-14518 (2019)

[16] R. Erik Holmlin, Xiaoxi Chen, Robert G. Chapman, Shuichi Takayama, George M.

Whitesides, Zwitterionic SAMs that Resist Nonspecific Adsorption of Protein from Aqueous Buffer. *Langmuir* **17**, 2841-2850 (2001)

[17] N. Nagahori, M. Abe, S.-I. Nishimura, Structural and functional glycosphingolipidomics by glycoblotting with aminooxy-functionalized gold nanoparticle. *Biochemistry* **48**, 583-594 (2009).

[18] S.-I. Nishimura, K. Niikura, M. Kurogochi, T. Matsushita, M. Fumoto, H. Hinou, R. Kamitani, H. Nakagawa, K. Deguchi, N. Miura, K. Monde, H. Kondo, High Throughput Protein Glycomics: Combined Use of Chemoselective Glycoblotting and MALDI-TOF/TOF Mass Spectrometry. *Angew. Chem. Int. Ed.* **44**, 91-96 (2004)

[19] R. S. Tan, K. Naruchi, M. Amano, H. Hinou, S.-I. Nishimura, Rapid Endolysosomal Escape and Controlled Intracellular Trafficking of Cell Surface Mimetic Quantum-Dots-Anchored Peptides and Glycopeptides. *ACS Chem. Biol.* **10**, 2073-2086 (2015)

[20] R. Koide, N. Hirane, D. Kambe, Y. Yokoi, M. Otaki, S.-I. Nishimura, Antiadhesive nanosome elicits role of glycocalyx of tumor cell-derived exosomes in the organotropic cancer metastasis. *Biomaterials* **280**, 121314 (2020)

[21] K. Murakami, D. Kambe, Y. Yokoi, H. Wakui, S. Hayakawa, N. Hirane, R. Koide, M. Otaki, N. Nagahori, S.-I. Nishimura, Smart Nanomedicine Targeting Endocytosis Mediated by Cancer Cell Surface Neuraminidase-1. *Adv. NanoBiomed. Res.* **3**, 2300076 (2023)

[22] Alanna M. Gilmour, Samar Abdulkhalek, Timothy S.W. Cheng, Farah Alghamdi, Preethi Jayanth, Leah K. O'Shea, Olivia Geen, Luis A. Arvizu, Myron R. Szewczuk, A novel epidermal growth factor receptor-signaling platform and its targeted translation in pancreatic cancer. *Cell Signal.* **25**, 2587–2603 (2013).

[23] Y-C. Liu, H-Y. Yen, C-Y. Chen, C-H. Chen, P-F. Cheng, Y.-H. Juan, C-H. Chen, K-H. Khoo, C-J. Yu, P-C. Yang, T-L. Hsu, C-H. Wong, Sialylation and fucosylation of epidermal growth factor receptor suppress its dimerization and activation in lung cancer cells. *Proc. Natl. Acad. Sci. USA* **108**, 11332-11337 (2011)

[24] Erik P. Lilleho, Sang Won Hyun, Chiguang Feng, Lei Zhang, Anguo Liu, Wei Guang, ChinhNguyen, Irina G. Luzina, Sergei P. Atamas, Antonino Passaniti, William S. Twaddell,

Adam C. Puch, Lai-Xi Wang, Alan S. Cross, Simeon E. Goldblum, NEU1 Sialidase Expressed in Human Airway Epithelia Regulates Epidermal Growth Factor Receptor (EGFR) and MUC1 Protein Signaling. *J. Biol. Chem.* **287**, 8214-8231 (2012)

[25] Qicheng Zhao, Xiuli Guo, Gerard B Nash, Philip C Stone, John Hilkens, Jonathan M Rhodes, Lu-Gang Yu, Circulating galectin-3 promotes metastasis by modifying MUC1 localization on cancer cell surface, *Cancer Res.* **69**, 6799-6806 (2009)

[26] Qicheng Zhao, Monica Barclay, John Hilkens, Xiuli Guo, Hannah Barrow, Jonathan M Rhodes, Lu-Gang Yu, Interaction between circulating galectin-3 and cancer-associated MUC1 enhances tumour cell homotypic aggregation and prevents anoikis. *Mol. Cancer* **9**, 154 (2010)

[27] Kiven E. Lukong, Volkan Seyrantepe, Karine Landry, Stephanie Trudel, Ali Ahmad, William A. Gahl, Stephane Lefrancois, Carlos R. Morales, Alexey V. Pshezhetsky, Intracellular Distribution of Lysosomal Sialidase Is Controlled by the Internalization Signal in Its Cytoplasmic Tail. *J. Biol. Chem.* **276**, 46172-46181 (2001)

[28] Feng Liang, Volkan Seyrantepe, Karine Landry, Rasheed Ahmad, Ali Ahmad, Nicholas M. Stamatos, Alexey V. Pshezhetsky, Monocyte Differentiation Up-regulates the Expression of the Lysosomal Sialidase, Neu1, and Triggers Its Targeting to the Plasma Membrane via Major Histocompatibility Complex Class II-positive Compartments. *J. Biol. Chem.* **281**, 27526-27538 (2006)

[29] Jan C. Lumibao, Jacob R. Tremblay, Jasper Hsu, Dannielle D. Engle, Altered glycosylation in pancreatic cancer and beyond. *J. Exp. Med.* **219**, e20211505 (2022)

[30] M. S. Macauley, P. R. Crocker, J. C. Paulson, Siglec-mediated regulation of immune cell function in disease. *Nat. Rev. Immunol.* **14**, 653-666 (2014)

[31] Ernesto Rodriguez, Kelly Boelaars, Kari Brown, R. J. Eveline Li, Laura Kruijssen, Sven C. M. Bruijns, Thomas van Ee, Sjoerd T. T. Schetters, Matheus H. W. Crommentuijn, Joost C. van der Horst, Nicole C. T. van Grieken, Sandra J. van Vliet, Geert Kazemier, Elisa Giovannetti, Juan J. Garcia-Vallejo, Yvette van Kooyk, Sialic acids in pancreatic cancer cells drive tumour associated macrophage differentiation via the Siglec receptors Siglec-7 and Siglec-9. *Nat. Commun.* **12**, 1270 (2021)

[32] H. Hinou, M. Kurogochi, H. Shimizu, S.-I. Nishimura, Characterization of *Vibrio cholerae* Neuraminidase by a Novel Mechanism-Based Fluorescent Labeling Reagent. *Biochemistry* **44**, 11669-11675 (2005)

[33] S. Carvalho, Mauro Sola-Penna, Isadora A Oliveira, Samuel Pita, Arlan S Gonçalves, Bianca C Neves, Francisco R Sousa, Leonardo Freire-de-Lima, Masaki Kurogochi, Hiroshi Hinou, Shin-Ichiro Nishimura, Lucia Mendonça-Previato, Jose O Previato, Adriane R Todeschini, A new class of mechanism-based inhibitors for *Trypanosoma cruzi trans*-sialidase and their influence on parasite virulence. *Glycobiology* **20**, 3772-3776 (2010)

[34] Sandrine Barbier, Benjamin Beaufils, Ricardo de Miguel, Melissa Reyre, Yannick Le Meitour, Andreanne Lortie, Marc Hillairet de Boisferon, Sophie Chaumeron, Anne Espirito, Lina Fossati, Pauline Lagarde, Stephan Klinz, Arunthathi Thiagalingam, Stephane Lezmi, Florence Meyer-Losic, Liposomal Irinotecan Shows a Larger Therapeutic Index than Non-liposomal Irinotecan in Patient-Derived Xenograft Models of Pancreatic Cancer. *Oncol Ther* **11**, 111-128 (2023)

[35] Oluwabukunmi Olajubutu, Omotola D. Ogundipe, Amusa Adebayo, Simeon K. Adesina, Drug Delivery Strategies for the Treatment of Pancreatic Cancer. *Pharmaceuticals* **15**, 1318 (2023)

[36] Hwang, S. H.; Wecksler, A. T.; Zhang, G.; Morisseau, C.; Nguyen, L. V.; Fu, S. H.; Hammock, B. D., Synthesis and biological evaluation of sorafenib- and regorafenib-like sEH inhibitors. *Bioorg. Med. Chem. Lett.* 2013, ***23***, 3732-3737.

[37] Zev A Wainberg, Davide Melisi, Teresa Macarulla, Roberto Pazo Cid, Sreenivasa R Chandana, Christelle De La Fouchardière, Andrew Dean, Igor Kiss, Woo Jin Lee, Thorsten O Goetze, Eric Van Cutsem, A Scott Paulson, Tanios Bekaii-Saab, Shubham Pant, Richard A Hubner, Zhimin Xiao, Huanyu Chen, Fawzi Benzaghou, Eileen M O'Reilly, NALIRIFOX versus nab-paclitaxel and gemcitabine in treatment-naive patients with metastatic pancreatic ductal adenocarcinoma (NAPOLI 3): a randomised, open-label, phase 3 trial. Lancet **402**, 1272-1281 (2023).

3-6. Supporting Information

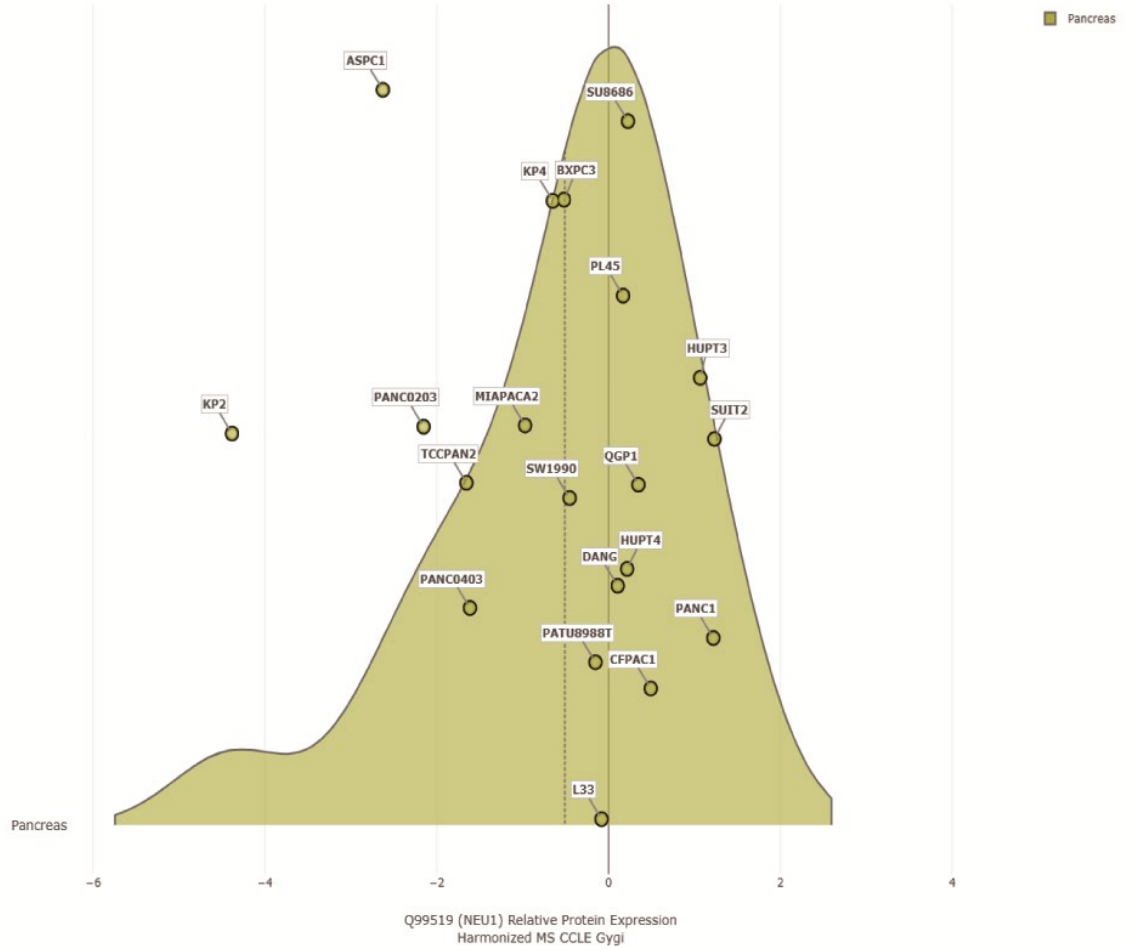

Figure S3-1. Relative expression levels of NEU1 sialidase in human pancreatic cancer cells. This figure was made by modification of an original data presented in the database linked by, https://depmap.org/portal/gene/NEU1?tab=characterization&characterization=proteomics_283458).

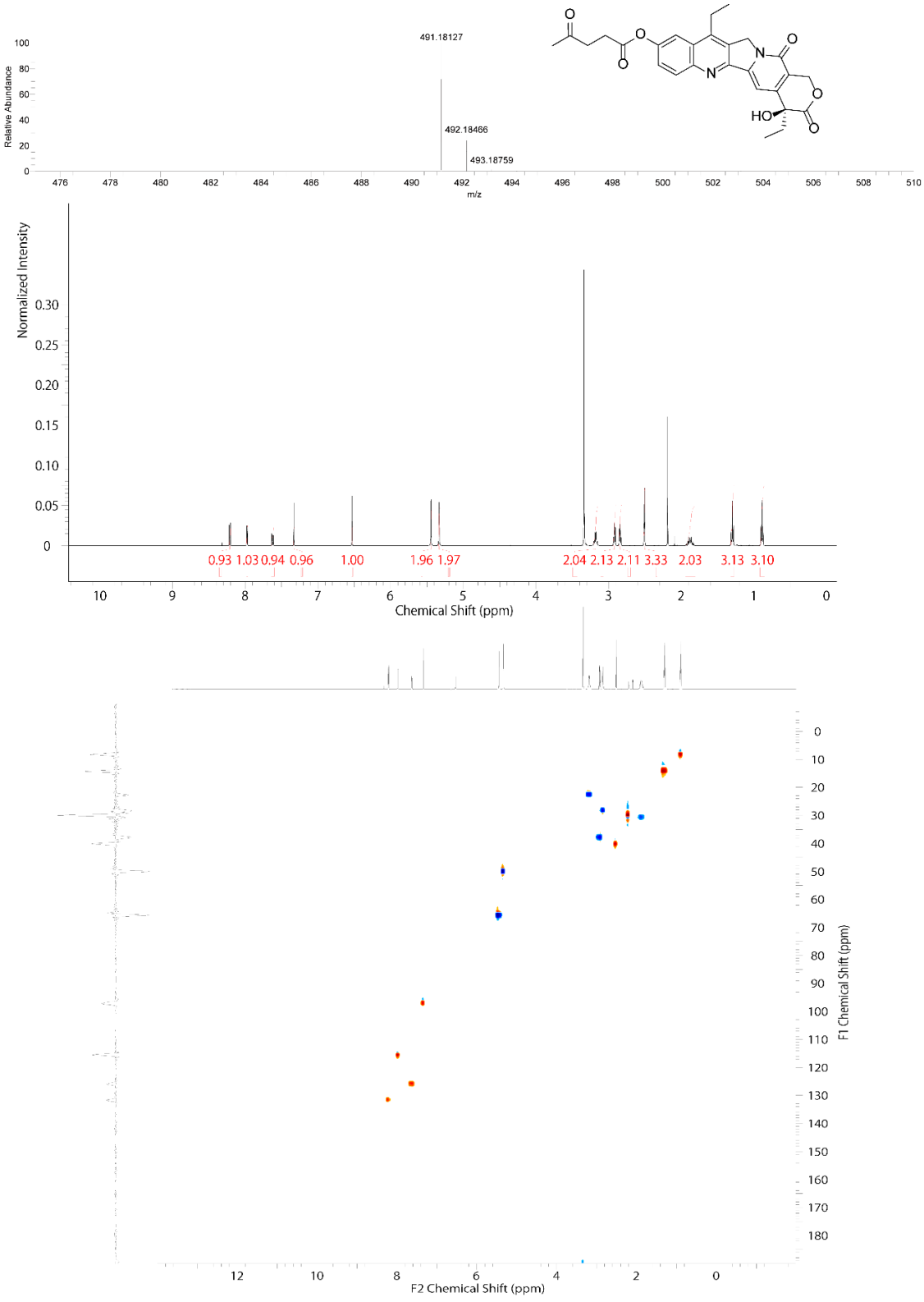

Figure S3-2. HR-MS and NMR spectra of compound **038**

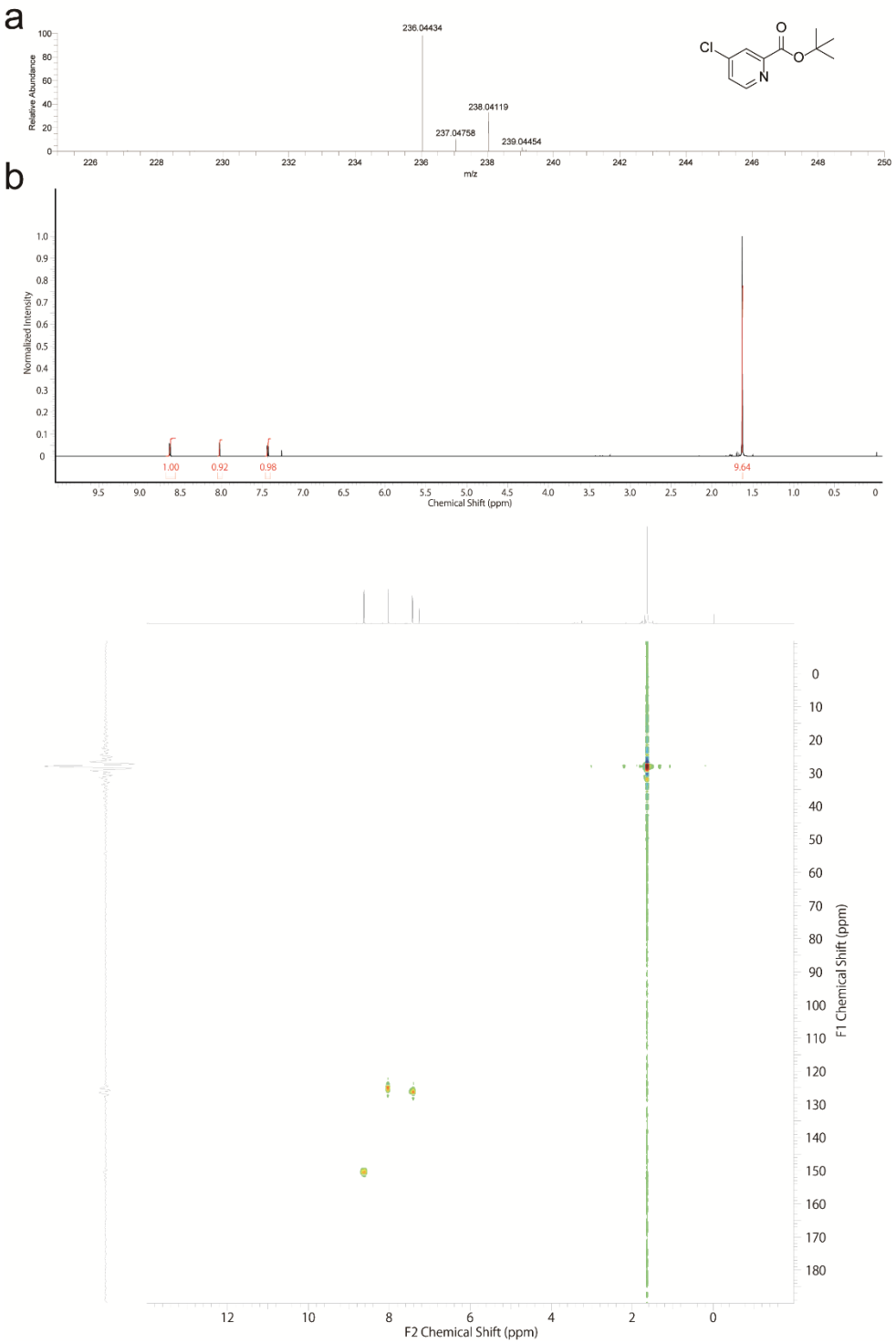

Figure S3-3. HR-MS and NMR of compound **9**.

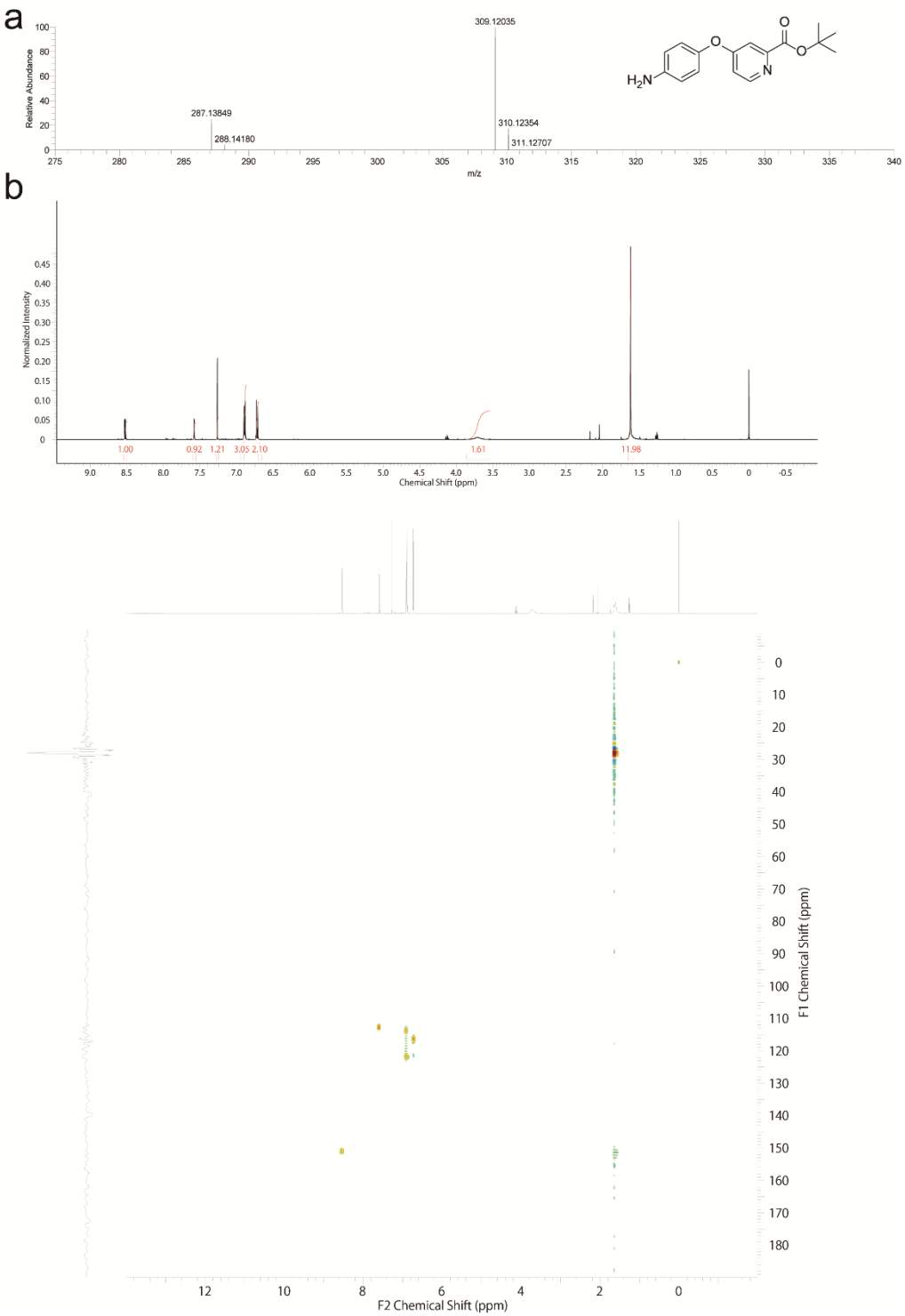

Figure S3-4. HR-MS and NMR of compound **10**.

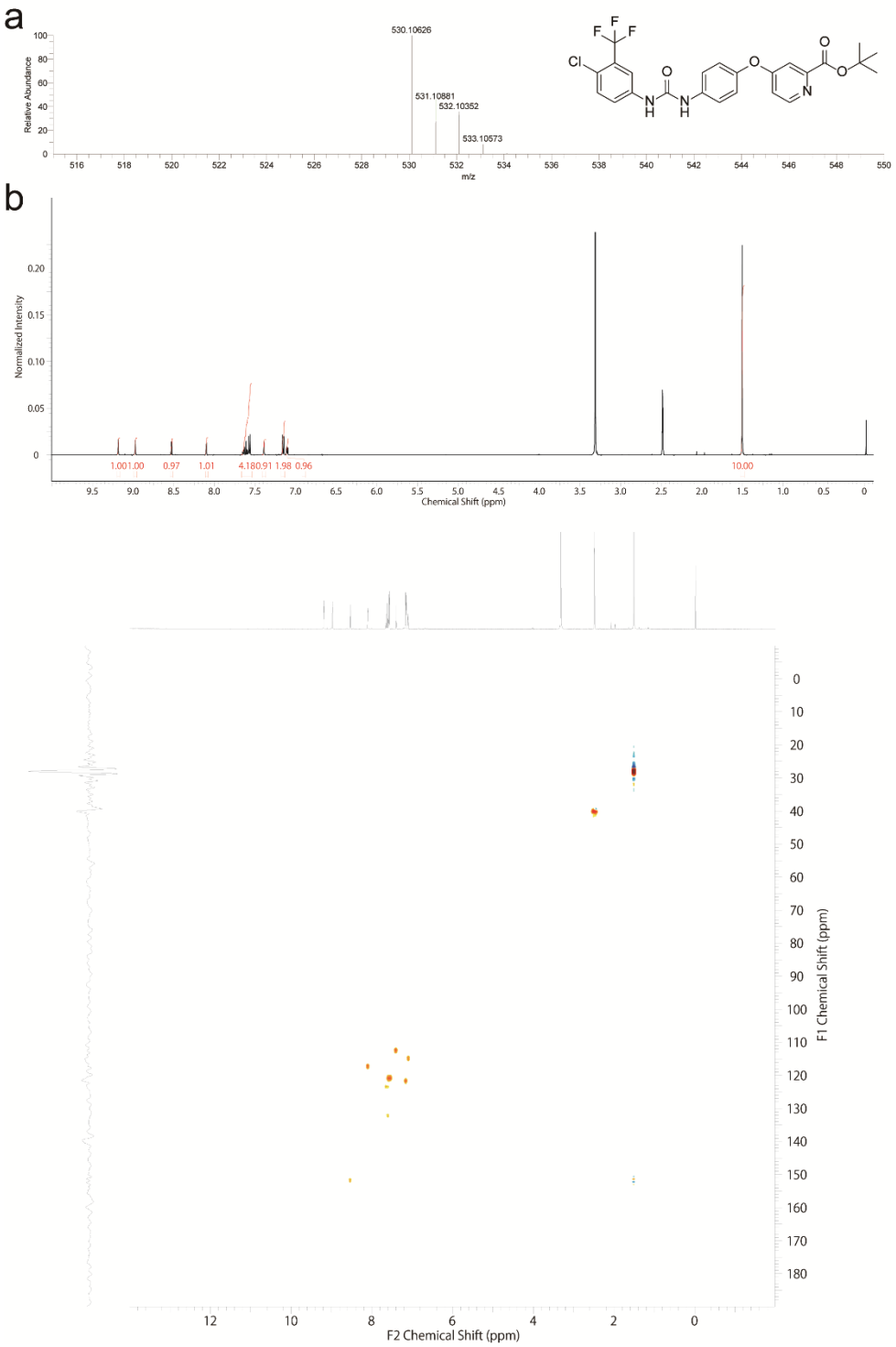

Figure S3-5. HR-MS and NMR of compound **11**.

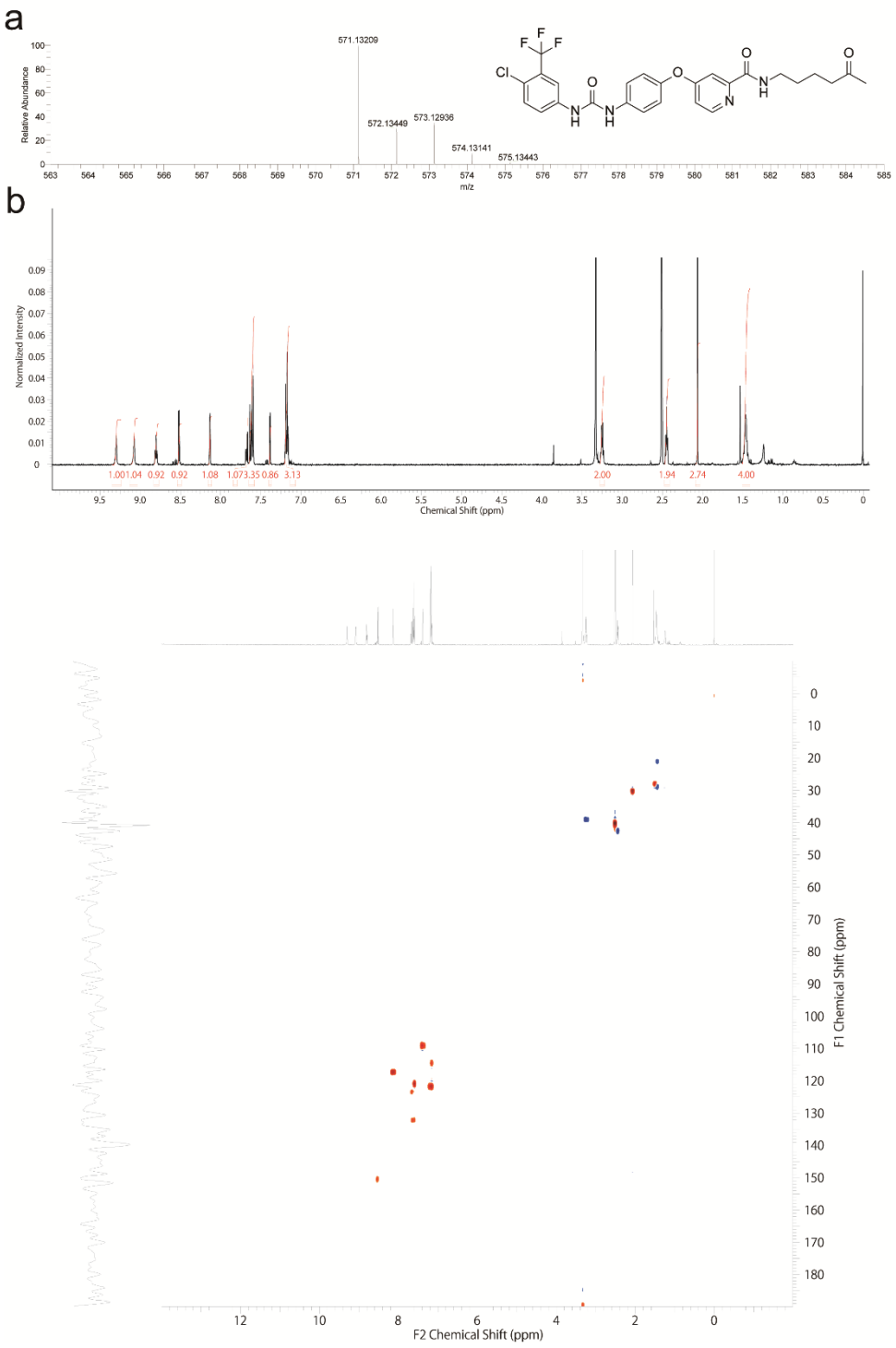

Figure S3-6. HR-MS and NMR of compound **201**.

a

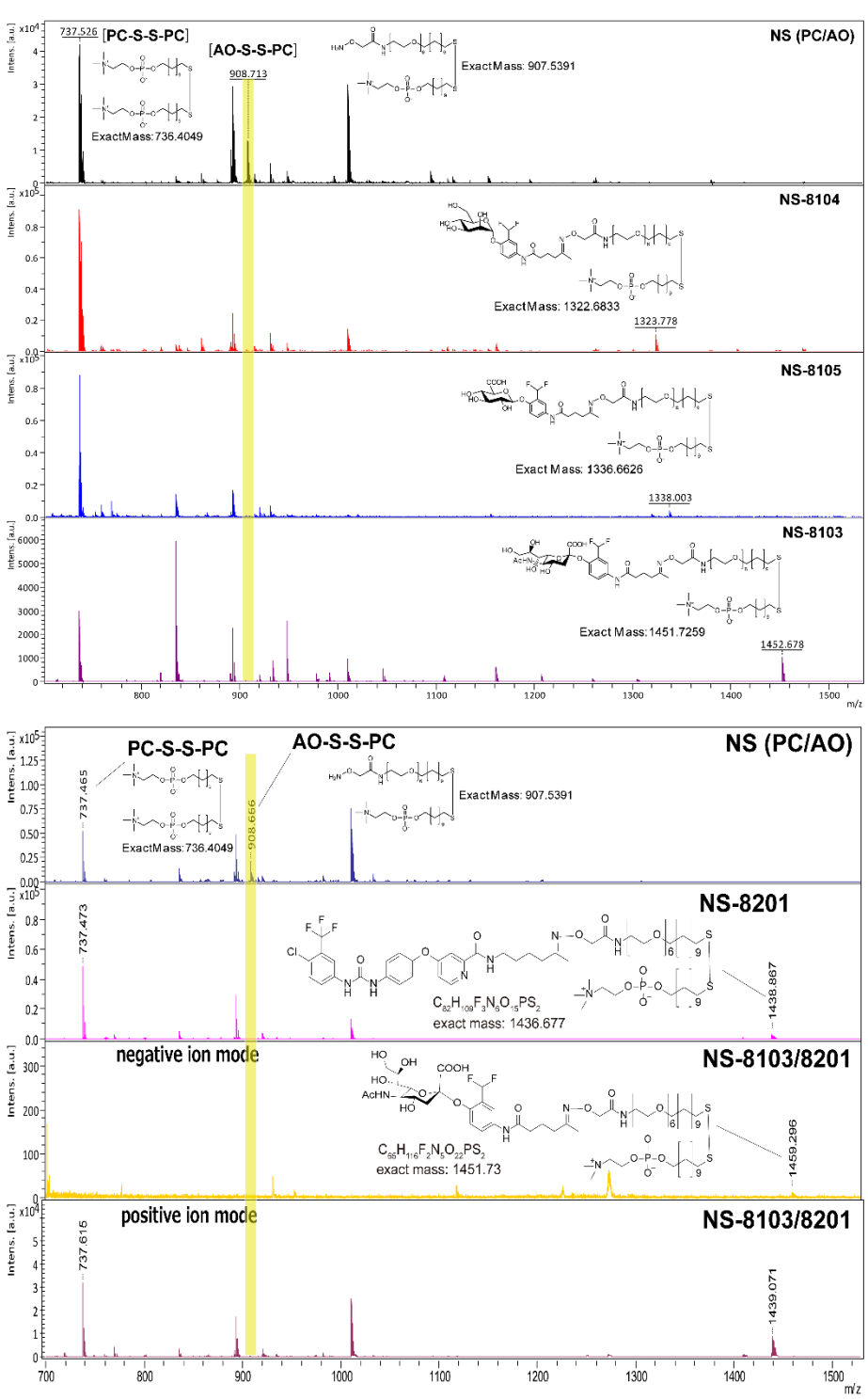
737.526 [PC-S-S-PC]
[AO-S-S-PC]
908.713
ExactMass: 907.5391
ExactMass:736.4049
NS (PC/AO)
NS-8104
ExactMass: 1322.6833
1323.778
NS-8105
Exact Mass: 1336.6626
1338.003
NS-8103
Exact Mass:1451.7259
1452.678
Intens. [a.u.]
m/z
PC-S-S-PC
AO-S-S-PC
737.465
908.666
NS-8201
737.473
C82H109F3N5O15PS2
exact mass: 1436.677
1438.867
negative ion mode
NS-8103/8201
C85H116F2N5O22PS2
exact mass: 1451.73
1459.296
positive ion mode
737.616
1439.071

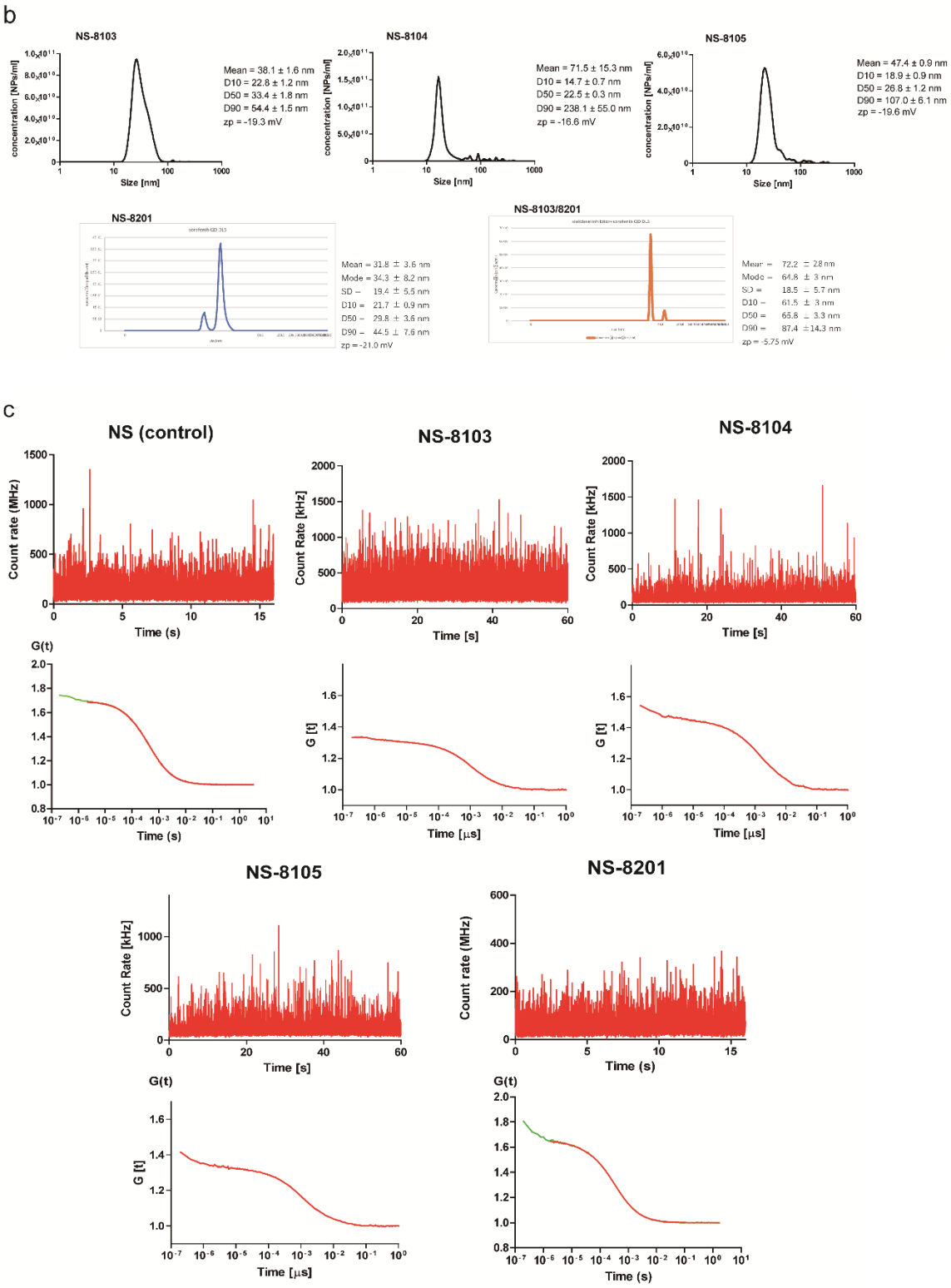
b
NS-8103
concentration [NPs/ml]
Size [nm]
Mean = 38.1 ± 1.6 nm
D10 = 22.8 ± 1.2 nm
D50 = 33.4 ± 1.8 nm
D90 = 54.4 ± 1.5 nm
zp = -19.3 mV
NS-8104
concentration [NPs/ml]
Size [nm]
Mean = 71.5 ± 15.3 nm
D10 = 14.7 ± 0.7 nm
D50 = 22.5 ± 0.3 nm
D90 = 238.1 ± 55.0 nm
zp = -16.6 mV
NS-8105
concentration [NPs/ml]
Size [nm]
Mean = 47.4 ± 0.9 nm
D10 = 18.9 ± 0.9 nm
D50 = 26.8 ± 1.2 nm
D90 = 107.0 ± 6.1 nm
zp = -19.6 mV
NS-8201
Mean = 31.8 ± 3.6 nm
Mode = 34.3 ± 8.2 nm
SD = 19.4 ± 5.5 nm
D10 = 21.7 ± 0.9 nm
D50 = 29.8 ± 3.6 nm
D90 = 44.5 ± 7.6 nm
zp = -21.0 mV
NS-8103/8201
Mean = 72.2 ± 28 nm
Mode = 64.8 ± 3 nm
SD = 18.5 ± 5.7 nm
D10 = 61.5 ± 3 nm
D50 = 65.8 ± 3.3 nm
D90 = 87.4 ± 14.3 nm
zp = -5.75 mV
c
NS (control)
Count rate (MHz)
Time (s)
G(t)
Time (s)
NS-8103
Count Rate [kHz]
Time [s]
G (t)
Time [µs]
NS-8104
Count Rate [kHz]
Time [s]
G (t)
Time [µs]
NS-8105
Count Rate [kHz]
Time [s]
G(t)
G (t)
Time [µs]
NS-8201
Count rate (MHz)
Time (s)
G(t)
Time (s)

Figure S3-7. Characterization of nanosomes prepared in this study. (a) Facile and rapid confirmation of the ligand exchange and oxime formation on the nanosomes is achieved by direct MALDI-TOFMS. Disappearance of the signal at *m/z* 908.7 corresponding to the ion composed of AO and PC linkers can be used as a convenient and universal marker to monitor the progress of the reaction with cargo molecules having a ketone/aldehyde auxiliary. (b) Hydrodynamic diameter and Zeta potential of the nanosomes prepared in this study. (c) Measurements of fluorescence fluctuation by fluorescence correlation spectrometry in 100% FBS represent surface antiadhesive nature of the nanosomes.

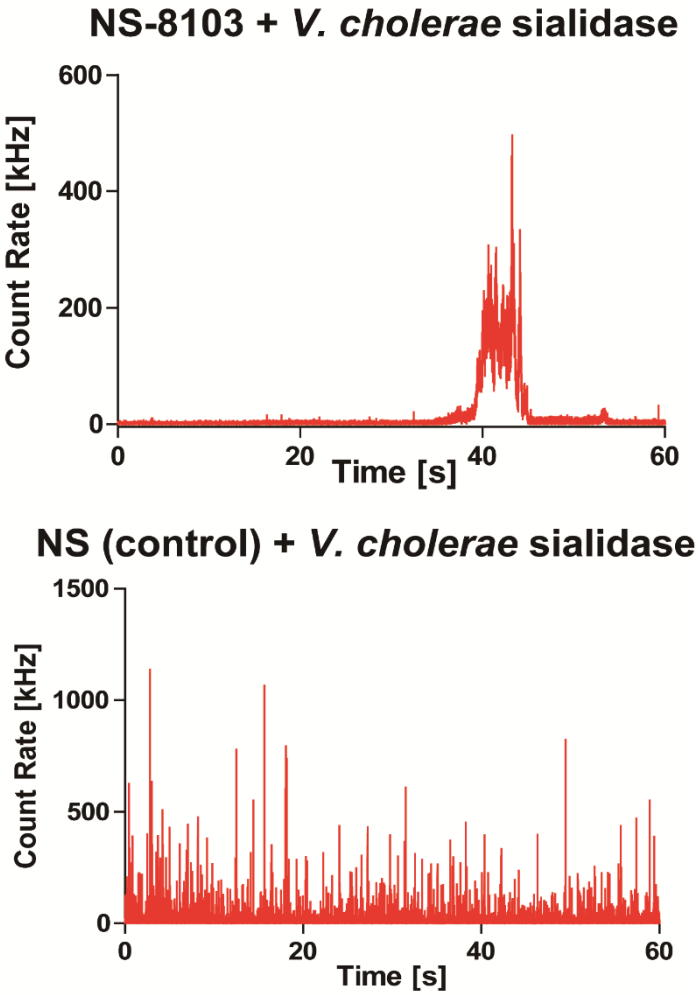

Figure S3-8. FCS analysis shows fluorescence fluctuations of **NS-8103** and **NS** (control) in the presence of commercially available *Vibrio cholerae* sialidase. Fluorescence fluctuations were measured according to the method reported previously[15,16] by fluorescence correlation spectroscopy (LSM 510 META Confocor 2, Carl Zeiss Inc., Germany).

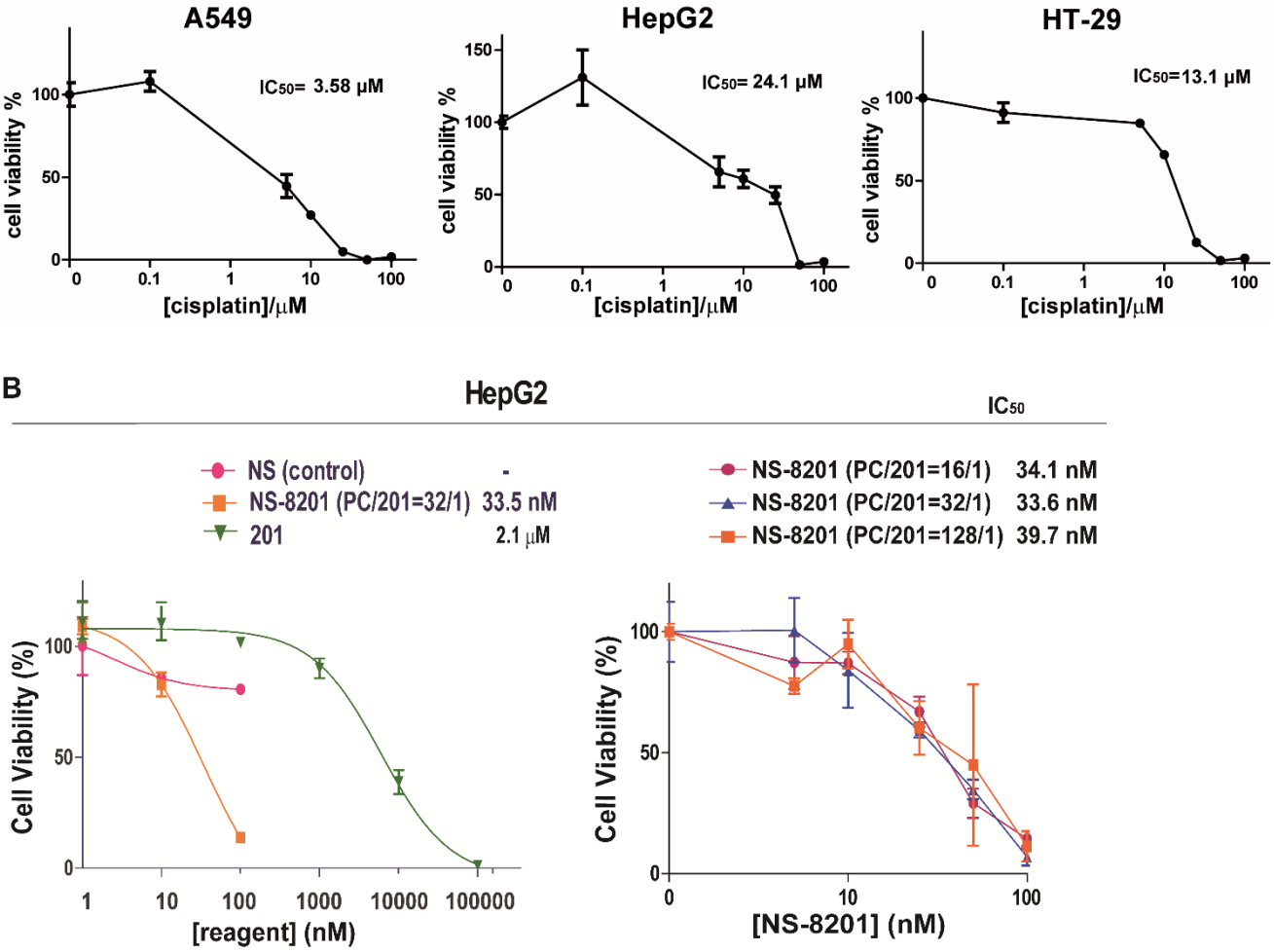

Figure S3-9. Antitumor activity of cisplatin against A549, HepG2, and HT-29 cells (A), and sorafenib derivative **201** and NSs carrying **201**. Loss of cell viability after 96 h coincubation with cisplatin was observed according to the experimental procedure for cell viability assay described in the supporting information.

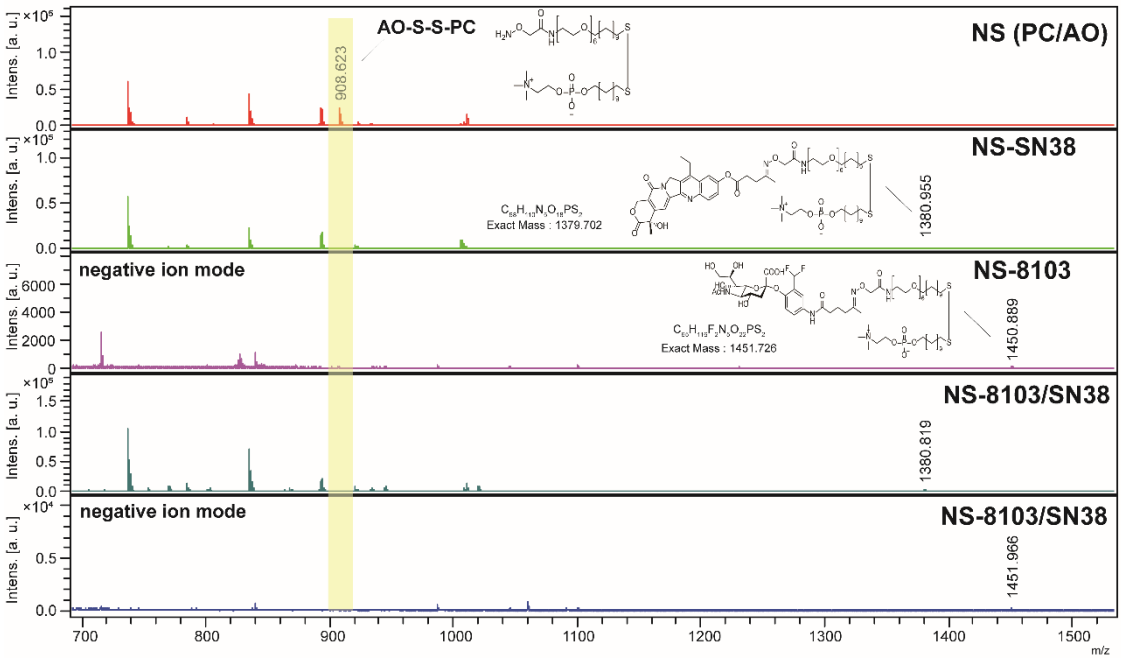

Figure S3-10. Facile and rapid confirmation of the ligand exchange and oxime formation on the nanosome is achieved by direct MALDI-TOFMS. Disappearance of the signal at *m/z* 908.7 corresponding to the ion composed of AO and PC linkers can be used as a convenient and universal marker to monitor the progress of the reaction with cargo molecules having a ketone/aldehyde auxiliary.

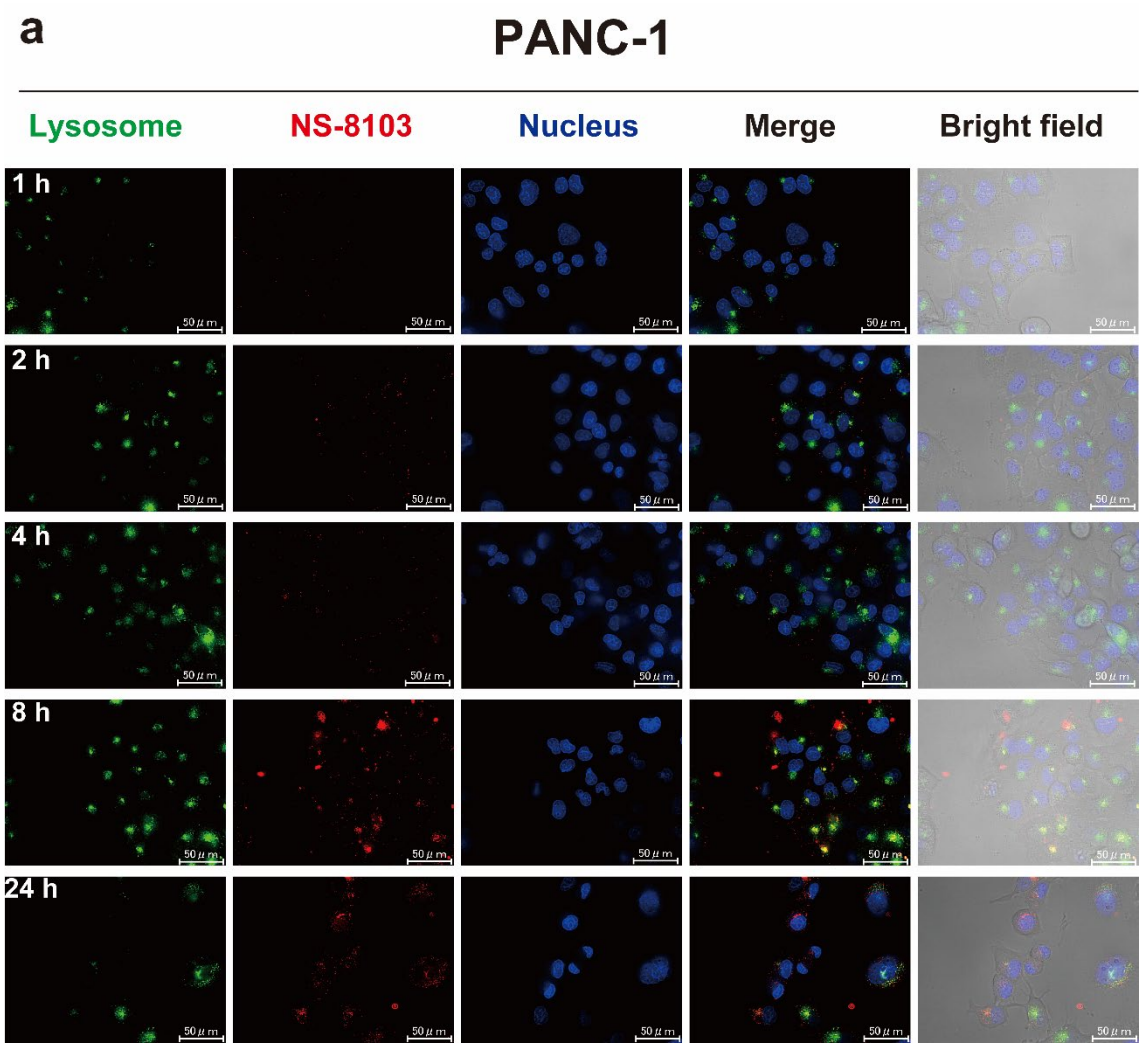
a
PANC-1
Lysosome
NS-8103
Nucleus
Merge
Bright field
1 h
2 h
4 h
8 h
24 h
50 μm

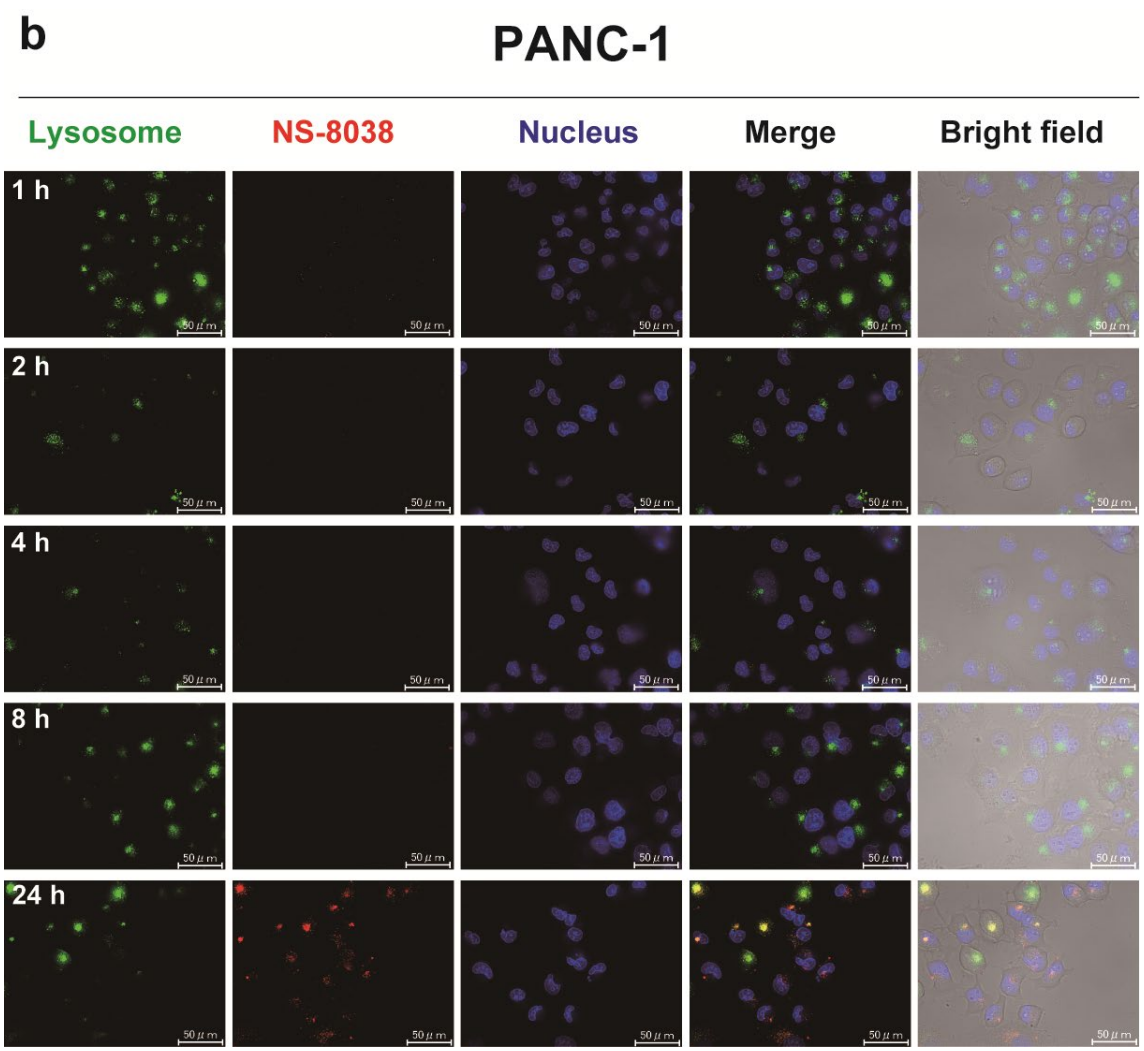
b
PANC-1
Lysosome
NS-8038
Nucleus
Merge
Bright field
1 h
2 h
4 h
8 h
24 h
50 μm

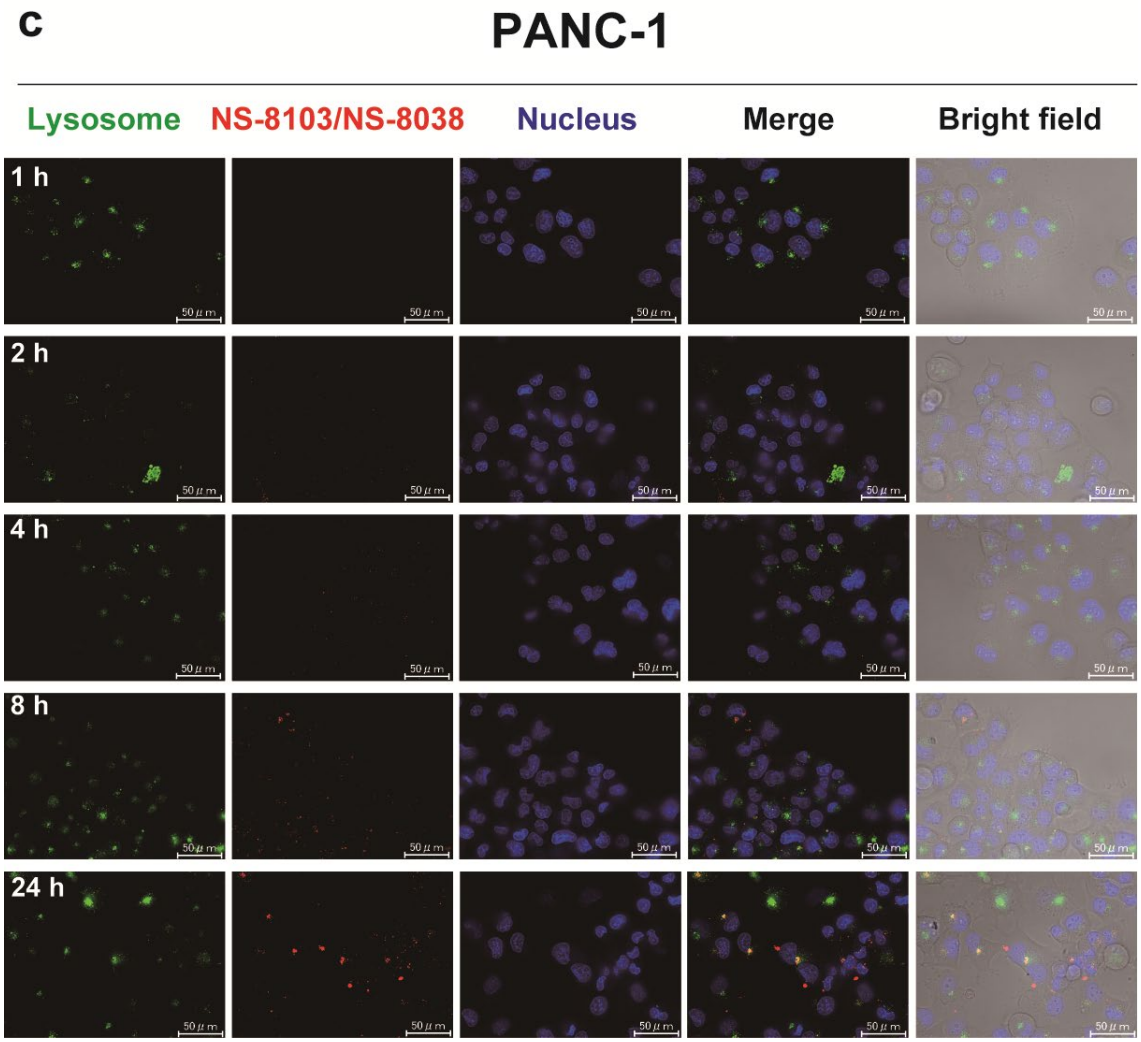
c
PANC-1
Lysosome
NS-8103/NS-8038
Nucleus
Merge
Bright field
1 h
2 h
4 h
8 h
24 h
50 μm

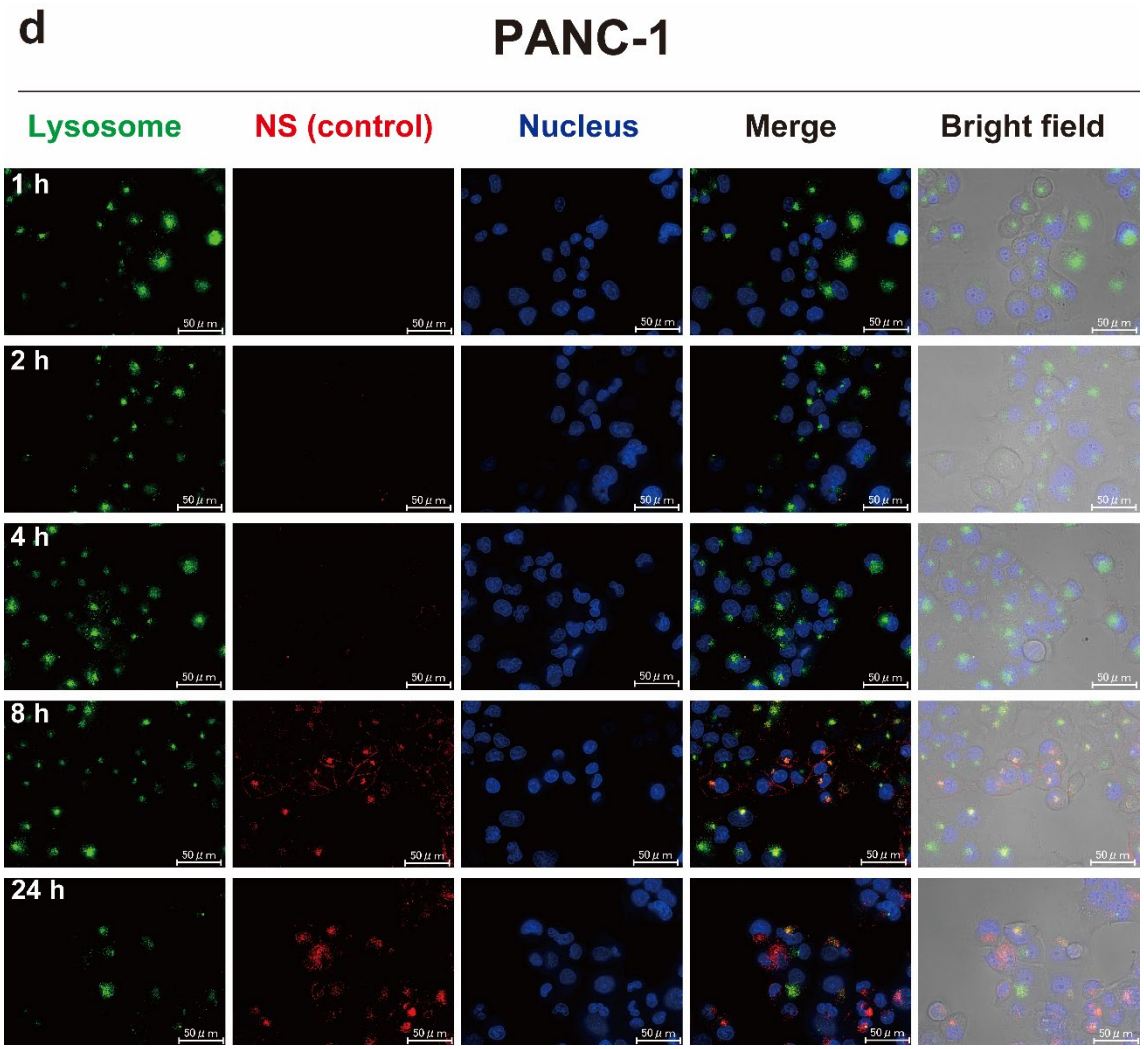

Figure S3-11. Representative cell images showing intracellular distribution of nanosomes after exposure of PANC-1 cells to 10 nM nanosomes. Scale bar, 50 μm. Cells were co-incubated with nanosomes (red) for 1, 2, 4, 8, and 24 h respectively. Lysosomes were stained with LysoTracker Green DND-26 (green), while the nuclei were stained with Hoechst 33342 (blue). (a)~(d) Merged pictures of 10 nM **NS-8103**, **NS-8038**, **NS-8103/8038**, and control **NS**.

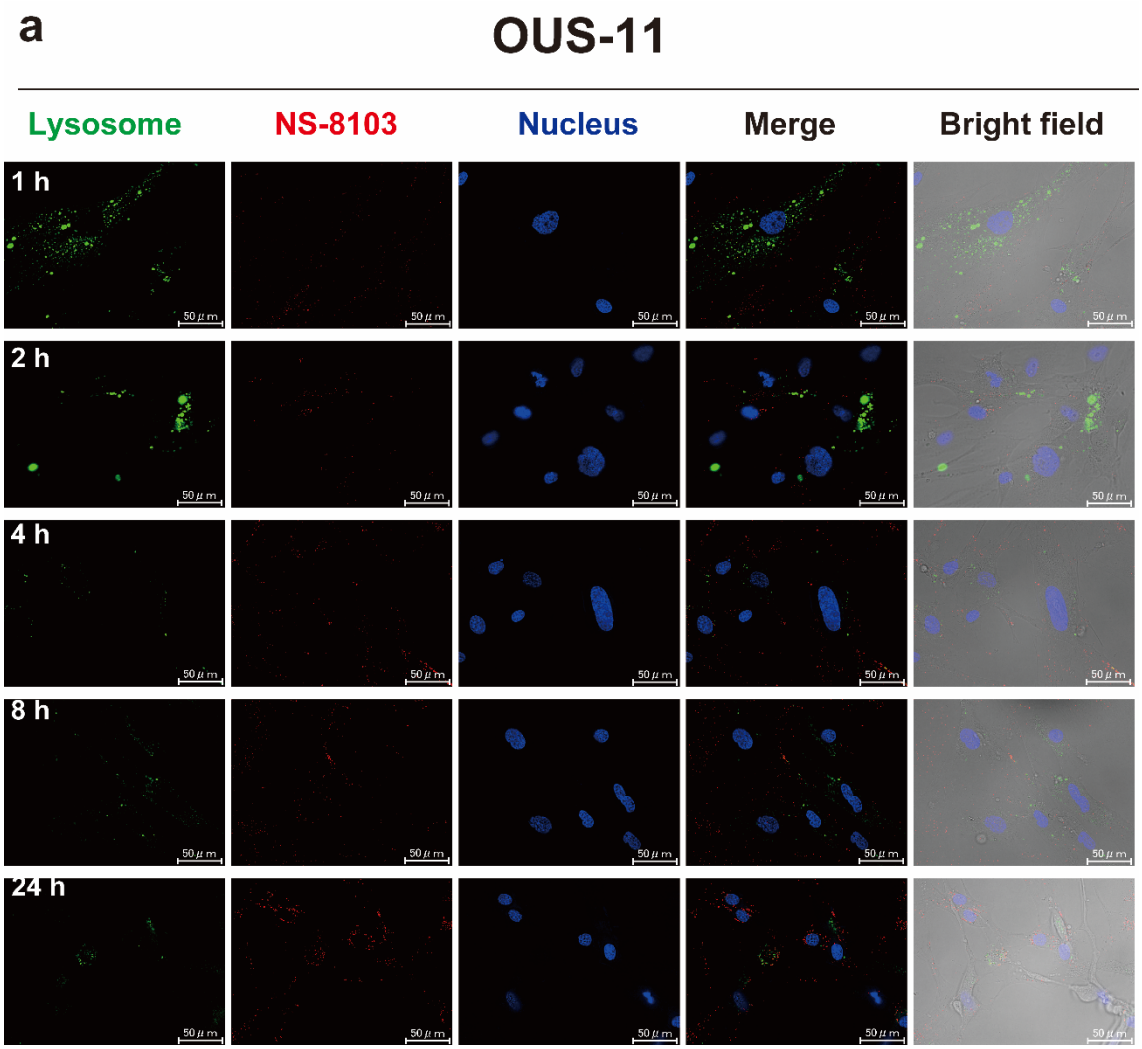
a
OUS-11
Lysosome
NS-8103
Nucleus
Merge
Bright field
1 h
2 h
4 h
8 h
24 h
50 μm

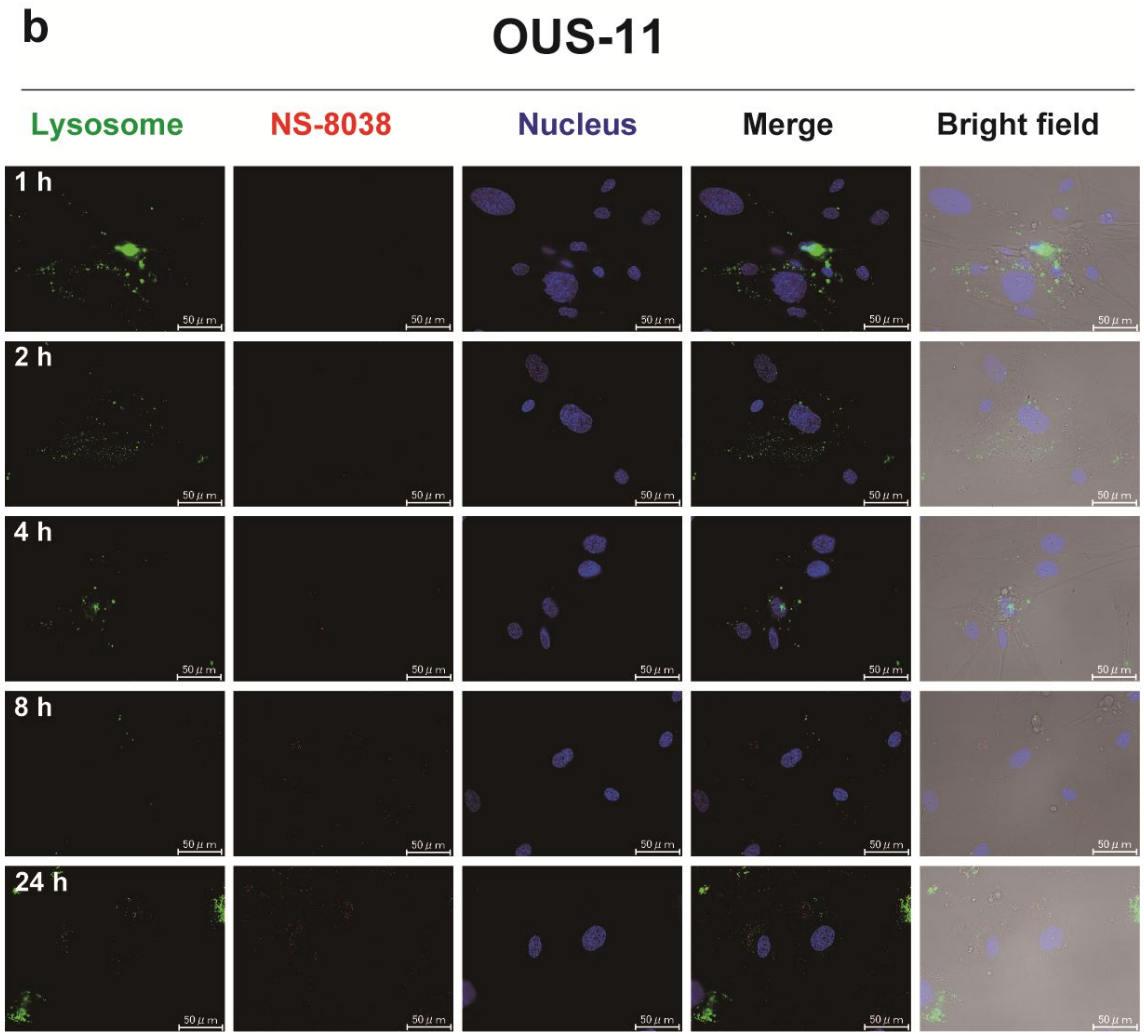
b
OUS-11
Lysosome
NS-8038
Nucleus
Merge
Bright field
1 h
2 h
4 h
8 h
24 h
50 μm

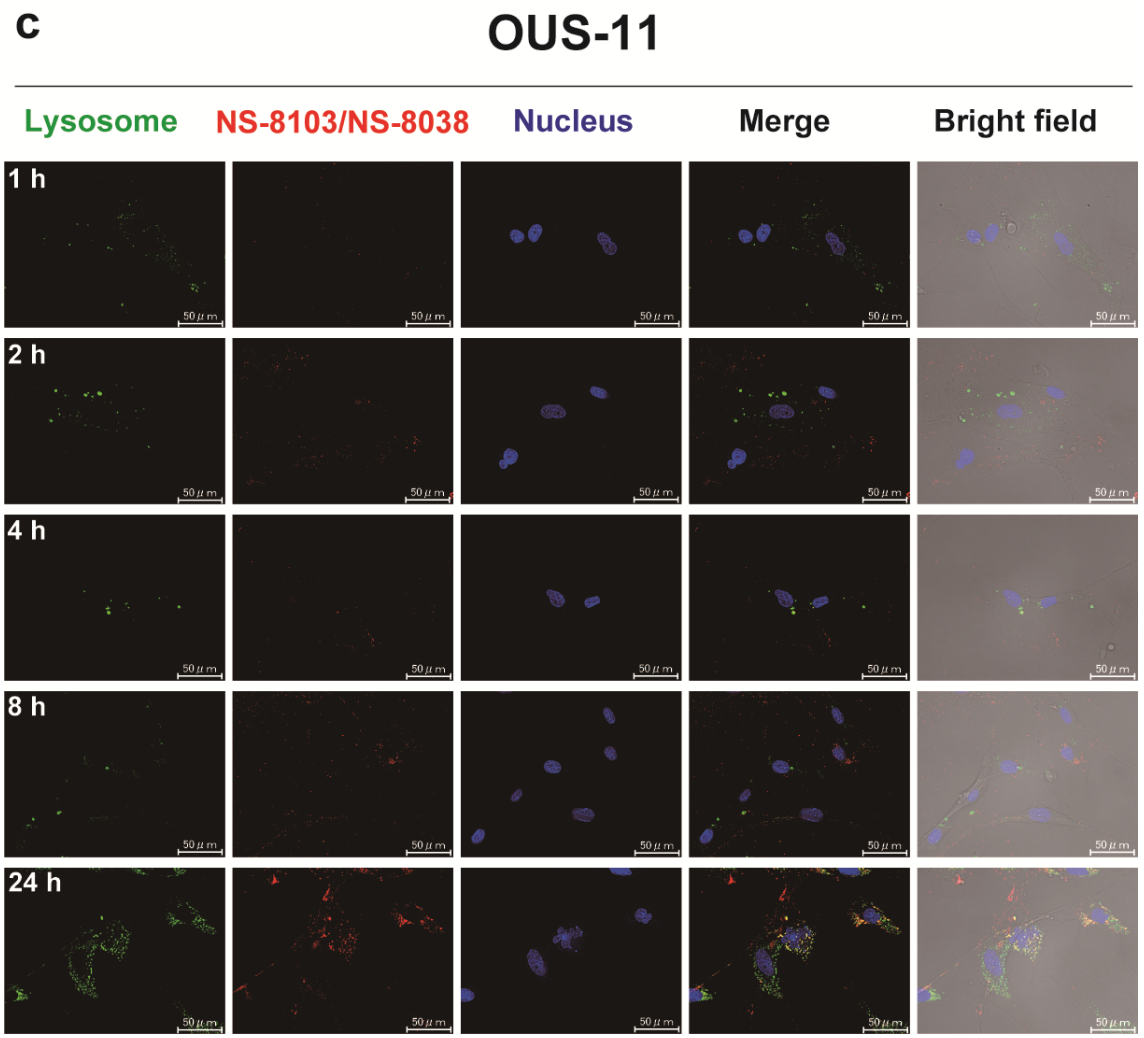
c
OUS-11
Lysosome
NS-8103/NS-8038
Nucleus
Merge
Bright field
1 h
2 h
4 h
8 h
24 h
50 μm

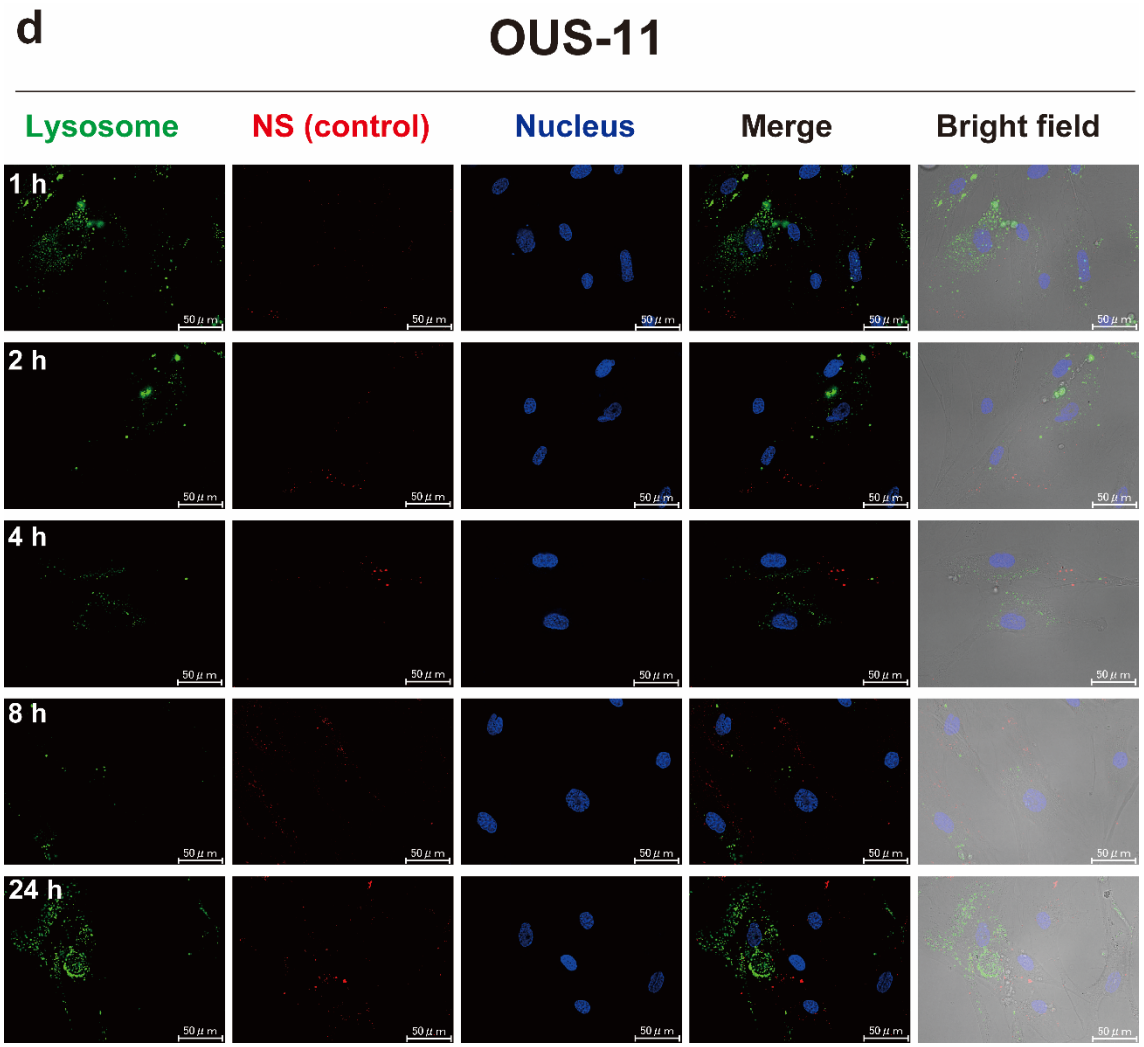

Figure S3-12. Representative cell images showing intracellular distribution of nanosomes after exposure of OUS-11 cells to 10 nM nanosomes. Scale bar, 50 μm. Cells were co-incubated with nanosomes (red) for 1, 2, 4, 8, and 24 h respectively. Lysosomes were stained with LysoTracker Green DND-26 (green), while the nuclei were stained with Hoechst 33342 (blue). (a)~(d) Merged pictures of 10 nM **NS-8103**, **NS-8038**, **NS-8103/8038**, and control **NS**.

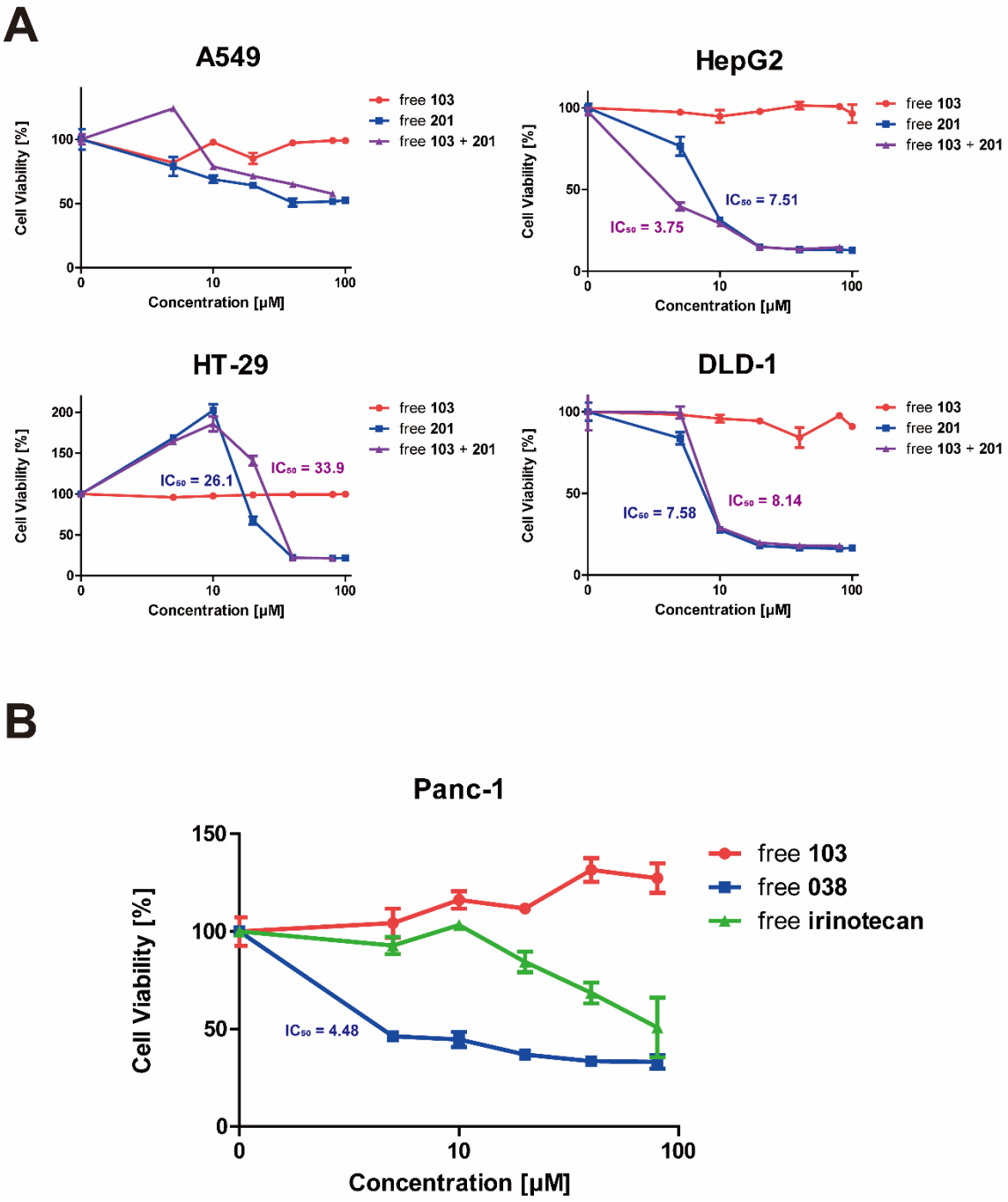

Figure S3-13. Antitumor activity of free compounds (A) free **103**, **201** against A549, HepG2, HT-29, DLD-1 and (B) free **103**, **038** and **irinotecan** against Panc-1 cell. Loss of cell viability after 48 h coincubation with compounds was observed according to the experimental procedure for cell viability assay described in the supporting information.

Chapter 4　Animal Experiment

4-1. Introduction

As described above, nanoparticles, including those containing globular serum albumin (nab-paclitaxel) and liposomes (NALIRIFOX/ONIVYDE)[1,2], are emerging as potent drug delivery platforms that improve the pharmacokinetics of free, cytotoxic chemotherapeutics. Indeed, ONIVYDE (liposomal irinotecan) promotes the controlled, sustained release of irinotecan.[1-4] It also facilitates passive delivery to solid tumors via the enhanced permeability and retention (EPR) effect of newly formed leaky tumor vasculature.[5] However, despite the significantly improved and higher therapeutic efficacy of liposomal irinotecan than non-liposomal irinotecan,[6] the extent of their use (dosing schedules) is limited by severe toxic side effects of irinotecan on normal tissues.[1,2] Notably, the PDAC tumor microenvironment (TME) consists of highly complex populations of heterogeneous fibroblasts, a dense extracellular matrix, and diverse, mostly suppressive immune cell populations.[7,8] Considering that a dense fibrotic stroma "desmoplasia" of PDAC TME acts as a barrier to chemotherapy penetration and contributes to multidrug resistance, the EPR effect is not sufficient for the extravasation and transportation of nanoparticles into PDAC TME.[9] Given that the lethality of PDAC patients is due to difficulty detecting the disease until a late stage in progression, development of much more efficient and beneficial therapeutic strategies than currently approved systemic chemotherapies is urgently needed. Targeting pancreatic cancer-specific molecules with high-performance nanoparticles could facilitate the active delivery of various chemotherapeutic agents to PDAC cells within the tumor microenvironment (TME) without severe off-target toxicity. In Chapter 4, we focused on the in vivo dynamics of nanosomes and their anti-tumor activity in a tumor-bearing mouse model.

4-2. Results and Discussion

4-2-1. Circulation and biodistribution of nanosomal irinotecan in mice

Our previous studies have demonstrated that the surface decoration of nanosomes with glycans strongly influences their circulation and biodistribution after intravenous administration.[10,11] Live animal near-infrared (NIR) fluorescence imaging of QD-core nanosomes after administration into the tail vein of the mouse revealed that attachment of the suicide substrate **103** of NEU1 sialidase dramatically improves circulation and systemic tissue distribution of nanosomes **NS-8103** and **NS-8103/8038** when compared with control NS and **NS-8038** (Figure 4-1). Nanosomes bearing multiple sialic acid residues involved in the "suicide substrate" of NEU1, **NS-8103** and **NS-8103/8038**, showed distinct long-term delocalization and retained in the whole body over 2 h after intravenous administration (Figure 4-1c and 4-1d), while NIR fluorescence of control NS and **NS-8038** appeared to be quenched rapidly after intravenous injection (Figure 4-1a and 4-1b). Importance of sialic acid residues in vivo dynamics in the tissue distribution of nanosomes was demonstrated by surgical dissection at 2 h after injection (Figure 4-1e~4-1h). Notably, nanosomes having Neu5Ac residues of **103**, **NS-8103** and **NS-8103/8038**, distributed in major tissues such as brain, lung, liver, spleen, kidney in addition to pancreas without any significant local accumulation. In contrast, fluorescence of NS and **NS-8038** seemed to be reduced rapidly in most tissues due to hepatobiliary clearance, although clearance mechanism of these nanosomes remains mostly unclear.[10,12,13] These results and in vitro anti-tumor activity of nanosomes greatly encouraged us to examine in vivo anti-PDAC activity of NEU1 targeted nanosomal irinotecan **NS-8103/8038** using pancreatic cancer cell subcutaneous xenograft model mice.

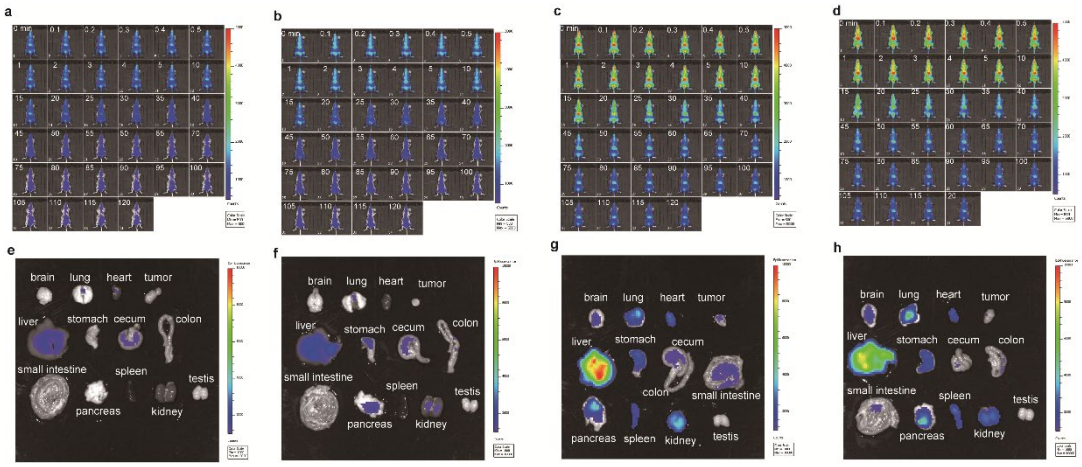

Figure 4-1. Live animal NIR fluorescence imaging analysis of nanosomes. Imaging after intravenous injection of QD-core nanosomes (1 μM x 100 μL), control NS (a), **NS-8038** (b), **NS-8103** (c), and **NS-8103/8038** (d). (e)~(h) Photographs of major organs isolated from tested mice by surgical dissection of mice at 2 h after intravenous administration.

4-2-2. Anti-pancreatic cancer activity of NEU1 targeted nanosomal irinotecan in Panc-1 subcutaneous xenografts

Our interest was focused on the in vivo anti-tumor activity of NEU1 targeted nanosomal irinotecan (**NS-8103/8038**) of a range 59~85 nm in a diameter prepared from the core AuNP of a range 8~10 nm in a diameter using Panc-1 subcutaneous xenograft mouse model. The pancreatic tumor-bearing mice received a nanosomal dose of 5 mg/kg per intravenous injection every 4 days for six injections when their mean tumor volume was ~100 mm^3 at day 0 (Figure 4-2a). For example, an intravenous injection of a dose of 5 mg/kg **NS-8103/8038** corresponds to the treatment with 2.1 mg/kg of **103** (suicide substrate of NEU1) and 1.7 mg/kg of **038** (irinotecan prodrug), respectively. Surprisingly, the treatments with nanosomes were found to be tolerable without any body weight loss relative to day 0 in all AuNP-core nanosomes tested, control NS, **NS-8038** (equivalent to 2.1 mg/kg of **038**), **NS-8103** (equivalent to 2.4 mg/kg of **103**), and **NS-8103/8038** (equivalent to 2.1 mg/kg of **103** and 1.7 mg/kg of **038**), whereas a significant loss of the body weight was observed only in the control groups (Figure 4-2b). The tumor size increased rapidly in the saline and control NS group, while the tumor growth rate was lowered obviously in the therapies by **NS-8038**, **NS-8103**, and **NS-8103/8038** (Figure 4-2c and 4-2d, $p < 0.05$). Note that treatment with NEU1 targeted nanosomal irinotecan **NS-8103/8038** and **NS-8103** remarkably reduced tumor progression compared to the therapeutic effects by **NS-8038**. Indeed, the treatment by the AuNP-core nanosome **NS-8103/8038** resulted in the smallest tumors at 25 days with significantly reduced volume (~80 mm^3) compared to the tumor volume (~100 mm^3) on day 0 (Figure 4-2c and 4-2d). Pictures of tumors at 25 days of Panc-1 cells also demonstrated the superior anti-PDAC therapeutic effect of NEU1 targeted nanosomal irinotecan **NS-8103/8038** (Figure 4-2e and 4-2f). Notably, a dose of ONIVYDE (50 mg/kg) administered weekly for three injections was shown to have a fourfold broader therapeutic index than non-liposomal irinotecan under optimal treatment schedules for evaluating antitumor efficacy in mice with subcutaneous, patient-derived xenograft (PDX) pancreatic tumors.[6] However, most mice receiving three cycles of liposomal irinotecan (50 mg/kg/week) had moderate to severe body weight loss up to day [14]. Given the results that pancreatic tumor-bearing mice

receiving six injections of **NS-8103/8038** (5 mg/kg/4 days) had no body weight loss, active delivery of nanosomal irinotecan by targeting NEU1 sialidase is highly beneficial modality to enhance therapeutic efficacy and reduce off-target toxicity of irinotecan in the normal tissues, concurrently.

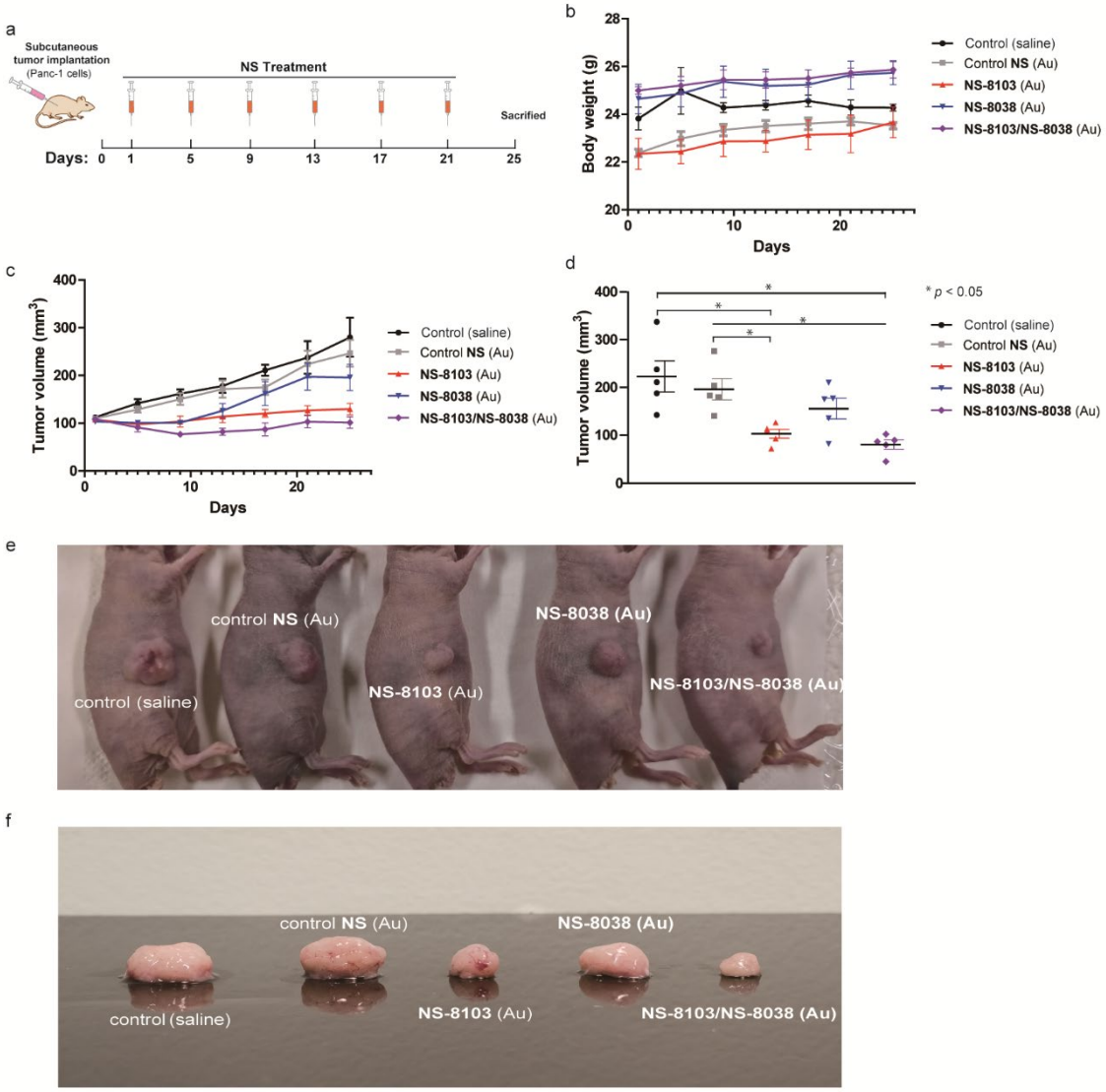

Figure 4-2. Treatment of Panc-1 subcutaneous xenografts by nanosomes made from AuNP core. (a) Scheme of therapy. The pancreatic tumor-bearing mice received a nanosomal dose of 5 mg/kg per intravenous injection every 4 days for six injections. (b) Body weight changes mice during treatments. These data are shown as the mean ± s.d. (n = 5). (c) and (d) Tumor growth curves during treatment by nanosomes. These data are shown as the mean ± s.d. (n = 5), *p < 0.05 (Student's t test). (e) and (f) Pictures of mice and isolated tumor samples treated by nanosomes at the termination of the experiments.

4-3. Conclusion

PDAC is the most lethal cancer. Most studies have highlighted the distinct and abnormal pathological barrier of the PDAC tumor microenvironment (TME), which impedes the efficient delivery of drugs to pancreatic cancer cells.[7,9] It is important to note that PDAC is specifically characterized by a dense desmoplastic stroma composed of cancer-associated fibroblasts, extracellular matrix (ECM), and diverse, suppressive immune cell populations. Recent general therapies involving immune checkpoint inhibitors and antibody drug conjugates (ADCs) have proven difficult for patients with PDAC.[8,15] In the past decade, two major combination chemotherapeutic regimens have emerged as the first-line therapy in patients with advanced PDAC; FOLFIRINOX[16] and nab-paclitaxel plus gemcitabine[17] approved by the US FDA in 2011 and 2013, respectively. Additionally, the US FDA approved the new NALIRIFOX regimen, which includes liposomal irinotecan (ONIVYDE), oxaliplatin, 5-fluorouracil (5-FU), and leucovorin, for the first-line treatment of metastatic PDAC in 2024. The efficacy of this treatment was evaluated in NAPOLI 3 (NCT04083235), a randomized, multicenter, open-label, active-controlled trial involving 770 patients with metastatic PDAC.[2] NAPOLI 3 revealed a quite similar efficacy and safety of NALIRIFOX when compared to those of nab-paclitaxel and gemcitabine as first-line therapy for metastatic PDAC. However, given evidence that median overall survival of the patients was 11.1 months with NALIRIFOX versus 9.2 months with nab-paclitaxel–gemcitabine, demonstrating that no substantial improvements in treatment for patients with advanced PDAC have been observed. Obviously, the exploitation of much more effective and beneficial chemotherapeutic strategies than currently approved medicines for the patients with advanced PDAC remains challenging.

Our present study elicited that targeting nanosomal irinotecan to NEU1 sialidase-mediated endocytosis enables creation of new class of anti-PDAC therapeutic modality to enhance significantly the therapeutic efficacy and safety of the liposomal irinotecan. Nanosomes are composed of a hard/high density core nanoparticle such as semiconductor single crystal QD and gold nanoparticle (AuNP), and softshell of antifouling mixed-SAM membrane that facilitates design and synthesis of various ligands and payloads for the development of active DDS. Advantage of AuNP (8~10 nm) as a core material of nanosome (59~85 nm) is evident because chemical coating by mixed SAM with designated alkanethiols (PC- and AO-linkers) provides core AuNP with an antiadhesive surface and cargo-attachment functions, concurrently.[7,38,11] Importantly, the core AuNP has a strong impact of superior physicochemical stability, higher specific gravity (19.32 g/cm3), and distinctly lower toxicity than other inorganic materials.[18,19] It is also noteworthy that nanosomes (38~59 nm) prepared from core QD (5~10 nm, > 5 g/cm3) can be used as a counterpart of the nanosomes derived

from core AuNP to allow for direct fluorescence imaging analysis in animals (Figure 4-1). Live mouse NIR fluorescence imaging of QD-core nanosomes highlighted the importance of the sialic acid residues of **NS-8103** and **NS-8103/8038** in the long-term circulation and delocalized biodistribution of the nanosomal irinotecan (Figure 4-1). As expected by the assessment using QD-core nanosomes, in vivo antitumor activities of nanosomal irinotecan demonstrated that pancreatic tumor-bearing mice receiving the treatment of **NS-8103/8038** at a dose of 5 mg/kg (1.7 mg/kg equivalent to irinotecan) six times at 4-day intervals had no body weight loss at 24 days after the first injection, while this treatment inhibited completely tumor proliferation (Figure 4-2). Notably, there is a limitation of the dosing schedule for the repetitive injections with a dose of ONIBYDE (10 mg/kg/week or 25 mg/kg/week) in the treatment of patients with advanced PDAC due to the acute toxicity caused by free irinotecan or SN-38 derived from liposomal irinotecan.

Characteristic features of the nanosomal platform are attributed to the simple core-shell structure and facile protocols of the preparation and quality control of the nanosomes, despite the highly beneficial chemotherapeutic effects by active DDS. The merit of the active delivery strategy of nanosomal irinotecan to the NEU1 of PDAC is clear. Enhanced efficacy and reduced off-target toxicity of **NS-8103/8038** enable a much more flexible molecular design, as well as optimization of the ratio of compositional payloads and the extent of use. Notably, this includes a dosing schedule suited to individual patients with advanced PDAC, which is superior to the currently approved therapeutic regimens.

4-4. Experimental Section

Preparation of Nanosomes using gold nanoparticles (AuNPs).

Gold nanoparticles with an average diameter of 10 nm were synthesized TOPO (25 g) and stearylamine (10 g) were added to 100 mL of cyclohexanol in a 300 mL flask, and the mixture was heated to 150 ℃. Under vigorous stirring, $HAuCl_4 \cdot 4H_2O$ (1 mL, 1 M/EtOH) and $NaBH_4$ (0.5 mL, 100 mM/EtOH) were injected, and the mixture was kept at 150 ℃ and stirred for 30 min. MeOH (200 mL) was added to the reaction mixture and the solution was centrifuged twice at 5,000 G for 5 min. Then, the supernatant was removed, and the precipitates were distributed in toluene (50 mL). The concentration of AuNP solution was determined from the mean diameter of AuNP from TEM images. The average Au atoms per nanoparticle were calculated as $N = \pi \rho D3/6M$, where ρ was the density for face-centered cubic gold (19.3 g/cm3), M was the molecular weight of gold (197 g/mol), and D was the average diameter of AuNPs from TEM images. AuNPs were coated by PC linker and AO linker in the same protocol described above.

Cell culture

PANC-1 (ECACC, UK), human pancreatic cancer cell, was cultured in D-MEM (Wako, Osaka, Japan) containing 10% fetal bovine serum at 37 ℃ with 5% CO_2

Evaluation of *in vivo* tumor growth inhibition

To establish PANC-1 tumors in mice, cells were cultured, detached by trypsinization, washed, and resuspended in serum-free DMEM. 2.0×10^7 cells were mixed with Matrigel (1:1) and BALB/c Slc-nu/nu mice (4 weeks old, male), housed under standard laboratory conditions (pathogen-free conditions with a 12 h light/12 h dark schedule), were s.c. injected into the right flank of the mouse. When tumors grew 100 mm^3, the mice were randomly assigned into 5 groups (n=5). Saline, NS (Au), **NS-8103** (Au), **NS8038** (Au), **NS-8103/8038** (Au) were injected into the tail vein of the tumor-bearing mice (200 μL, 1 μM/saline) on day 1, 5, 9, 13, 17, and 21. Tumor size was measured on day 1, 5, 9, 13, 17, 21 and 25, and calculated based on the following equation: volume = 0.5 × (major diameter) × (minor diameter).

Living animal imaging in tumor bearing mice

To establish PANC-1 tumors in mice, cells were cultured, detached by trypsinization, washed, and resuspended in serum-free DMEM. 2.0×10^7 cells were mixed with Matrigel (1:1) and BALB/c Slc-nu/nu mice (4 weeks old, male) were s.c. injected into the right flank of the mouse. When the tumor grew to 200 mm^3, nanosomes (1 μM, 100 μL) were injected into the tail vein of PANC-1 tumor mice. The mice were then anesthetized with isoflurane, and images were captured using an IVIS imaging system (Sumisho Pharma International Corporation, Tokyo, Japan). The exposure time was 1 second, the excitation wavelength was 710 nm, and the emission wavelength was 820 nm. Mice were imaged for 2 hours after intravenous injections; after 2 hours of imaging, mice were dissected, and fluorescent images were taken. Major organs were isolated from all mice, and fluorescence images of the organs were also observed.

4-5. Reference

[1] Andrea Wang-Gillam, Chung-Pin Li, György Bodoky, Andrew Dean, Yan-Shen Shan, Gayle Jameson, Teresa Macarulla, Kyung-Hun Lee, David Cunningham, Jean F Blanc, Richard A Hubner, Chang-Fang Chiu, Gilberto Schwartsmann, Jens T Siveke, Fadi Braiteh, Victor Moyo, Bruce Belanger, Navreet Dhindsa, Eliel Bayever, Daniel D Von Hoff , Li-Tzong Chen, Nanoliposomal irinotecan with fluorouracil and folinic acid in metastatic pancreatic cancer after previous gemcitabine-based therapy (NAPOLI-1): a global, randomised, open-label, phase 3 trial. *Lancet* **387**, 545–557 (2016)

[2] Zev A Wainberg, Davide Melisi, Teresa Macarulla, Roberto Pazo Cid, Sreenivasa R Chandana, Christelle De La Fouchardière, Andrew Dean, Igor Kiss, Woo Jin Lee, Thorsten O Goetze, Eric Van Cutsem, A Scott Paulson, Tanios Bekaii-Saab, Shubham Pant, Richard A Hubner, Zhimin Xiao, Huanyu Chen, Fawzi Benzaghou, Eileen M O'Reilly, NALIRIFOX versus nab-paclitaxel and gemcitabine in treatment-naive patients with metastatic pancreatic ductal adenocarcinoma (NAPOLI 3): a randomised, open-label, phase 3 trial. *Lancet* **402**, 1272-1281 (2023)

[3] Drummond DC, Noble CO, Guo Z, Hong K, Park JW, Kirpotin DB., Development of a highly active nanoliposomal irinotecan using a novel intraliposomal stabilization strategy. *Cancer Res.* **66**, 3271-3277 (2006)

[4] Ashish V. Kalra, Jaeyeon Kim, Stephan G. Klinz, Nancy Paz, Jason Cain, Daryl C. Drummond, Ulrik B. Nielsen, and Jonathan B. Fitzgerald, Preclinical Activity of Nanoliposomal Irinotecan Is Governed by Tumor Deposition and Intratumor Prodrug Conversion. *Cancer Res.* **74**, 7003-7013 (2014)

[5] H. Maeda, K. Tsukigawa, J. Fang, A Retrospective 30 Years After Discovery of the Enhanced Permeability and Retention Effect of Solid Tumors: Next-Generation Chemotherapeutics and Photodynamic Therapy-Problems, Solutions, and Prospects. *Microcirculation* **23**, 173-182 (2016)

[6] Sandrine Barbier, Benjamin Beaufils, Ricardo de Miguel, Melissa Reyre, Yannick Le Meitour, Andreanne Lortie, Marc Hillairet de Boisferon, Sophie Chaumeron, Anne Espirito,

Lina Fossati, Pauline Lagarde, Stephan Klinz, Arunthathi Thiagalingam, Stephane Lezmi, Florence Meyer-Losic, Liposomal Irinotecan Shows a Larger Therapeutic Index than Non-liposomal Irinotecan in Patient-Derived Xenograft Models of Pancreatic Cancer. *Oncol Ther* **11**, 111-128 (2023)

[7] Christopher J. Halbrook, Costas A. Lyssiotis, Marina Pasca di Magliano, Anirban Maitra, Pancreatic cancer: Advances and challenges. *Cell* **186**, 1729-1754 (2023)

[8] Adham S. Bear, Robert H. Vonderheide, Mark H. O'Hara, Challenges and Opportunities for Pancreatic Cancer Immunotherapy. *Cancer Cell* **38**, 788-802 (2020)

[9] Oluwabukunmi Olajubutu, Omotola D. Ogundipe, Amusa Adebayo, Simeon K. Adesina, Drug Delivery Strategies for the Treatment of Pancreatic Cancer. *Pharmaceuticals* **15**, 1318 (2023)

[10] T. Ohyanagi, N. Nagahori, K. Shimawaki, H. Hinou, T. Yamashita, A. Sasaki, T. Jin, T. Iwanaga, M. Kinjo, S.-I. Nishimura, Importance of sialic acid residues illuminated by live animal imaging using phosphorylcholine self-assembled monolayers-coated quantum dots. *J. Am. Chem. Soc.* **133**, 12507-12517 (2011).

[11] K. Murakami, D. Kambe, Y. Yokoi, H. Wakui, S. Hayakawa, N. Hirane, R. Koide, M. Otaki, N. Nagahori, S.-I. Nishimura, Smart Nanomedicine Targeting Endocytosis Mediated by Cancer Cell Surface Neuraminidase-1. *Adv. NanoBiomed. Res.* **3**, 2300076 (2023)

[12] R. Koide, S.-I. Nishimura, Antiadhesive nanosomes facilitate targeting of lysosomal GlcNAc salvage pathway through derailed cancer endocytosis. *Angew. Chem. Int. Ed.* **58**, 14513-14518 (2019).

[13] R. Koide, N. Hirane, D. Kambe, Y. Yokoi, M. Otaki, S.-I. Nishimura, Antiadhesive nanosome elicits role of glycocalyx of tumor cell-derived exosomes in the organotropic cancer metastasis. *Biomaterials* **280**, 121314 (2020)

[14] S.-I. Nishimura, K. Niikura, M. Kurogochi, T. Matsushita, M. Fumoto, H. Hinou, R. Kamitani, H. Nakagawa, K. Deguchi, N. Miura, K. Monde, H. Kondo, High Throughput Protein Glycomics: Combined Use of Chemoselective Glycoblotting and MALDI-TOF/TOF Mass Spectrometry. *Angew. Chem. Int. Ed.* **44**, 91-96 (2004)

[15] Mubin Tarannum, Juan L. Vivero-Escoto, Nanoparticle-based therapeutic strategies targeting major clinical challenges in pancreatic cancer treatment. *Adv. Drug Deliv. Rev.* **187**, 114357 (2022)

[16] Thierry Conroy, Françoise Desseigne, Marc Ychou, Olivier Bouché, Rosine Guimbaud, Yves Bécouarn, Antoine Adenis, Jean-Luc Raoul, Sophie Gourgou-Bourgade, Christelle de la Fouchardière, Jaafar Bennouna, Jean-Baptiste Bachet, Faiza Khemissa-Akouz, Denis Péré-Vergé, Catherine Delbaldo, Eric Assenat, Bruno Chauffert, Pierre Michel, Christine Montoto-Grillot, Michel Ducreux, FOLFIRINOX versus Gemcitabine. *N. Engl. J. Med.* **364**, 1817-1825 (2011)

[17] Daniel D. Von Hoff, Thomas Ervin, Francis P. Arena, E. Gabriela Chiorean, Jeffrey Infante, M.D., Malcolm Moore, M.D., Thomas Seay, M.D., Sergei A. Tjulandin, M.D., Wen Wee Ma, M.D., Mansoor N. Saleh, Marion Harris, Michele Reni, Scot Dowden, Daniel Laheru, Nathan Bahary, Ramesh K. Ramanathan, Josep Tabernero, Manuel Hidalgo, David Goldstein, Eric Van Cutsem, Xinyu Wei, Jose Iglesias, Markus F. Renschler, Increased Survival in Pancreatic Cancer with nab-Paclitaxel plus Gemcitabine. *N. Engl. J. Med.* **369**, 1691-1703 (2013)

[18] J. Christopher Love, Lara A. Estroff, Jennah K. Kriebel, Ralph G. Nuzzo, George M. Whitesides, Self-Assembled Monolayers of Thiolates on Metals as a Form of Nanotechnology. *Chem. Rev.* **105**, 1103-1116 (2005)

[19] Alaaldin M. Alkilany, Catherine J. Murphy, Toxicity and cellular uptake of gold nanoparticles: what we have learned so far? *J. Nanopart. Res.* **12**, 2313–2333 (2010)

4-6. Supporting Information

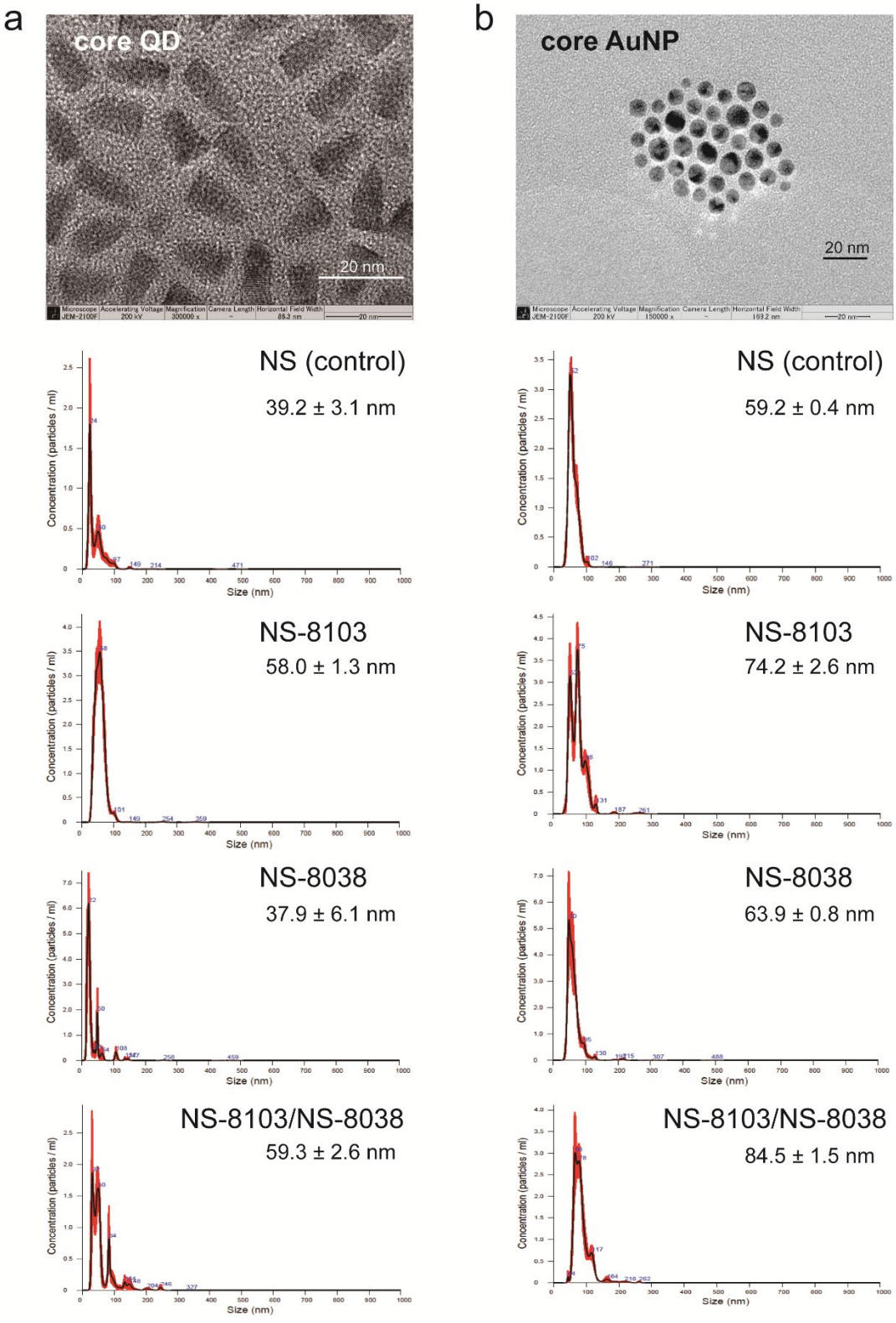

Figure S4. TEM and Hydrodynamic diameter of nanosomes. (a) QD core series, (b) AuNP core series

Chapter 5　Conclusion Remarks

Human neuraminidase-1 (NEU1) plays a much more profound function in human cancers than previously considered. We demonstrate that cancer cell surface NEU1 is a desired gatekeeper for an innovative anticancer therapeutic nanomedicine enabling active drug-targeting delivery by specific endocytosis into the cytoplasm.

In Chapter 2, we synthesized five types of lysosomal glycosidase enzymes, loaded them onto nanosomes, and demonstrated their antitumor effects on breast cancer cells, liver cancer cells, and colon cancer cells. This study reports for the first time that NEU1 distributed widely in cancer cell surfaces is a promising molecular target for creating an innovative anticancer therapeutic nanomedicine exhibiting potent and universal inhibitory effect on the proliferation of various cancer cells, and concurrently a desired "gatekeeper" for enabling transport of small molecular drugs to the intracellular space via specifically NEU1-mediated endocytic pathway.

In chapter 3, the merit of the present strategy to new generation nanocarrier based on the membrane tethered NEU1-mediated endocytosis is evident because **NS-8103/8201** bearing both irreversible NEU1 inhibitor **103** and sorafenib derivative **201** and **NS-8103/8038** bearing both **103** and irinotecan analog exhibits an enhanced higher anticancer activity to HepG2 cell growth (IC_{50}=6.2 nM) and Panc-1 cell growth (IC_{50}=8.07 nM) than **NS-8201** and **NS-8103** co-incubation and **NS-8038** and **NS-8103** co-incubation. The result clearly shows that antiadhesive nanosomal platform enables targeted delivery of hydrophobic sorafenib derivative **201** and irinotecan analog **038** into the cancer cells cytoplasm by the NEU1-mediated endocytosis conducted through irreversible inactivation with suicide substrate **103** on **NS-8103/8201**. Therefore, antiadhesive NSs having multiple irreversible NEU1 inhibitor **103** would be an ideal nanocarrier allowing for in vivo targeting cancer tissue/organ cell surface-NEU1 and subsequent endocytic intracellular delivery of various small antitumor reagents modified with a suited ketone/aldehyde auxiliary. More importantly, the concept and chemistry of the antiadhesive nanomedicine targeting endocytosis mediated by cancer cell surface-NEU1 can be expanded widely to other nanoparticular modalities such as gold nanoparticles, dendrimers, small exosome-like liposomes as well as new class non-toxic Cd-free QDs.

In chapter 4, animal experiment elicits a promising and highly potent therapeutic efficacy by NEU1 targeted nanosomal irinotecan **NS-8103/8038** due to the synergistic effects by two distinctive payloads of the nanosome, notably multiple "suicide substrate **103**" targeting NEU1-mediated endocytosis and irinotecan analog **038** targeting intracellular DNA topoisomerase, respectively. In addition, our results imply that a core AuNP/QD of high specific gravity with antiadhesive mixed-SAM surface is essential for active delivery of NEU1 targeted nanosomes **NS-8103** and **NS-8103/8038** into the pancreatic tumors across a

dense desmoplastic stroma. Characteristic features of the nanosomal platform are attributed to the simple core-shell structure and facile protocols of the preparation and quality control of the nanosomes, despite the highly beneficial chemotherapeutic effects by active DDS. Merit of active delivery strategy of nanosomal irinotecan to NEU1 sialidase of PDAC is clear because enhanced efficacy and reduced off-target toxicity of NS-8103/8038 enable much more flexible molecular design and optimization of the ratio of compositional payloads and extent of the use, notably “dosing schedule”, suited for the individual patients with advanced PDAC than currently approved therapeutic regimens.

Acknowledgements

First of all, I would like to express my sincere gratitude to Professor Shin-Ichiro Nishimura and Professor Hiroshi Hinou for their helpful suggestions, discussions, and encouragements. This work described herein would not have been successful without them.

I would like to express my special thanks to Professor Toyoyuki Ose and Dr. Akira Kitamura in Hokkaido University for critical suggestions and tenderhearted encouragement.

I would like to express my grateful thanks to Dr. Yasuhiro Yokoi and Mr. Daiki Kambe for supporting. And I want to express grateful thanks to my colleagues in Nishimura laboratory members for daily support, discussions, and encouragement.

Finally, I wish to express my sincere gratitude to my parents for their invaluable mental support and affectionate encouragement.